Master's Thesis

Molecular Design and Modification of Organic Materials for Opto-electronic and Tribo-electric Devices

Hye Jin Cho

Department of Energy Engineering

(Energy Engineering)

Graduate School of UNIST

2017

Molecular Design and Modification of Organic Materials for Opto-electronic and Tribo-electric Devices

Hye Jin Cho

Department of Energy Engineering

(Energy Engineering)

Graduate School of UNIST

Molecular Design and Modification of Organic Materials for Opto-electronic and Tribo-electric Devices

A thesis/dissertation
submitted to the Graduate School of UNIST
in partial fulfillment of the
requirements for the degree of
Master of Science

Hye Jin Cho

5/28/2017 of submission

Approved by

Advisor

Changduk Yang

Molecular Design and Modification of Organic Materials for Opto-electronic and Tribo-electric Devices

Hye Jin Cho

This certifies that the thesis of Hye Jin Cho is approved.

05. 28. 2017 of submission

signature

Advisor: Changduk Yang

signature

Hyesung Park: Thesis Committee Member #1

signature

Sung You Hong: Thesis Committee Member #2

Abstract

Over the past two decades, energy harvesting using wasting is critical issue. Energy harvesting is essential, as it is abundant in our life environment. Among harvesters, organic photovoltaics (OPVs) using cunjugated polymers or smallmolecules, organic field-effect transistors (OFETs), and triboelectric nanogenerators (TENGs) are representative harvesters and exhibit good performance.

Among a large number of materials reported in the related literature such as benzodithiophene (BDT), diketopyrrolopyrrole (DPP), isoindigo (IIG), TPTI is a promising material for optoelectronic device application (polymer solar cells and organic field-effect transistors).

In accordance with this, **in chapter 1**, I performed in-depth study about the relationship between random terpolymer and polymer solar cell performance based on TPTI as the donor and PCBM as the acceptor. Incorporating random terpolymerization strategy unlike alternating donor-acceptor copolymer, TPTI-based random terpolymers with thiophene and bithiophene moieties (PTPTI-Tx) were investigated for polymer solar cells (PSCs). Particularly, correlation between crystalline allignment from surface to the whole film depth in the TPTI-Tx:PCBM blend films and the PSCs performance was investigated deeply.

In chapter 2, with TPTI-Tx random terpolymers which described in chapter 1, a fused-aromatic-ring-based acceptor (m-ITIC) was introduced as non-fullerene acceptor. I explored TPTI-Tx:m-ITIC blends characters including optical, electrical energy, morphology, crystalline packing in the non-fullerene polymer solar cells.

Also, **in chapter 3**, I simultaneously tuning the molecular weight and alkyl substituents based on thienoisoindigo-naphthalene copolymer (PTIIG-Np) for organic field-effect transistors (OFETs). Through stoichiometry imbalance of monomers, I systematically synthesized low and high molecular weight PTIIG-Np polymers with three different alkyl substituents.

In chapter 4, I deeply studied about modulating of PVDF dielectric material via Atom Transfer Radical Polymerization (ATRP) to enhance triboelectric nanogenerator performance. By controlling the reaction time with the fixed catalyst system and monomer conditions, PVDF-graft tert-butyl acrylate copolymers (PVDF-*Gn*) have been synthesized and characterized. Inducing improved dielectric constant, Difference of TENG performance depending on the graft extend and degree of dielectric constant has been demonstrated relating to the structure of PVDF-*Gn*. Also, we intertwined the morphology and crystalline structure of PVDF graft copolymers with the TENGs performance.

Table of Contents

List of Figures

patterns of TPTI-T-based neat terpolymer films (a, b, c, and d: upper line) and blend films with $PC_{71}BM$ (e, f, g and h: lower line) depicted in the bulk region: (a and e for PTPTI-T100, b and f for PTPTI-T70, c and g for PTPTI-T50, and d and h for PTPTI-T30). i,j, Pole figures extracted from (010) diffraction in surface (i) and bulk (j) regions of the blend films on the SiO_2/Si substrates, indicating that // and $\perp$ are parallel and perpendicular to the substrates, respectively (surface region: $\alpha_i = 0.11° <$ critical angle, bulk region: $\alpha_i = 0.12° >$ critical angle).

Figure 20. 2D-GIWAXD images of the polymer:$PC_{71}BM$ blend films measured below the critical angle of films ($\alpha_i = 0.11° < \alpha_c$). (a) PTPTI-T100:$PC_{71}BM$, (b) PTPTI-T70:$PC_{71}BM$, (c) PTPTI-T50:$PC_{71}BM$, and (d) PTPTI-T30:$PC_{71}BM$ blend films, respectively.

Figure 21. Pole figures of azimuthal-cuts along the (010) π-π stacking peaks in the polymer:$PC_{71}BM$ blend films both in surface ($\alpha_i = 0.11° <$ critical angle) and bulk ($\alpha_i = 0.12° >$ critical angle) region of the films. a, PTPTI-T100:$PC_{71}BM$ b, PTPTI-T70:$PC_{71}BM$ c, PTPTI-T50:$PC_{71}BM$, and d, PTPTI-T30:$PC_{71}BM$ blend films, respectively. The stronger intensity appeared at 90° (and 0° and 180°) in the pole figures represents orientation of (010) π-π stacking is mainly parallel (and perpendicular) to the substrate.

Figure 22. Charge-carrier dynamic characterizations of TPTI-T-based polymer:$PC_{71}BM$ solar cells. Net photocurrent density of TPTI-T-based polymer solar cells as a function of effective voltage (a), V_{OC} (b), and J_{SC} (c) versus the natural logarithm of light intensity for the devices, and FF (d) of the photovoltaic devices are shown for various light intensities of 4–100 mW cm^{-2}.

Figure 23. ^{1}H-NMR spectra of four TPTI-T based polymers in $CDCl_3$. The broad peaks in the range of 1.56-1.00 are assigned to methylene protons (-CH_2-R, methylene) of the hexyldecyl side chain groups.

Figure 24. (a) Chemical structures of PTPTI-Tx donor polymers and *m*-ITIC acceptor. (b) Optical absorption spectra of PTPTI-Tx:*m*-ITIC blend films. (c) Energy level diagram of PTPTI-Tx and *m*-ITIC.

Figure 25. (a) *J-V* curves of PTPTI-Tx:*m*-ITIC (1/1.25 w/w) solar cells under 100 mW cm^{-2} AM 1.5G solar illumination. (b) Corresponding EQE spectra.

Figure 26. (a) GIWAXS images of the PTPTI-Tx:*m*-ITIC blend films: (i) PTPTI-T100:*m*-ITIC, (ii) PTPTI-T70:*m*-ITIC, (iii) PTPTI-T50:*m*-ITIC, (iv) PTPTI-T30:*m*-ITIC. (b) Corresponding in-plane and out-of-plane line cuts of the GIWAXS images of PTPTI-Tx:*m*-ITIC blend films.

Figure 27. Pole figure plots from the (100) lamellar diffraction in the PTPTI-Tx:*m*-ITIC blend films: (i) PTPTI-T100:*m*-ITIC, (ii) PTPTI-T70:*m*-ITIC, (iii) PTPTI-T50:*m*-ITIC, (iv) PTPTI-T30:*m*-ITIC, the fraction values in parentheses are the ratios of integrated 0–45° and 135–180° (A_{xy}) to 45–135° (A_z) area.

Figure 28. (a) AFM height images and (b) TEM images of the PTPTI-Tx:*m*-ITIC blend films: (i) PTPTI-T100:*m*-ITIC, (ii) PTPTI-T70:*m*-ITIC, (iii) PTPTI-T50:*m*-ITIC, (iv) PTPTI-T30:*m*-ITIC.

Figure 39. AFM and SEM images of the PVDF-Gn films. (a) 3-dimensional AFM images and (b) Cross-sectional SEM images for PVDF-based films with various PtBA mole percent ranging from 0 to 18%.

Figure 40. XRD pattern of PVDF-Gn films. (a) The high-resolution XRD patterns of pristine PVDF and PVDF-Gn films as a function of PtBA mole percent. (b) The expanded view of t he 2nd peak in Fig. 7A. The peak can be deconvoluted into two peaks, α (110) (red) and β (200) phase (blue).

List of Tables

List of Schemes

Research Background of Organic Photovoltaics, Organic Field-effect Transistors, and Triboelectric Nanogenerators

1. Principle of Organic Photovoltatics (OPVs)

Figure 1. Illustration of photovoltaic effect

Organic Photovoltaic (OPV) devices convert solar energy to electrical energy. A typical OPV device consists of one or several photoactive materials sandwiched between two electrodes. **Figure 1** depicts organic photovoltaic effect.

To improve organic photovoltaics, various research works have been investigated using conjugated polymers. The substantial researches have been started from the discovery of perylene-iodine complex in 1954 which has highly conducting properties. After that, high electrical conductivity material, polyacetylene with iodine doped, discovered by Shirakawa, Heeger, and MacDiarmid helped to initiate the field of organic conductive polymers.

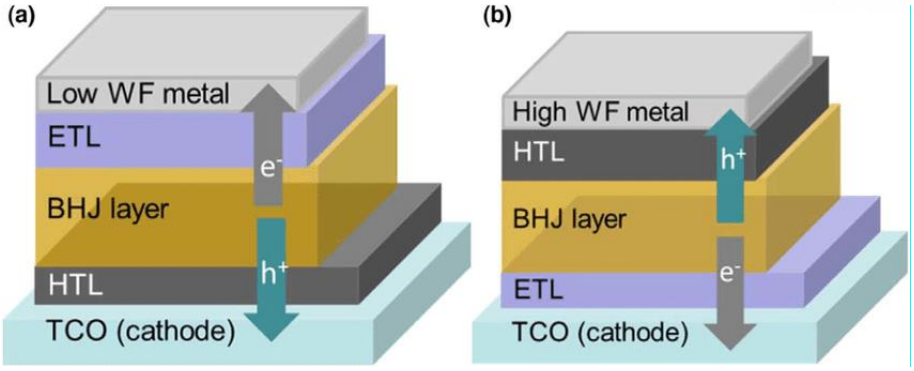

Figure 2. (a) conventional and (b) inverted device structure of OPVs

When sunlight exposed the photoactive layers composed of donor and acceptor semiconducting organic materials to generate photocurrents. The donor material (D) donates electrons and mainly transports holes and the acceptor material (A) withdraws electrons and mainly transports electrons. Typical device structure of OPV, which is categorized as conventional and inverted structure is demontrated in **Figure 2**. As depicted in **Figure 3**, those photoactive materials harvest photons from sunlight to form excitons, in which electrons are excited from the valence band into the conduction band (**Light Absorption**). The excitons diffuse to the donor/acceptor interface (**Exciton Diffusion**) and separate into free holes (positive charge carriers) and electrons (negative charge carriers) (**Excition dissociation**). When the holes and electrons move to the corresponding electrodes and the charges are collected by following either donor or acceptor phase, it is called photovoltaic (**Charge collection**).

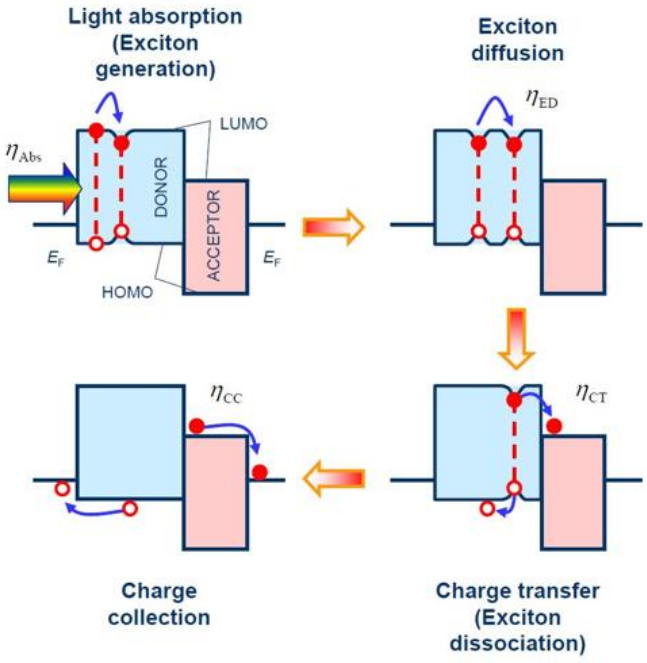

Figure 3. operating mechanism of OPVs

The power conversion efficiency (η) is the percentage of the solar energy shining on the PV devices that is converted into electrical energy and η is given by the following equation:

$$\text{PCE } (\eta) = V_{OC} \times J_{SC} \times FF/P_{in}.$$

Where P_{in} is the input power, J_{SC} is the short-circuit current density obtained under short circuit conditions (V = 0), V_{OC} is the open-circuit voltage obtained when there is no current flow, *FF* is defined as the ratio of its maximum power to the product of J_{SC} and V_{OC}. These factors are crucial for solar cells with high performance efficiency.

The quantum efficiency (QE) is the ratio of the number of carriers collected by the solar cell to the number of photons of a given energy incident on the solar cell.

- External Quantum Efficiency (EQE) is the ratio of the number of charge carriers collected by the solar cell to the number of photons of a given energy shining on the solar cell from outside (incident photons).
- Internal Quantum Efficiency (IQE) is the ratio of the number of charge carriers collected by the solar cell to the number of photons of a given energy that shine on the solar cell from outside and are absorbed by the cell.

$$EQE = \eta_A \bullet \eta_{IQE} = \eta_A \bullet \eta_{ED} \bullet \eta_{CT} \bullet \eta_{CC}$$

Where

Photon absorption ($\boldsymbol{\eta_A}$) : Exciton generation by absorption of light

Exciton diffusion ($\boldsymbol{\eta_{ED}}$) : diffusion over ~LD (~20 nm)

Charge-transfer reaction ($\boldsymbol{\eta_{CT}}$) : Exciton dissociation by rapid and efficient charge transfer

Collection of the carriers ($\boldsymbol{\eta_{CC}}$) : Charge extraction by the internal electric field

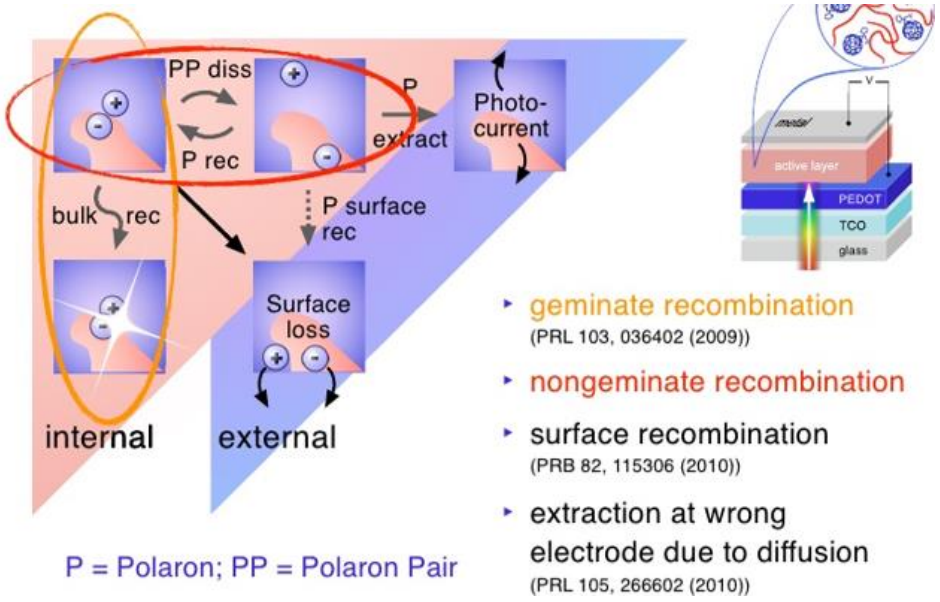

Figure 4. Recombination illustration of OPVs

When the charge generation occur, some degree of charge recombination could exist.

Exciton – electron-hole pair (Tightly bound pair- Frenkel exciton, weekly bound pair- Wannier-Mott exciton)

Polaron – charge + disortion of the surrounding

Polaron pair – Bound pair of electron and electron polarons in different molecules

Exciplex: D*-A (A: ground); an excited molecul and an adjacent ground-state molecule can form instantaneous complex that emits fluorescence at a longer wavelength than the excited molecule itself

Eximer: D*-D (D: ground); interaction between an excited molecules and an adjacent ground-state molecule (if two molecules are the same type)

Recombination of mobile charge carriers could limit FF. there are several types of recombination following below as shown in **Figure 4**.

Geminate recombination: recombination of an electron with hole wich are still bound

Non-Geminate recombination: recombination of a free mobile electron with a trapped hole

Molecular recombination: involves one electron and one hole at a time

Bimolecular recombination: involves two free carriers simultaneously, such as direct band-to-band recombination

2. Principle of Organic Field-effect Transistors (OFETs)

The field-effect transistor (FET) was first proposed by J.E. Lilienfeld, who received a patent for his idea in 1930. He proposed that a field-effect transistor behaves as a capacitor with a conducting channel between a source and a drain electrode. Applied voltage on the gate electrode controls the amount of charge carriers flowing through the system. The first field-effect transistor was designed and prepared in 1960 by Kahng and Atalla using a metal–oxide–semiconductor (MOSFET). However, rising costs of materials and manufacturing, as well as public interest in more environmentally friendly electronics materials have supported development of organic based electronics in more recent years. In 1987, Koezuka and co-workers reported the first organic field-effect transistor based on a polymer of thiophene molecules. The thiophene polymer is a type of conjugated polymer that is able to conduct charge, eliminating the need to use expensive metal oxide semiconductors. Additionally, other conjugated polymers have been shown to have semiconducting properties. OFET design has also improved in the past few decades.

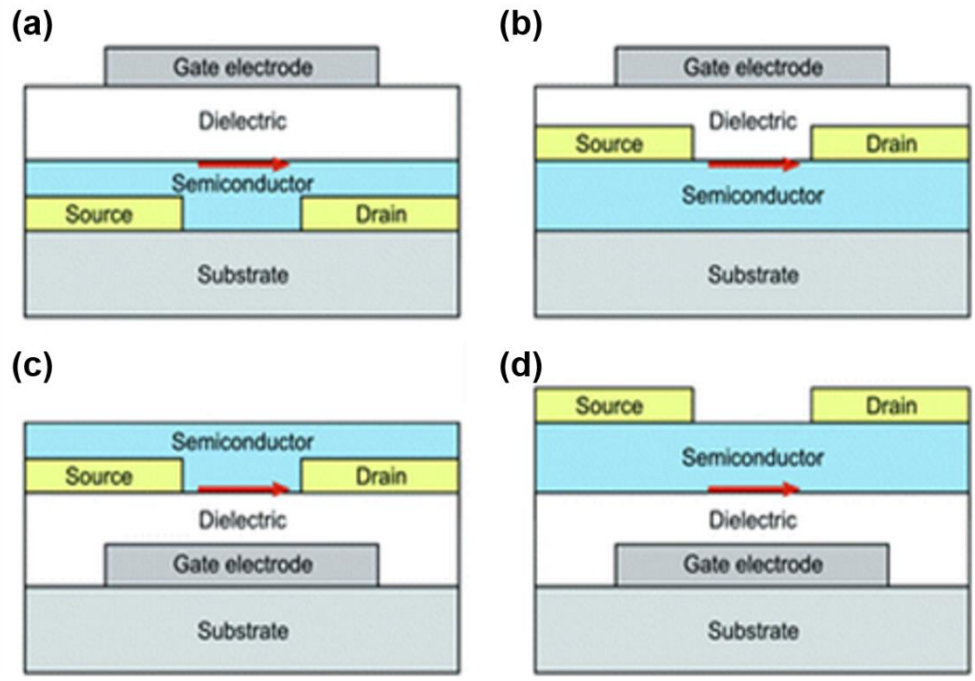

Figure 5. Typical device structures of OFETs. (a) top gate-bottom contact, (b) top gate-top contact, (c) bottom gate-bottom contact, (d) bottom gate-top contact, respectively.

There are representative four types of OFET device structures as shown in **Figure 5**. Voltage gives rise to an electric field in the semiconductor that attract, accumulates, charges. These create a channel for charges and let them more easily move between source and drain contact. Drain current (I_d) varies linearly with drain-source voltage (V_{DS}), channel has the characteristics of a resistor.

3. Brief Concept of Random Polymerization

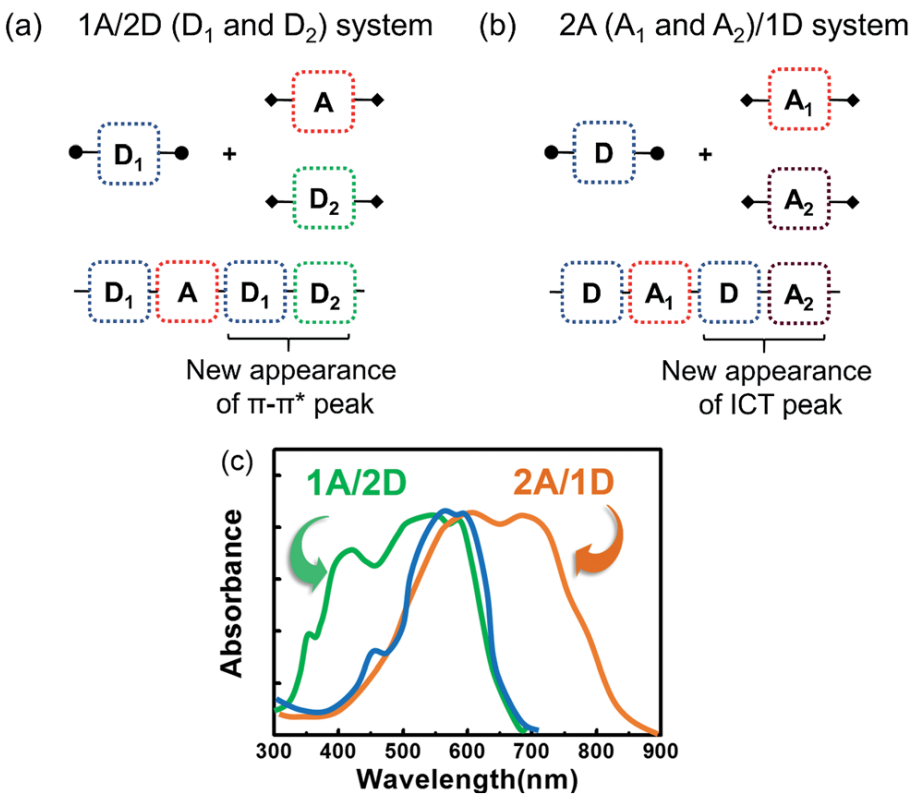

Figure 6. Two different approaches for random terpolymers. (a) 1A/2D system, (b) 2A/1D system, and (c) their concept absorption profiles

A promising strategy to overcome alternating donor-acceptor polymer limitations is using the concept of random terpolymer strategy. There are two types of random terpolymers as shown in **Figure 6**. First is 1D-2A random terpolymers comprising one donor and two acceptor units in the polymer backbone, because introducing a third acceptor component can induce a positive effect on light absorption profiles, endowing a great potential for simultaneously improving J_{SC} and EQE values. Another type of random terpolymer is 2D-1A type terpolymer consisting of two donor and one acceptor units, which was used to control the crystallinity of terpolymers. Therefore, a proper choice of two donor co-monomers in the 2D-1A type terpolymers backbone can provide an effective mean of optimizing morphology and maximizing the performances of the PSCs.[1]

4. The synthetic method of Stille Coupling Reaction

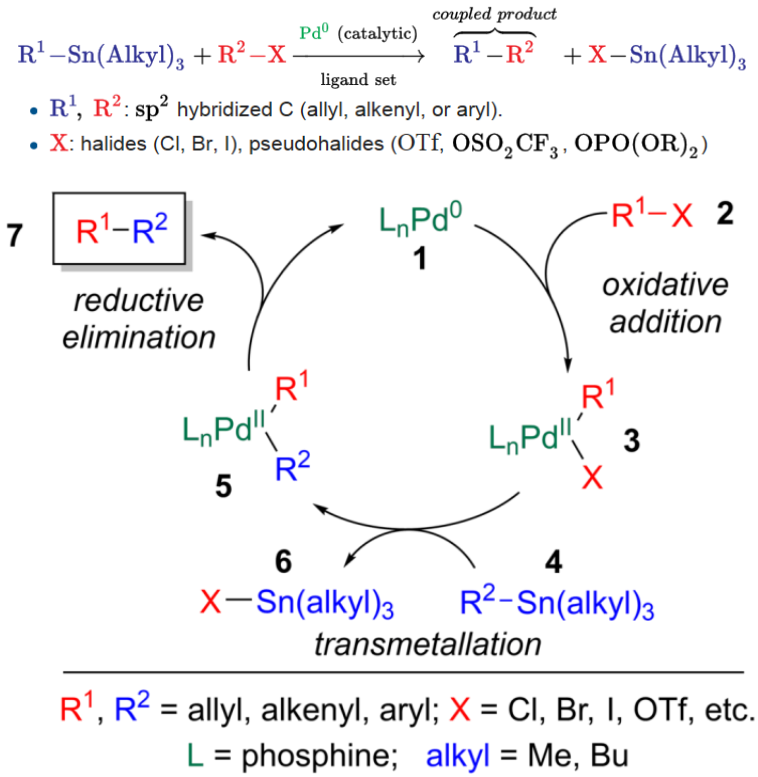

Figure 7. Mechanism of Stille coupling reaction

The Stille reaction, or the Migita-Kosugi-Stille coupling, discovered in 1977, is the powerful organic reaction between stannanes and halides or pseudohalides forming C-C bond using a palladium catalyst. The reaction is usually conducted under inert condition to prevent unwanted homo coupling of organic stannyl compounds. Tetrakis(triphenylphosphine)palladium(0), in short $Pd(pph_3)_4$, and tris(dibenzylideneacetone)dipalladium(0), in short $Pd_2(dba)_3$ is commonly used as the catalyst. The mechanism, as depicted in **Figure 7**, begins with oxidative addition of the organo halide to the Pd(0) to form a Pd(II) complex (**3**). After this increasing oxidation state of Pd, transmetallation and reductive elimination are followed, regenerating the palladium catalyst and yielding the compound.

5. The synthetic method of Suzuki Coupling Reaction

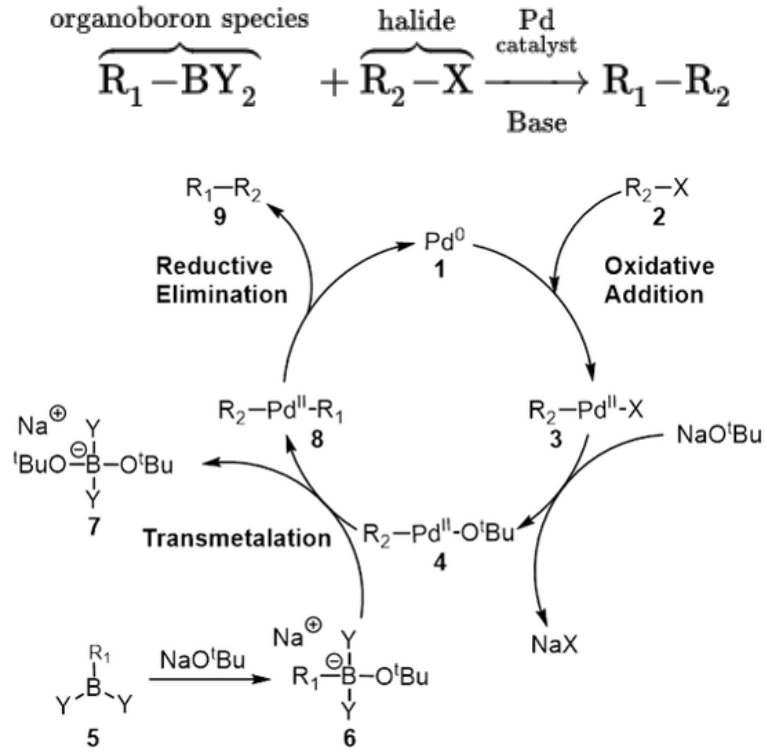

Figure 8. Mechanism of Suzuki coupling reaction

The **Suzuki reaction** is an organic reaction, classified as a coupling reaction, where the coupling partners are a boronic acid and an organohalide catalyzed by a palladium(0) complex. It was first published in 1979 by Akira Suzuki. The mechanism, as depicted in **Figure 8**, begins with oxidative addition of the organo halide to the Pd(0) to form a Pd(II) complex (**3**). After this increasing oxidation state of Pd, transmetallation and reductive elimination are followed, regenerating the palladium catalyst and yielding the compound.

6. Principle of TENGs

The triboelectric effect (also known as triboelectric charging) is a type of contact electrification in which certain materials become electrically charged after they come into frictional contact with a different material.

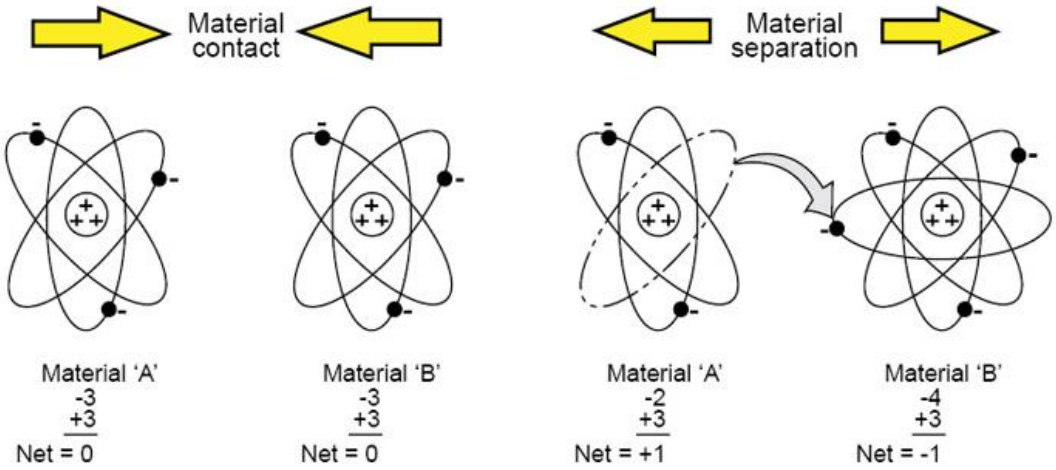

Figure 9. Illustration of triboelectric effect

Figure 10. Illustration of Triboelectric Series

Triboelectric series is the term used to refer to a list of materials organized by electric affinity, only that it refers to negative and positive affinities from certain materials. Johan Carl Wilcke published the first triboelectric series in a 1757 paper on static charges. Materials are often listed in order of the polarity of charge separation when they are touched with another object. A material towards the bottom of the series, when touched to a material near the top of the series, will acquire a more negative charge. The farther away two materials are from each other on the series, the greater the charge transferred. Materials near to each other on the series may not exchange any charge.

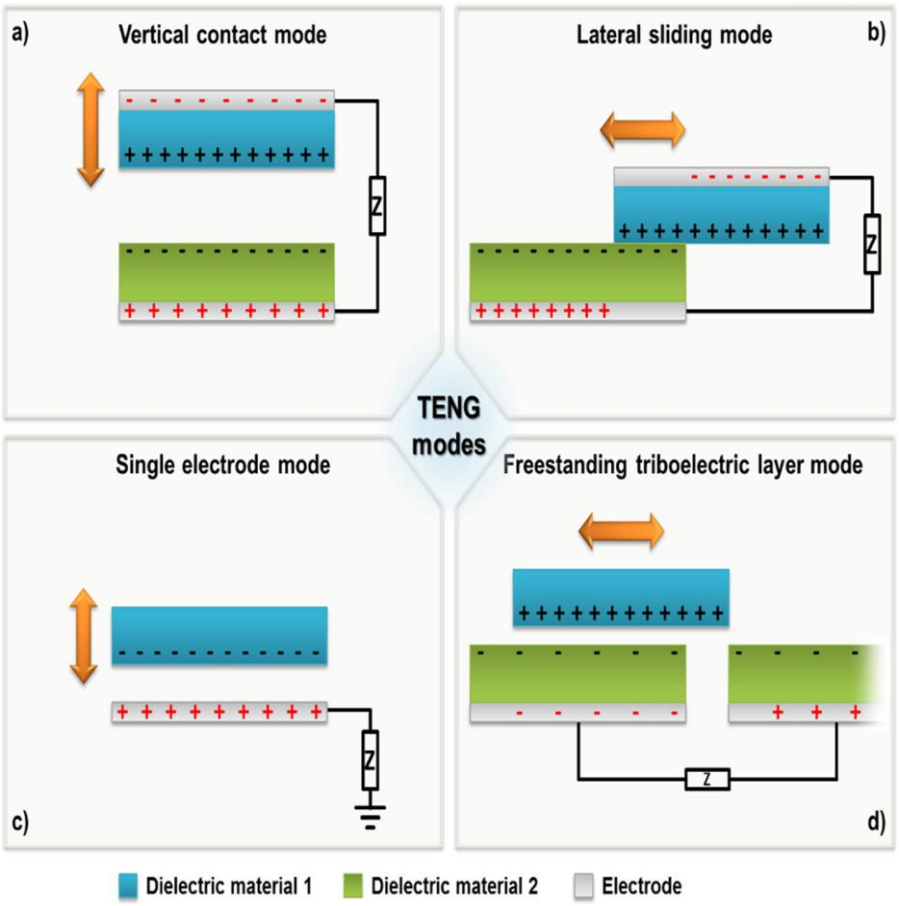

Figure 11. Four different operating mode of TENGs. (a) vertical contact mode, (b) lateral sliding mode, (c) single electrode mode, and (d) freestanding triboelectric layer mode, respectively.

Triboelectric Nanogenerators (TENGs) which convert mechanical energy to electric using triboelectrification and electrostatic induction, is promising self-powered system. In general, four operation working modes of TENGs have been established (**Figure 11**); the vertical contact mode, the lateral sliding mode, single-electrode mode, and freestanding triboelectric layer mode, respectively.

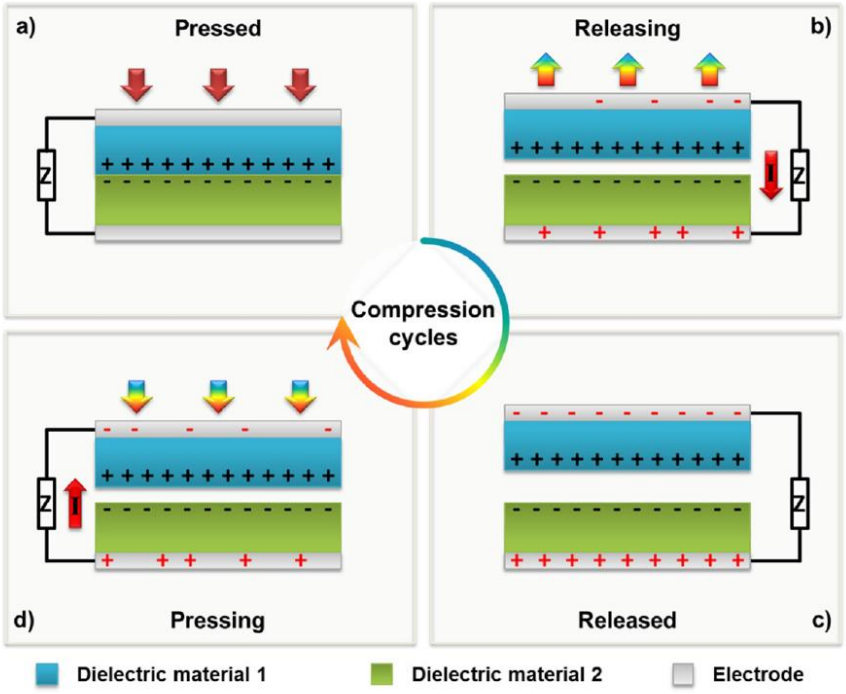

Figure 12. operating mechanism of TENGs

The electronic generation process can be demonstrated the coupling between triboelectric effect and electrostatic effect as sketched in **Figure 12**. Two different dielectric layers face each other. Then two electrodes are connected on the top and bottom surface of the stacked dielectric structure. As applied an external force on the device, this generates opposite triboelectric charges at the interface. If the external force is released and the surfaces are separated more far away, a potential difference generated between dielectric films, resulting that electrons in one electrode will flow to the other electrode to balance the electrostatic field, and this generates a current. If the seperation is closed again due to an external force, the triboelectric potential difference disappears, and then the electrons flow back dirrection to generate an opposite current.[2]

7. The synthetic method of Atom Transfer Radical Polymerization

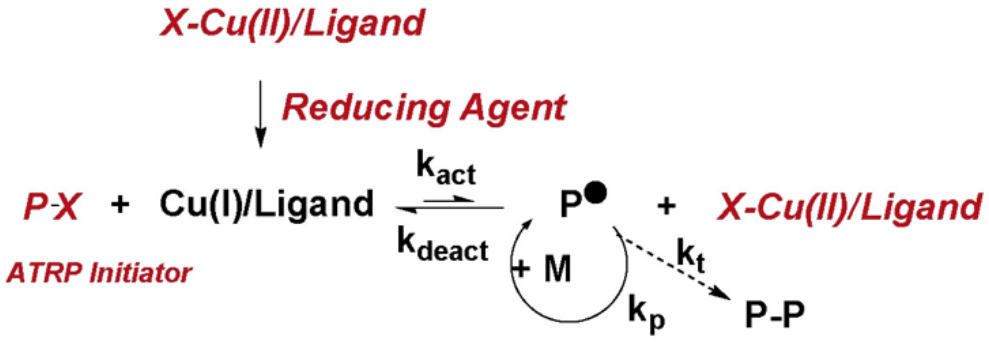

Figure 13. (a) Schematic illustration and (b) operating mechanism of OPVs

Atom transfer radical polymerization (ATRP) is an example of a reversible-deactivation radical polymerization. As the name implies, the atom transfer step is the key step in the reaction responsible for uniform polymer chain growth. ATRP (or transition metal-mediated living radical polymerization) was independently discovered by Mitsuo Sawamoto and by Jin-Shan Wang and Krzysztof Matyjaszewski in 1995. ATRP usually employs a transition metal complex as the catalyst with an alkyl halide as the initiator (R-X). Various transition metal complexes, namely those of Cu, Fe, Ru, Ni, Os, etc., have been employed as catalysts for ATRP. In an ATRP process, the dormant species is activated by the transition metal complex to generate radicals via one electron transfer process. Simultaneously the transition metal is oxidized to higher oxidation state. This reversible process rapidly establishes an equilibrium that is predominately shifted to the side with very low radical concentrations. The number of polymer chains is determined by the number of initiators. Each growing chain has the same probability to propagate with monomers to form living/dormant polymer chains (R-P_n-X). As a result, polymers with similar molecular weights and narrow molecular weight distribution can be prepared.

Chapter 1. A Study on TPTI-based Random Terpolymers by Tuning Composition Ratio in Fullerene-based Polymer Solar Cells

1.1. Introduction

The power-conversion efficiency (PCE) of polymer solar cells (PSCs) has rapidly improved from below 1% to over 10% in the past 10 years—mainly due to significant advances in the design and synthesis of better semiconducting polymers, based on an increased understanding of structure–property relations [3-13]. Over the years, significant research efforts have been directed toward developing alternating donor–acceptor (D–A) copolymers to extend absorption and harvest more solar energy [14-17]. However, compared with commercial inorganic solar cells, the narrow intrinsic absorption of alternating D–A copolymers limits the short-circuit current density (J_{SC}) with low external quantum efficiencies (EQEs) [18-24]. A promising strategy to overcome these limitations is using the concept of 1D-2A random terpolymers comprising one donor and two acceptor units in the polymer backbone, because introducing a third acceptor component can induce a positive effect on light absorption profiles, endowing a great potential for simultaneously improving J_{SC} and EQE values[19, 25-27]. Unfortunately, despite their broadened and intensified absorptions, very few successful PSCs based on 1D-2A random terpolymers that have PCEs surpassing those of the state-of-the-art PSCs based on alternating copolymers have been reported[1, 18, 28-30]. This is because the irregular sequence in the backbone causes adverse effects on not only morphological properties but also charge transport characteristics, which obscures the real potential of the random terpolymer strategy. There is another type of random terpolymer consisting of two donor and one acceptor units, named as 2D-1A type terpolymer, which was used to control the crystallinity of terpolymers[31-32]. Therefore, a proper choice of two donor co-monomers in the 2D-1A type terpolymers backbone can provide an effective mean of optimizing morphology and maximizing the performances of the PSCs[25, 29].

Here, I synthesized a new series of 2D-1A random terpolymers (PTPTI-Tx) from thieno[2′,3′:5′,6′]pyrido[3,4-*g*]thieno[3,2-*c*]isoquinoline-5,11(4*H*,10*H*)-dione (TPTI) acceptor unit in conjugation with two donor moieties (thiophene (T) and bithiophene (2T)), with a view to inducing different crystalline behaviors of the resulting polymers (see Fig. 1a for the molecular structures).

1.2. Results and discussion

1.2.1. Synthesis and Characterization

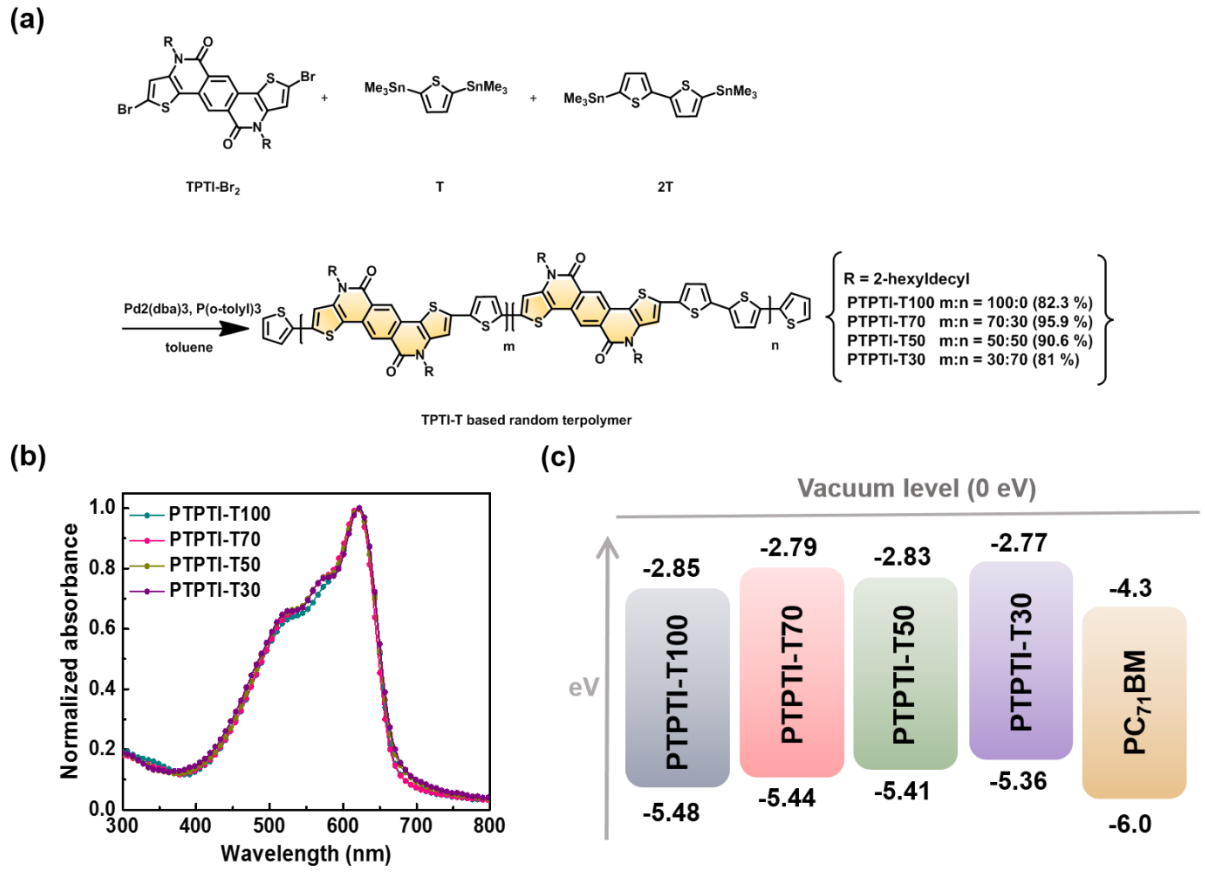

Figure. 14. TPTI-T-based random polymers with chemical structures and optical and electrical properties. (a) Structure of the four terpolymers with different ratios of T and 2T moieties; (b) UV–visible absorption spectra of the four neat polymers in the film state; (c) Energy level diagram of the four polymers and $PC_{71}BM$ (energy values are in eV with respect to the vacuum level).

A Stille coupling polymerization of three monomers, 2,8-dibromo-4,10-bis(2-hexyldecyl)thieno[2′,3′:5′,6′]pyrido[3,4-*g*]thieno[3,2-*c*]isoquinoline-5,11(4*H*,10*H*)-dione (TPTI-Br_2), 2,5-bis(trimethylstannyl)thiophene (T), and 5,5′-bis(trimethylstannyl)-2,2′-bithiophene (2T), is carried out using $Pd_2(dba)_3$ and P(*o*-tolyl)$_3$ as the catalyst system to produce a series of TPTI-T-based polymers, where different T:2T feed molar ratios of 100:0, 70:30, 50:50, and 30:70 are used[29, 33]. The corresponding polymers are referred to as PTPTI-T100, PTPTI-T70, PTPTI-T50, and PTPTI-T30, respectively (see **Figure 14a**). All polymers show good solubility in common organic solvents such as chloroform (CF), chlorobenzene (CB), and *o*-dichlorobenzene. For a systematic investigation, we also attempt to prepare PTPTI-T0 (without T units), *i.e.*, a PTPTI-2T alternating copolymer[34]. However, this

precipitates out during the polymerization due to very limited solubility, and thus, is not studied further.

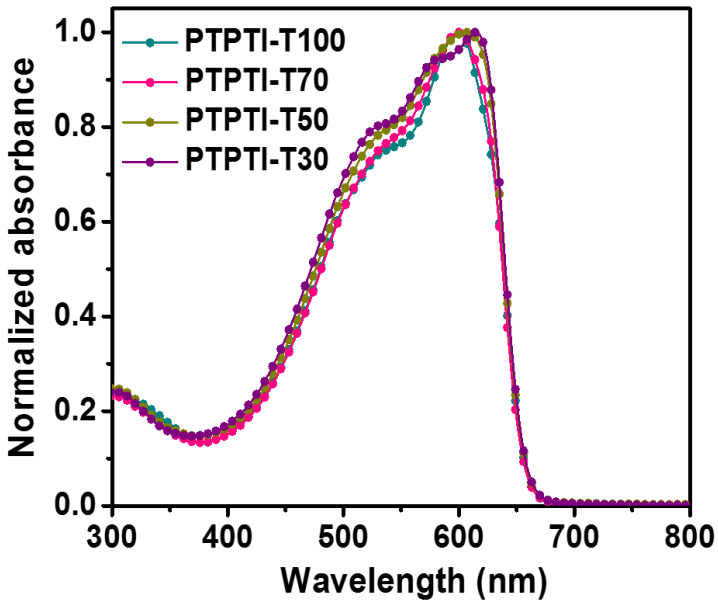

Figure 15. UV-vis absorption spectra of the TPTI-T based polymers in solution (1×10^{-5} M in chloroform).

All polymers show very similar well-defined absorption features (in the range of 300–700 nm); the changes in the absorption peak and onset point among the polymers are within 10 nm. In addition, the absorption spectra shows that there are no significant bathochromic shifts on going from solution to thin film, indicating a similar rigid-rod conformation in both states[35-36]. Therefore, the calculated optical bandgaps (ΔE_g^{opt}) from the polymer film absorption edges fall within a small range of 1.84–1.85 eV.

Table 1. Optical and electrochemical parameters of TPTI-T based polymers.

Copolymer	λ_{max}^{sol} [nm]	λ_{max}^{film} [nm]	λ_{onset}^{film} [nm]	ΔE_g^{opta} [eV]	E_{HOMO} [eV]	E_{LUMO} [eV]	ΔE_g^{elecb} [eV]	M_n^c [kDa]	PDI[c]
PTPTI-T100	610	618	670	1.85	- 5.48	- 2.85	2.63	95.3	1.50
PTPTI-T70	605	615	669	1.85	- 5.44	- 2.79	2.65	118.3	1.48
PTPTI-T50	613	620	673	1.84	- 5.41	- 2.83	2.58	85.3	1.42
PTPTI-T30	615	621	673	1.84	- 5.36	- 2.77	2.59	84.1	2.04

[a]Optical energy bandgap estimated from the absorption onset of the thin films. $\Delta E_g^{opt} = 1240/\lambda_{onset}^{film}$; [b]$\Delta E_g^{elec}$ = LUMO-HOMO [c]Estimated from the gel permeation chromatography (GPC) against polystyrene standard in 1,2,4-trichlorobenzene (TCB) at 120 °C.

The molecular weight (M_n) and polydispersity index of the polymers are measured by gel permeation chromatography (GPC) against polystyrene standards in 1,2,4-trichlorobenzene at 120 °C; the data are summarized in **Table 1**. PTPTI-T100 and PTPTI-T70 show somewhat higher M_n values relative to the other polymers, reflecting a higher degree of chain aggregation in the GPC measurement for the samples with a higher 2T content.

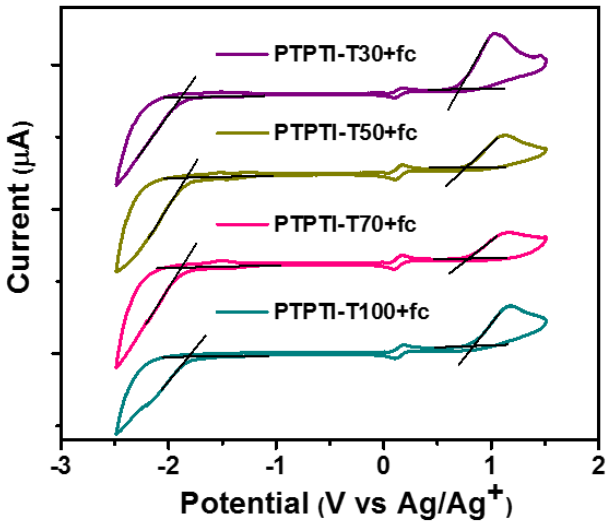

Figure 16. Cyclic voltammograms of TPTI-T based polymers with onset points drawn by black lines highlighted for reduction and oxidation, respectively (measurement with a three-electrode cell in a 0.1 M tetra-n-butylammonium hexafluorophosphate (n-Bu_4NPF_6) solution in acetonitrile at a scan rate of 100 mV/s at room temperature under argon).

The highest occupied molecular orbital (HOMO) and lowest unoccupied molecular orbital (LUMO) energy levels of TPTI-based polymers are determined by cyclic voltammetry (CV), and the results are shown in **Figure 16**. The HOMO and LUMO levels of PTPTI-T100 are located at −5.48 and −2.85 eV, respectively. Interestingly, introducing 2T into the backbone can slightly raise both the HOMO and LUMO levels. Note that the LUMO energy levels of the polymers are all located within a suitable range (−2.85 to −2.77 eV), yielding LUMO–LUMO offsets of >0.3 eV with the $PC_{71}BM$ acceptor, which should ensure efficient exciton dissociation[37-38].

1.2.2. Photovoltaic performance

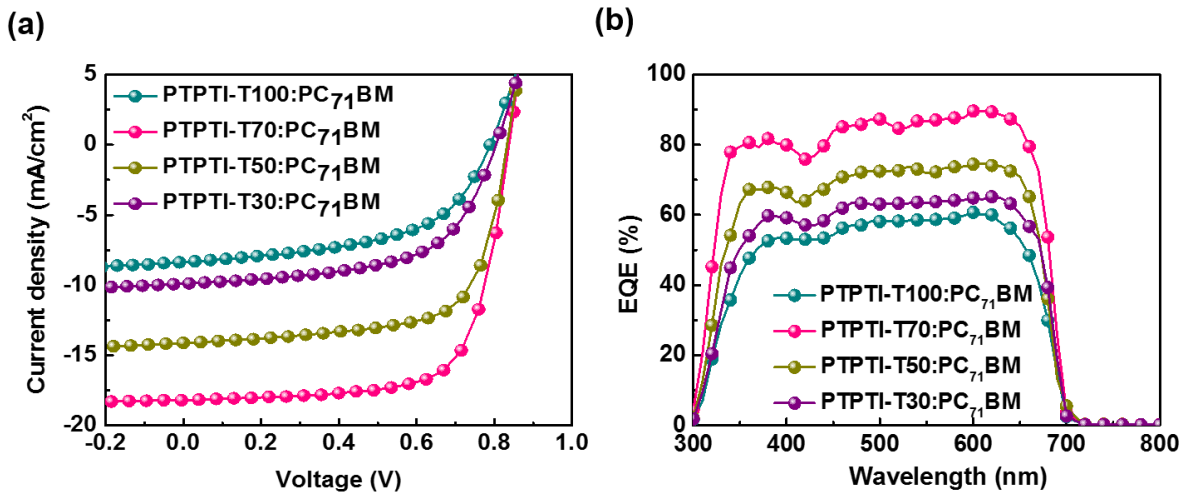

Figure 17. Photovoltaic performances and morphologies of TPTI-T based polymer:$PC_{71}BM$ single-junction solar cell systems. a,b, Illuminated *J–V* curves (a) and EQE spectra (b) of the TPTI-T based polymers:$PC_{71}BM$ based devices under simulated air mass 1.5G illumination (100 mW cm^{-2}).

Table 2. Photovoltaic performance parameters in the TPTI-T-based polymer solar cells with $PC_{71}BM$ under the optimized conditions.

Active layer	Thickness (nm)	V_{OC} (V)	J_{SC} (mA/ cm^2)	FF (%)	PCE^{best} (%)	PCE^{avg*} (%)	Hole mobility (μ_h) (cm^2 /V s)	Electron mobility (μ_e) (cm^2 /V s)	μ_h/μ_e
PTPTI-T100	194±2.5	0.80	8.2	53.9	3.53	3.02	1.45×10^{-4}	1.11×10^{-5}	13.06
PTPTI-T70	191±1.7	0.83	18.3	71.2	10.8	9.91	3.78×10^{-4}	2.13×10^{-4}	1.77
PTPTI-T50	203±2.2	0.82	14.7	66.4	8.02	7.82	7.01×10^{-4}	8.05×10^{-5}	8.70
PTPTI-T30	192±2.0	0.82	10.5	58.7	5.05	4.87	5.02×10^{-4}	4.11×10^{-5}	12.18

*The average PCE values were obtained from more than 16 separate devices.

To investigate the photovoltaic properties of all polymers, PSCs with a conventional structure of ITO/PEDOT:PSS/polymer:$PC_{71}BM$/ZnO/Al are examined throughout the study. For all cases, we use a solvent mixture of CB and CF (4:1 vol. ratio) with 3 vol% of 1,8-diiodooctane and a total solution concentration of 18 mg ml^{-1}, with a donor to acceptor ratio of 1:0.8 (w/w)[33, 39-40]. The detailed process is described in the Experimental section. The current density–voltage (*J–V*) curves and representative EQE spectra of the best-performing PSCs are shown in **Figure 17a and b** and the corresponding photovoltaic characteristics are summarized in **Table 2**. First, the PTPTI-T100:$PC_{71}BM$ control device shows a J_{SC} of 8.2 mA cm^{-2}, an open-circuit voltage (V_{OC}) of 0.80 V, and a fill factor (FF) of 53.9%, yielding a PCE of 3.53%. All random terpolymer-based PSCs exhibit V_{OC} values comparable to that of

the PTPTI-T100 device, which is in good agreement with the similar HOMO values measured by CV [41]. Surprisingly, although the energy levels and absorption coefficients of the employed donor polymers are very similar to each other, a dramatic improvement is seen in the J_{SC}s and FFs of the random terpolymer systems. In particular, the PTPTI-T70-based PSC induces the highest J_{SC} of 18.3 mA cm^{-2} and FF while maintaining high V_{OC} value, resulting in a surprising PCE of as high as 10.8%, which is comparable to those of the state-of-the-art PSCs based on polymers[42-43]. Note that both the J_{SC} and FF values of the random terpolymers show a gradual decrease as the 2T content increases in the backbone. As a result, the overall PCEs of the random terpolymers show a linear compositional dependence in the sequence of PTPTI-T70 (10.8%) > PTPTI-T50 (8.02%) > PTPTI-T30 (5.05%). **Figure 17b** presents the EQE of the devices, well-reflecting the spectral response spanning from 300 to 700 nm[44]. The terpolymer-based devices show much better EQE values over the whole wavelength region than that of the PTPTI-T100-based control device, and thus, the EQEs are in the order of PTPTI-T100 < PTPTI-T30 < PTPTI-T50 < PTPTI-T70, being essentially consistent with the J_{SC}s obtained from the J–V characteristics[44].

1.2.3. Film morphology and GIWAXS analysis

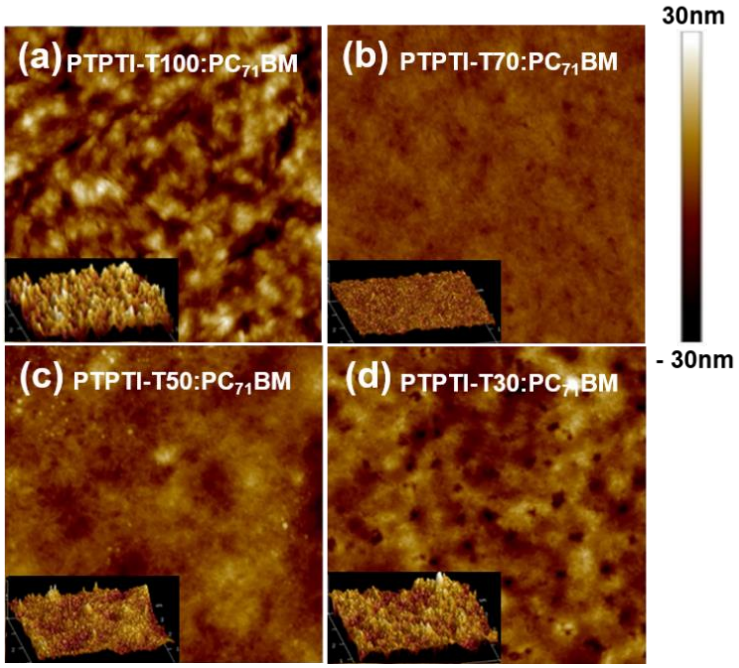

Figure 18. (a) Multi-mode AFM height images and 3D images (inset) of PTPTI-T100:$PC_{71}BM$ blend films for the optimal polymer solar cell fabrication; (b) AFM and 3D images of PTPTI-T70:$PC_{71}BM$; (c) AFM and 3D images of PTPTI-T50:$PC_{71}BM$; (d) AFM and 3D images of PTPTI-T30:$PC_{71}BM$, where the inner scale bar is 1 μm.

To understand the surface and bulk morphology of the active layer textures, we conduct atomic force microscopy (AFM) measurements. The blend films are prepared under the same conditions as the device fabrications. As shown in **Figure 18a-18d**, the PTPTI-T100:$PC_{71}BM$ film exhibits a distinctly aggregated surface with large irregular separated domains (root-mean-square (rms, R_q) roughness of 8.38 nm). On the other hand, all terpolymer-based blend films show smooth and uniform features with smaller surface roughness (R_q = 2.00 nm for PTPTI-T70, R_q = 4.54 nm for PTPTI-T50, and R_q = 6.12 nm for PTPTI-T30). The fine-dispersed nanoscale structures are known to result in more charge separation and transport[45]. Furthermore, relatively smaller surface roughness (smoother surface) can enable defect-free contact with the cathode layer, resulting in increasing FF values as well as photocurrent[46-47]. Thus, the trend in the R_q values correlates well with the observed trend in the PCEs above.

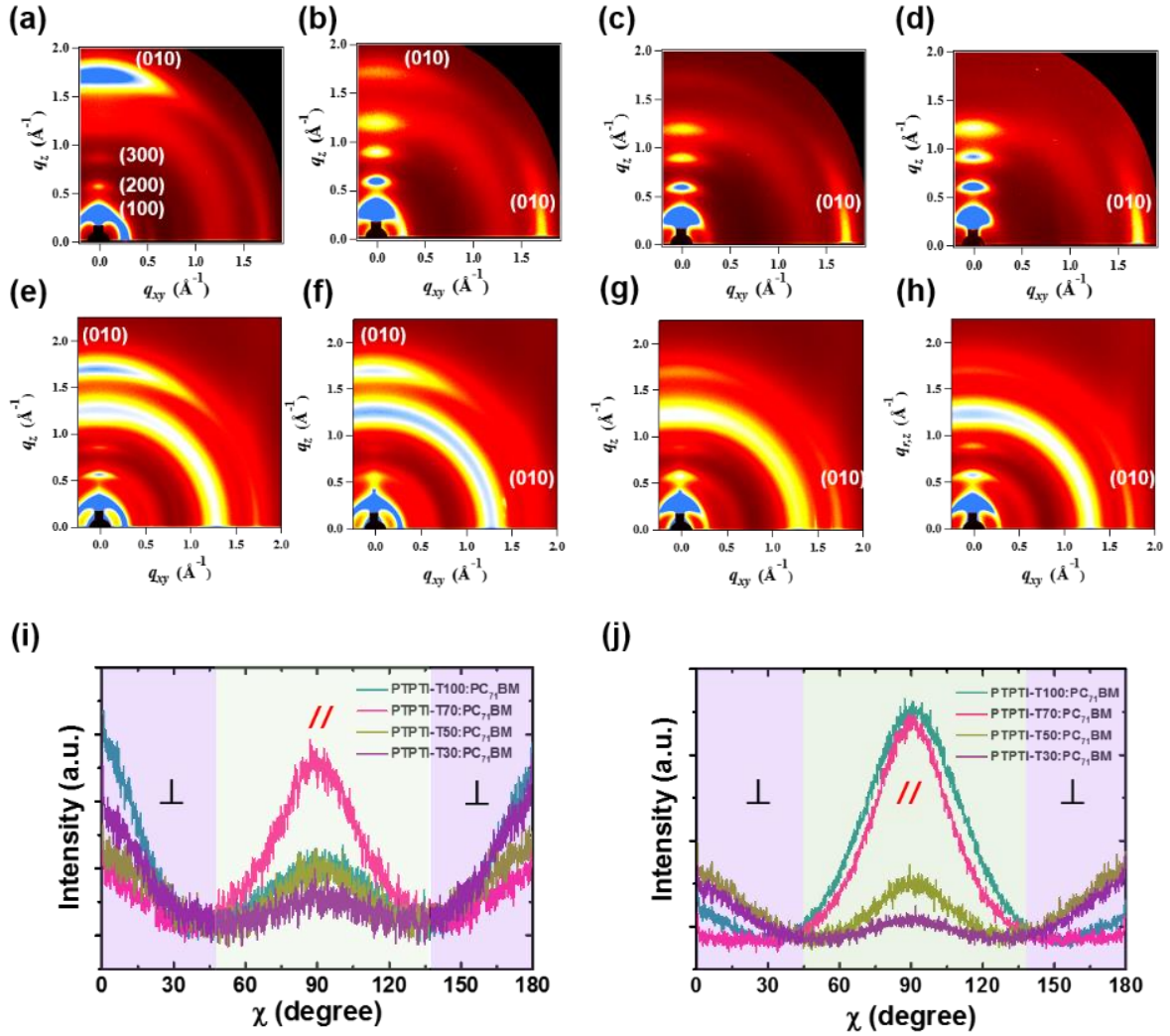

Figure 19. Crystalline orientation for TPTI-T-based polymer:$PC_{71}BM$ blend films. (a–h), 2D GIWAXD patterns of TPTI-T-based neat terpolymer films (a, b, c, and d: upper line) and blend films with $PC_{71}BM$ (e, f, g and h: lower line) depicted in the bulk region: (a and e for PTPTI-T100, b and f for PTPTI-T70, c and g for PTPTI-T50, and d and h for PTPTI-T30). i,j, Pole figures extracted from (010) diffraction in surface (i) and bulk (j) regions of the blend films on the SiO_2/Si substrates, indicating that // and ⊥ are parallel and perpendicular to the substrates, respectively (surface region: $\alpha_i = 0.11° <$ critical angle, bulk region: $\alpha_i = 0.12° >$ critical angle).

Grazing incidence wide-angle X-ray diffraction (GIWAXD) measurements with various incidence angles of the X-ray beam (α_i) are also employed [48-50]. **Figure 19a-19h** display the two-dimensional GIWAXD images of neat polymer films and their polymer:$PC_{71}BM$ blend films spun on SiO_2/Si substrates, where α_i is selected to be 0.12°, just above the critical angle of the film, to obtain maximum diffraction signal in the full film depth. The behavior of (010) π–π stacking diffraction peaks is

discussed in detail in the GIWAXD studies because charge transport in organic solar cells occurs via a π-conjugation system. The neat PTPTI-T100 film exhibits strong (010) π–π stacking peaks along the out-of-plane direction, whose intensity gradually fades away with increasing 2T content in the backbone, while affecting the intensity of the in-plane (010) π–π stacking peak, which implies a gradual shift of the parallel π–π stacking orientation to a perpendicular one[46, 51]. For their blend samples, although they show similar behavior, the shifts of the π–π stacking orientation are slightlyretarded in comparison to their neat counterparts, possibly because of the favorable interaction of $PC_{71}BM$ molecules with 2T units causing the perpendicular π–π stacking orientation[52]. For example, the π–π stacking peaks appear both along the in-plane and out-of-plane directions for the PTPTI-T70 neat film (**Figure 19b**), while still maintaining the parallel π–π stacking orientation for its blend film (**Figure 19f**). **Figure 19i and h** show the pole figures of (010) diffraction peaks for the surface and bulk regions, respectively, where the intensity of the azimuthal angle (χ) of 45–135° is attributed to the parallel (//) π–π stacking of the substrate and χ of 0–45° and 135–180° to the perpendicular (⊥) π–π stacking[53-54]. The PTPTI-Tx:$PC_{71}BM$ (x = 70, 50, and 30) blend films present quite similar χ dependences both in the surface and bulk regions, while the PTPTI-T100:$PC_{71}BM$ blend film shows much lower parallel π–π stacking intensity in the surface region than in the bulk region. These results clearly suggest that, although the portions of the parallel π–π stacking component vary in PTPTI-Tx:$PC_{71}BM$ (x = 70, 50, and 30) blend films, they comprise a well-organized 3D texture of parallel and perpendicular π–π stacking (*i.e.*, a bimodal orientation distribution) within the whole film depth [55].

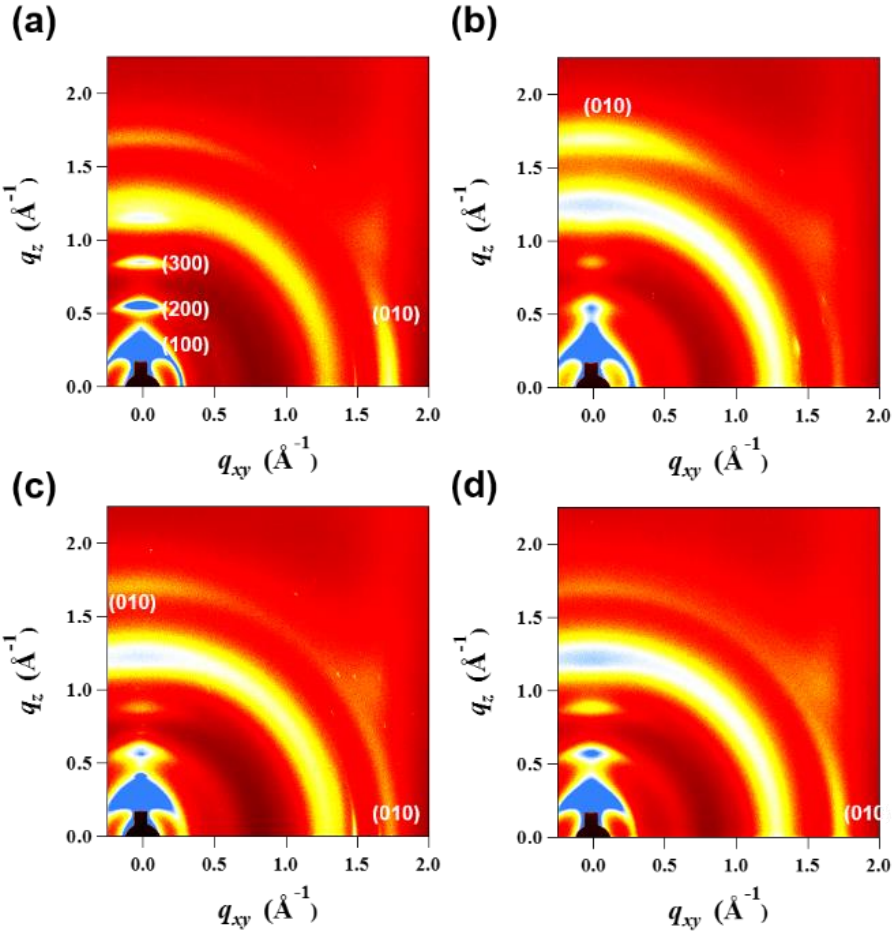

Figure 20. 2D-GIWAXD images of the polymer:$PC_{71}BM$ blend films measured below the critical angle of films ($\alpha_i = 0.11° < \alpha_c$). (a) PTPTI-T100:$PC_{71}BM$, (b) PTPTI-T70:$PC_{71}BM$, (c) PTPTI-T50:$PC_{71}BM$, and (d) PTPTI-T30:$PC_{71}BM$ blend films, respectively.

I further assess the surface packing orientation within ca. 15 nm depths of the blend films by evaluating GIWAXD at α_i of 0.11°, just below the critical angle [52, 55]. To a greater or lesser degree, all blend films show (010) π–π stacking peaks both along the in-plane and out-of-plane directions (**Figure 20**). Distinctively, the PTPTI-T100:$PC_{71}BM$ blend film shows a stronger π–π stacking peak along the in-plane rather than the out-of-plane direction, while the other blend films show quite similar orientations of π–π stacking peaks with respect to those of the neat polymers.

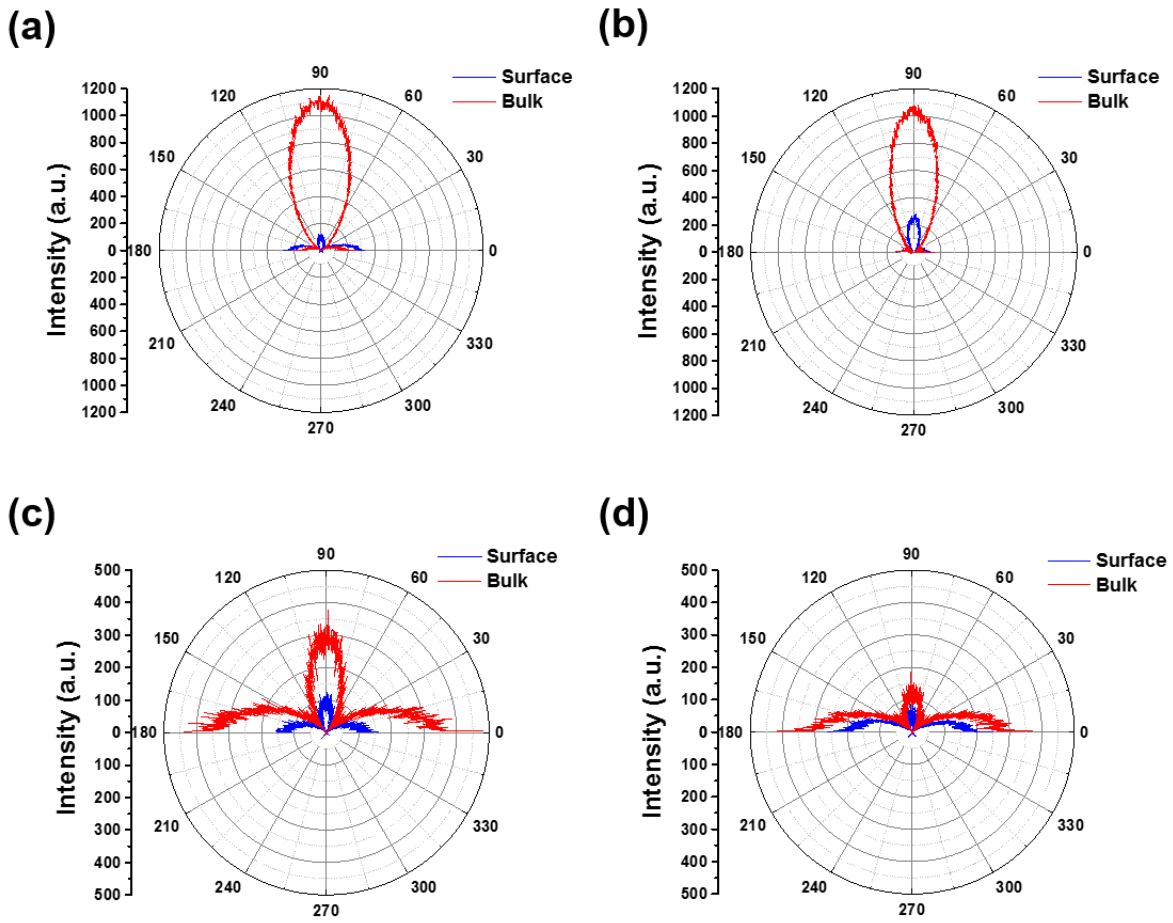

Figure 21. Pole figures of azimuthal-cuts along the (010) π-π stacking peaks in the polymer:$PC_{71}BM$ blend films both in surface (α_i = 0.11° < critical angle) and bulk (α_i = 0.12° > critical angle) region of the films. a, PTPTI-T100:$PC_{71}BM$ b, PTPTI-T70:$PC_{71}BM$ c, PTPTI-T50:$PC_{71}BM$, and d, PTPTI-T30:$PC_{71}BM$ blend films, respectively. The stronger intensity appeared at 90° (and 0° and 180°) in the pole figures represents orientation of (010) π-π stacking is mainly parallel (and perpendicular) to the substrate.

After the appropriate background subtractions, the deconvoluted intensities are plotted against azimuthal angle (χ) in **Figure 21**, where the intensity appearing at 90° in the pole figures represents the parallel orientation of (010) π–π stacking, while those at 0° and 180° represent the perpendicular orientation. Notably, the best-performing PTPTI-T70:$PC_{71}BM$ blend film again exhibits the highest population of parallel π–π stacking crystallites in both the surface and bulk regions [56]. This is the main reason why the PTPTI-T70:$PC_{71}BM$ system outperforms other cases since it is well known that such a parallel orientation of π–π stacking within the whole film depth is more favorable for photovoltaic devices because of its vertical charge transportation channel.

1.2.4. Charge carrier dynamics-generation, collection, and recombination

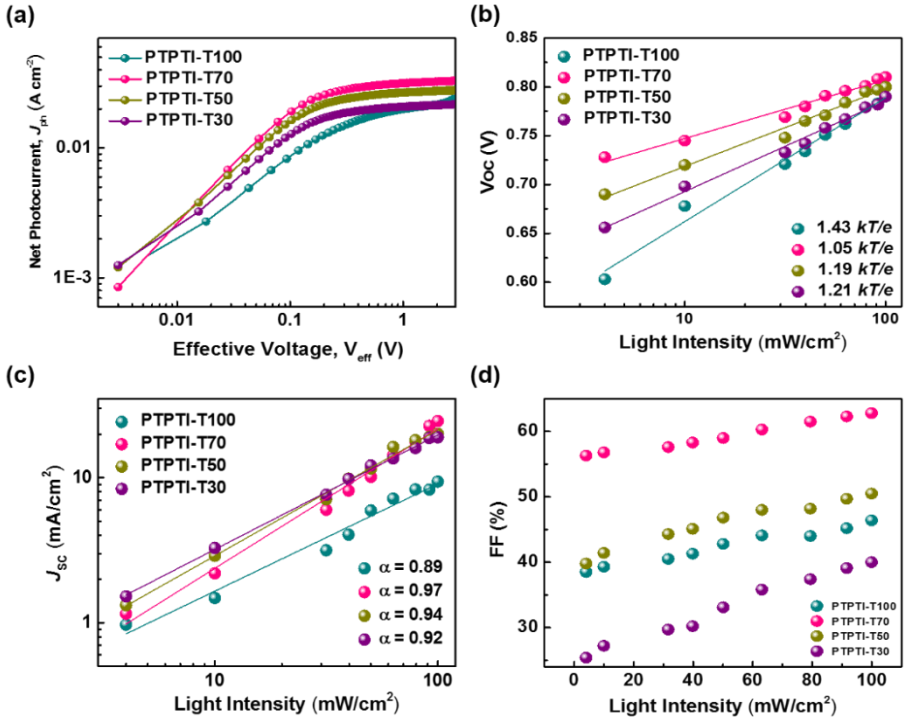

Figure 22. Charge-carrier dynamic characterizations of TPTI-T-based polymer:$PC_{71}BM$ solar cells. Net photocurrent density of TPTI-T-based polymer solar cells as a function of effective voltage (a), V_{OC} (b), and J_{SC} (c) versus the natural logarithm of light intensity for the devices, and FF (d) of the photovoltaic devices are shown for various light intensities of 4–100 mW cm^{-2}.

The J_{ph} under the internal field is reflected by $J_{ph} - V_{eff}$ (J_{ph} is defined as $J_L - J_D$, where J_L and J_D are the current densities under illumination and in the dark, respectively, and V_{eff} is defined as $V_0 - V$; we thoroughly investigate the charge carrier dynamics such as generation, collection, and recombination by measuring the photogenerated current (J_{ph}) versus V, where V_0 is the voltage at which J_{ph} is zero) [57]. As shown in **Figure 22a**, in addition to its linear dependence at low V_{eff}, J_{ph} reaches full saturation (J_{sat}) at a sufficiently high V_{eff} of over 1 V, which suggests that all photogenerated excitons are sufficiently dissociated into free carriers and collected by the electrodes [58]. However, the calculated charge dissociation probabilities *P(E,T)* are in the order of PTPTI-T100 (54%) < PTPTI-T30 (69%) < PTPTI-T50 (74%) < PTPTI-T70 (86%), which is essentially consistent with the aforementioned EQE trend in the same order. Therefore, one can conclude that the most effective charge dissociation and collection occur at the interface of the PTPTI-T70:$PC_{71}BM$ device, which is a key factor for achieving the PCE close to 11%. Considering that *P(E,T)* is strongly related to geminate recombination kinetics at the blend films, we first examine the dependence of V_{OC} on light intensity (4–100 mW cm^{-2}). The V_{OC} of the devices is given by $V_{OC} \propto nkT/qln(P_{light})$, where n is a constant, k is Boltzmann's constant, T is

temperature in Kelvin, q is the elementary charge, and P_{light} is the incident light intensity [59]. As shown in **Figure 22b**, the slopes for the PTPTI-T100, PTPTI-T70, PTPTI-T50, and PTPTI-T30 devices are 1.43 kT/q, 1.05 kT/q, 1.19 kT/q, and 1.21 kT/q, respectively. This suggests that PTPTI-T70:$PC_{71}BM$ has the least geminate recombination rate among the four blend systems [6, 59]. Besides, the relevant results are demonstrated in J_{SC} and FF as a function of light intensity in **Figure 22c and d**. By following the relation $J_{SC} \propto P_{light}^{\gamma}$ (power law), the γ values show the same trends as that observed in the light-intensity-dependent J_{SC} characteristics [60]; thus, the PTPTI-T70:$PC_{71}BM$ device exhibits the highest value ($\gamma = 0.97$), close to unity. This implies that PTPTI-T70:$PC_{71}BM$ has the weakest charge carrier losses for non-geminate recombination under the short-circuit condition. Additionally, as shown in the light-intensity-dependent FF characteristics (**Figure 22d**), the FF values in each device gradually decrease with decreasing light intensity, which is attributed to two main factors: series resistance and non-geminate recombination [61]. The declining tendency in FF is again in the sequence of PTPTI-T100 < PTPTI-T30 < PTPTI-T50 < PTPTI-T70, which is one of the reasons for the observed highest FF in PTPTI-T70:$PC_{71}BM$.

1.3. Experimental Section

The monomers TPTI-Br_2 (80 mg, 0.0859 mmol), T, and 2T were mixed in 12 mL of anhydrous toluene. After degassing under argon for 10 min, $Pd_2(dba)_3$ (2.359 mg, 2.57 μmol) and P(*o*-tolyl)$_3$ (3.13 mg, 10.28 μmol) were added as the catalyst and ligand. The reaction mixture was stirred at 100 °C for 3 days under argon. Then, 2-(tributylstannyl)thiophene and 2-bromothiophene were added to end-cap the polymer chain. The reaction mixture was cooled to room temperature and precipitated into methanol. The precipitate was purified by Soxhlet extraction in the sequences of methanol, acetone, hexane, and chloroform. The chloroform fraction was re-precipitated using methanol and dried. Finally, PTPTI-T series terpolymers were obtained as a dark purple solid.

PTPTI-T100: Isolated yield = 82.3% (60.3 mg). GPC (TCB, 120 °C, against PS standard) M_n = 95.3 kDa, M_w = 143.5 kDa, and PDI = 1.50; ^{1}H NMR (400 MHz, $CDCl_3$, δ): 8.6-7.71(br, Ar–H), 6.84-6.00 (br, Ar–H), 5.25-4.5 (br, N–CH_2), 1.56-1.00 (m, br, –CH, –CH_3), 0.97-0.4 (m, br, –CH_3). Anal. calcd for $C_{52}H_{72}N_2O_2S_3$: C 73.19, H 8.50, N 3.28, O 3.75 S 11.27; found: C 73.17, H 8.29, N 3.01, S 11.10.

PTPTI-T70: Isolated yield = 95.9 % (72.3 mg). GPC (TCB, 120 °C, against PS standard) M_n = 118.3 kDa, M_w = 175.0 kDa, and PDI = 1.48; ^{1}H NMR (400 MHz, $CDCl_3$, δ): 8.6-7.71(br, Ar–H), 6.84-6.00 (br, Ar–H), 5.25-4.5 (br, N–CH_2), 1.56-1.00 (m, br, –CH, –CH_3), 0.97-0.4 (m, br, –CH_3). Anal. calcd for $[(C_{52}H_{72}N_2O_2S_3)_{0.7} + (C_{56}H_{74}N_2O_2S_4)_{0.3}]$: C 72.80, H 8.34, N 3.19, S 12.00; found: C 72.12, H 8.30, N 2.68, S 11.50.

PTPTI-T50: Isolated yield = 90.6 % (69.7 mg). GPC (TCB, 120 °C, against PS standard) M_n = 85.3 kDa, M_w = 121.1 kDa, and PDI = 1.42; ^{1}H NMR (400 MHz, $CDCl_3$, δ): 8.6-7.71(br, Ar–H), 6.84-6.00 (br, Ar–H), 5.25-4.5 (br, N–CH_2), 1.56-1.00 (m, br, –CH, –CH_3), 0.97-0.4 (m, br, –CH_3). Anal. calcd for $[(C_{52}H_{72}N_2O_2S_3)_{0.5} + (C_{56}H_{74}N_2O_2S_4)_{0.5}]$: C 72.54, H 8.23, N 3.13, S 12.49; found: C 72.03, H 8.24, N 2.66, S 12.34.

PTPTI-T30: Isolated yield = 81 % (63.4 mg). GPC (TCB, 120 °C, against PS standard) M_n = 84.1 kDa, M_w = 172.2 kDa, and PDI = 2.04; ^{1}H NMR ($CDCl_3$, 400 MHz): δ (ppm) 8.6-7.71(br, Ar–H), 6.84-6.00 (br, Ar–H), 5.25-4.5 (br, N–CH_2), 1.56-1.00 (m, br, –CH, –CH_3), 0.97-0.4 (m, br, –CH_3). Anal. calcd for $[(C_{52}H_{72}N_2O_2S_3)_{0.3} + (C_{56}H_{74}N_2O_2S_4)_{0.7}]$: C 72.28, H 8.12, N 3.07, S 12.97; found: C 71.88, H 7.85, N 2.60, S 12.88.

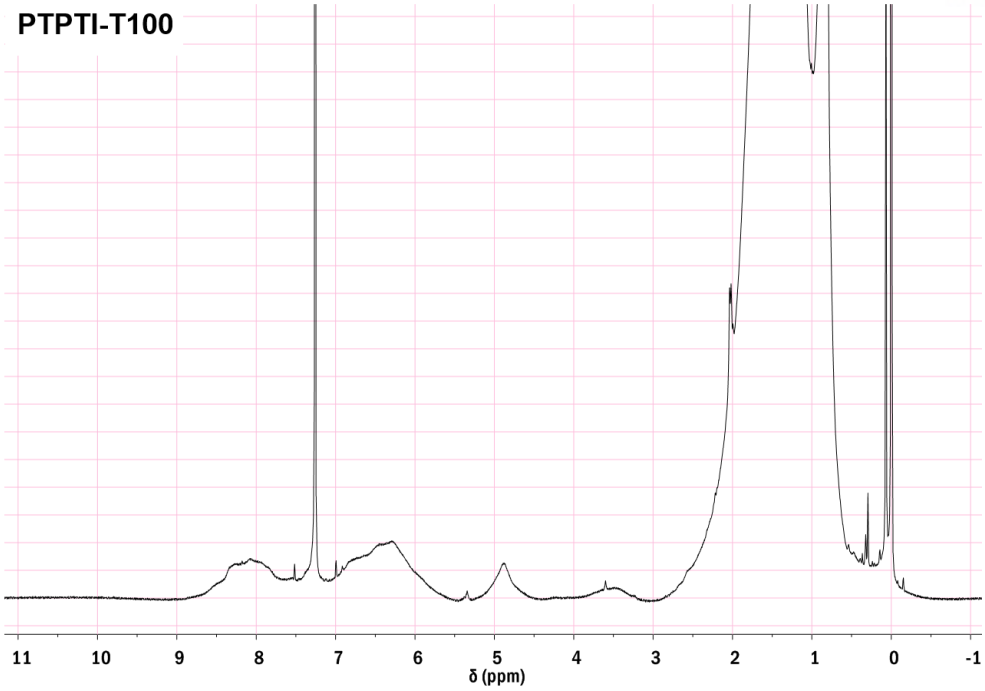

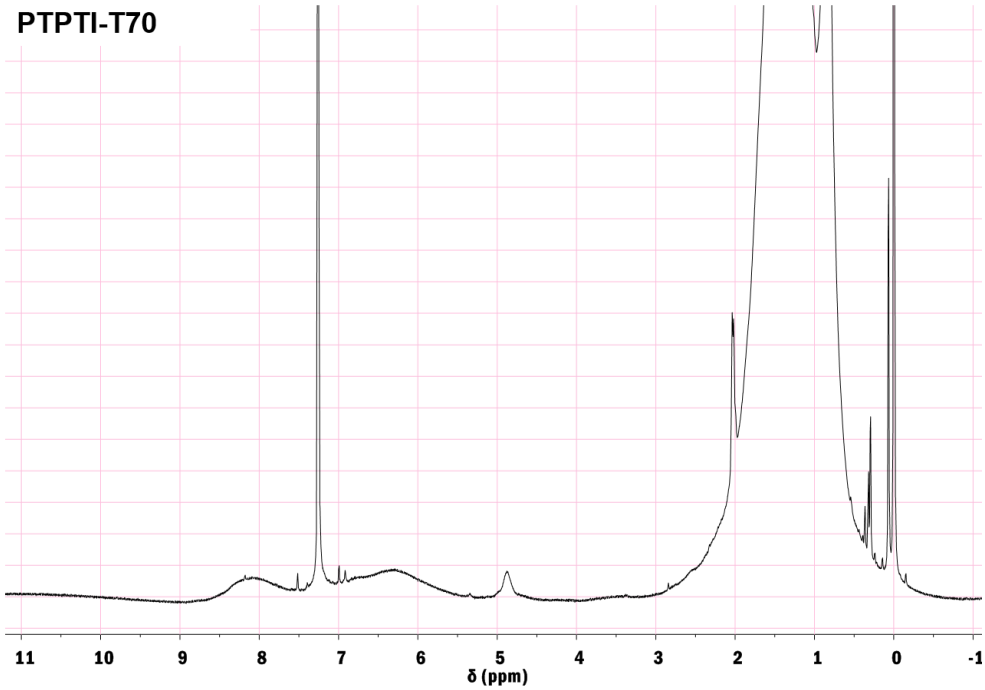

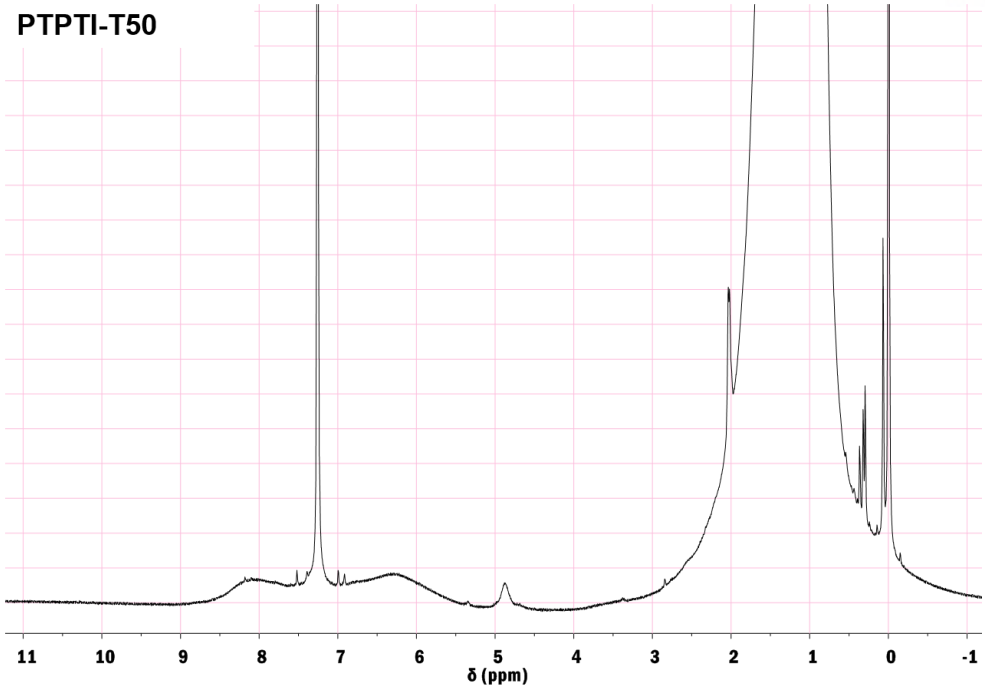

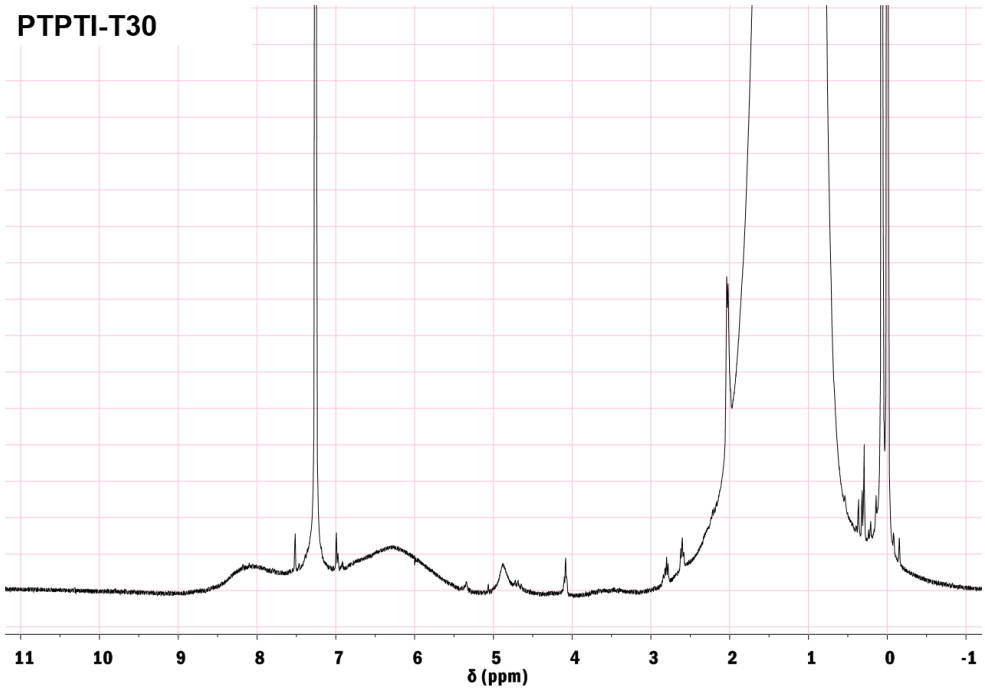

Figure 23. ^{1}H-NMR spectra of four TPTI-T based polymers in $CDCl_3$. The broad peaks in the range of 1.56-1.00 are assigned to methylene protons (-CH_2-R, methylene) of the hexyldecyl side chain groups.

1.4. Conclusion

In **Chapter 1**, we demonstrated using new TPTI-containing random terpolymers with high PCE close to 11% in the single-juction PSCs. Introducing 2T into the TPTI-T backbone entity was found to play a critical role in the morphology and charge transport characteristics, and charge carrier dynamics without significantly influencing the frontier molecular orbital energy levels and the light harvesting properties of the polymers. As a result, all random terpolymer-based PSCs yielded superior J_{SC}s and FFs compared to the alternating polymer-based reference device. In particular, a high J_{SC} of 18.3 mA cm^{-2} and FF of 71.2% were achieved in the PTPTI-T70:PC$_{71}$BM system. This is due to the multiple beneficial effects (promoting fine-morphological feature, achieving a more balanced μ_h/μ_e ratio, and reducing recombination probability) via a pronounced parallel π–π stacking alignment in the substrate at both the surface and whole film depth.

Chapter 2. A study of TPTI-based Random Terpolymerization in Non-fullerene Polymer Solar Cells

2.1. Introduction

Development of non-fullerene polymer solar cells (NF-PSCs) comprising *p*-type conjugated polymer donors and *n*-type non-fullerene acceptors in the active layer is an emerging photovoltaic technology that can be used to overcome the existing shortcomings of conventional fullerene-based PSCs, such as weak absorption in the visible spectral region and limited energy-level variability.[3, 6, 15, 62-68] The recent development of fused-aromatic-ring-based acceptors (e.g., ITIC and *m*-ITIC) has enabled significant breakthroughs in terms of improving the power conversion efficiency (PCE) of NF-PSCs, yielding values higher than 10%, which is considered as a milestone in the NF-PSCs.[17, 69-77] The development of state-of-the-art donor polymers mainly relies on the concept of the alternating donor–acceptor (D–A) design and application of precise control over the regularity of the polymer backbone.[68, 78-83] In the past few years, extensive studies have investigated a variety of D–A alternating donor polymers optimized for application in fullerene-based PSCs as well as the relations between their structure, morphology, and device performance.[33, 45, 51, 81, 84-86] However, only a few polymeric materials (e.g., D–A alternating copolymers based on benzodithiophene, difluorobenzotriazole, and alkoxycarbonyl-bithiophene units) have been successfully applied to achieve a high PCE in NF-PSCs.[71-72, 75-76] Considering that ITIC-based acceptors exhibit strong absorption in the spectral region from 600 to 780 nm, donor polymers that simultaneously possess complementary absorption and compatibility with ITIC-based acceptors can be the appropriate choice.[15, 87] Recently, a random terpolymerization approach, in which three different monomer species unite together to polymerize, was introduced to achieve synergetic effects of their inherent properties, such as optical absorption ability, charge mobility, and morphological compatibility with fullerene-based acceptors.[1, 20-21, 25, 28-29, 88-96] However, the irregularity in the backbone of the polymers fabricated via random polymerization can cause an adverse effect on molecular packing and charge transport by creating energetic and structural disorders. Therefore, preparation of highly efficient random polymer-based NF-PSCs is an interesting but very challenging issue.[31-32, 92, 97]

Here, I chose thieno[2',3':5',6']pyrido[3,4-*g*]thieno[3,2-*c*]isoquinoline-5,11(4*H*,10*H*)-dione-based random polymers (PTPTI-Tx) with various thiophene (T) and bithiophene (2T) ratios in the polymer backbone (**Figure 21a**) and performed systematic study of their optoelectronic properties and structural analysis; moreover, the characterization of NF-PSCs based on PTPTI-Tx as a donor and that of *m*-ITIC as an acceptor were performed.

2.2. Results and discussion

2.2.1. Synthesis and Characterization

The chemical structures of PTPTI-Tx polymers (**Figure 24a**) with various molar ratios of T and 2T (T:2T) of 100:0, 70:30, 50:50, and 30:70 are denoted as PTPTI-T100, PTPTI-T70, PTPTI-T50, and PTPTI-T30, respectively. All selected PTPTI-Tx donor polymers showed a complementary absorption ($\lambda_{max} \approx 620$ nm) well-matched with that of the *m*-ITIC acceptor ($\lambda_{max} \approx 700$ nm).[76] Therefore, the PTPTI-Tx:*m*-ITIC blend films cover a broad spectral range, from 300 to 800 nm (**Figure 24b**), which is a desirable feature for enhanced light harvesting and ultimate increase in photocurrent generation in NF-PSCs. Although the cyclic-voltammetry-derived values of the energy level offsets (ΔHOMO) between the PTPTI-Tx donor polymers and *m*-ITIC acceptor are 0.04–0.16 eV (**Figure 24c**), an efficient exciton dissociation is still exhibited at the heterojunction interface, as described in the following section, implying a relatively low photon energy loss (E_{loss}) in this system.[69, 98-101]

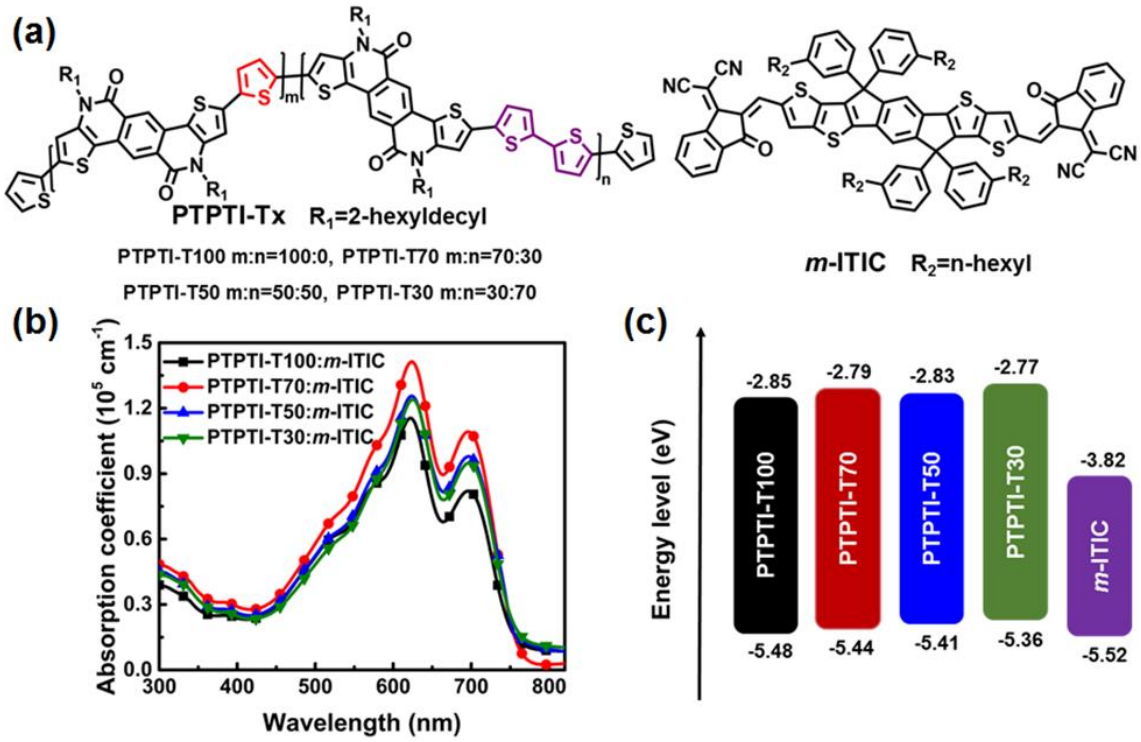

Figure 24. (a) Chemical structures of PTPTI-Tx donor polymers and *m*-ITIC acceptor. (b) Optical absorption spectra of PTPTI-Tx:*m*-ITIC blend films. (c) Energy level diagram of PTPTI-Tx and *m*-ITIC.

2.2.2. Photovoltaic performance

The evaluation of the photovoltaic properties of the PTPTI-Tx donor polymers was performed using NF-PSCs with a traditional device structure of ITO (indium tin oxide)/poly(3,4-ethylenedioxythiophene):poly(styrenesulfonate) (PEDOT:PSS)/active layer/perylenediimide functionalized with amino N-oxide (PDINO)[102]/Al. The active layers with a thickness of ~95 ± 10 nm were fabricated via spin-coating using chlorobenzene (CB)/chloroform (CF)/1,8-diiodooctane (DIO) (1/2/0.5 vol%) solutions with a donor/acceptor (D/A) weight ratio of 1/1.25 and subsequent thermal annealing at 150 °C for 10 min. As can be seen from the current density–voltage (*J*–*V*) curves (**Figure 25a**), corresponding external quantum efficiencies (EQEs) (**Figure 25b**), and relevant photovoltaic parameters (**Table 3**), when PTPTI-T100 is combined with *m*-ITIC, a PCE value of 9.10% is obtained along with a J_{SC} of 13.90 mAcm^{-2}, an open-circuit voltage (V_{OC}) of 0.957 V, and a fill factor (*FF*) of 68.34%. Favorably, the PTPTI-T70:*m*-ITIC-based device exhibited an impressive PCE of 11.02% along with significantly enhanced J_{SC} of 17.12 mAcm^{-2} and *FF* of 69.26%, and a slightly lower V_{OC} of 0.929 V. With further increase in the 2T moiety fraction in the main backbone, a decrease in the photovoltaic performance was observed (PCEs of 8.95% and 8.13% for PTPTI-T50 and PTPTI-T30, respectively). This remarkable difference in the PCEs can be mainly attributed to the change in the J_{SC} values. The higher absorption coefficient observed in the PTPTI-T70:*m*-ITIC blend (**Figure 25b**) is one of the factors responsible for the highest J_{SC} of the device. The variation in the V_{OC} values agreed with the trend of the HOMO levels of the corresponding PTPTI-Tx polymers. Moreover, the calculated E_{loss} values in the devices, defined as $E_{loss} = E_g^{opt} - eV_{OC}$, where E_g^{opt} is the lowest optical bandgap among the donor and acceptor components,[98] were in the range of 0.62–0.67 eV, which are lower than those of the majority of fullerene-based PSCs (0.7–1.0 eV), close to the empirically low threshold of 0.6 eV.[103-105] A low E_{loss} contributed to the high values of V_{OC} and J_{SC} simultaneously in PTPTI-Tx:*m*-ITIC-based NF-PSCs, which is one of the main factors for the observed performance enhancement.

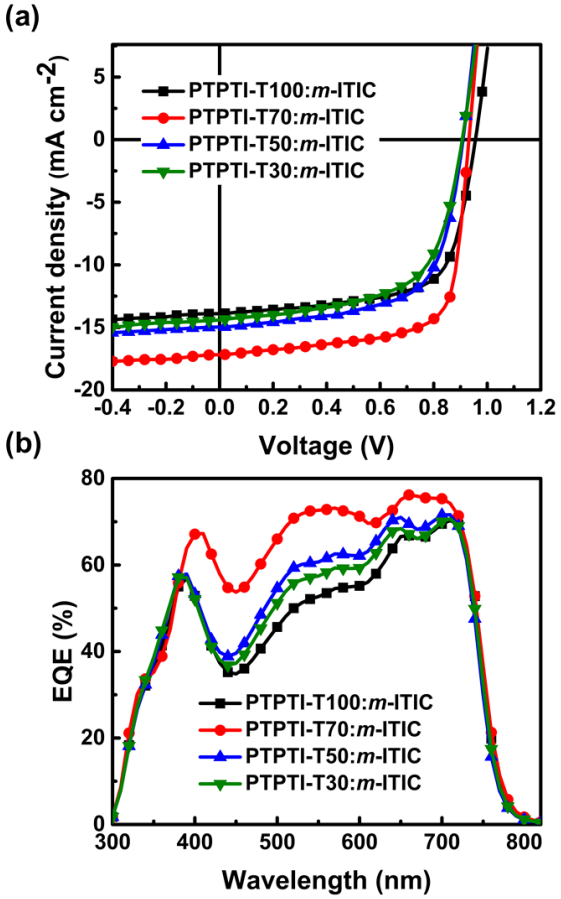

Figure 25. (a) *J-V* curves of PTPTI-Tx:*m*-ITIC (1/1.25 w/w) solar cells under 100 mW cm^{-2} AM 1.5G solar illumination. (b) Corresponding EQE spectra.

The EQE curves of the blend films (**Figure 25b**) demonstrate broad and high photoresponse covering the spectral region from 300 to 800 nm, which is in agreement with their absorption spectra. This confirms that absorptions of both the PTPTI-Tx donor polymers and *m*-ITIC acceptor in the blends efficiently contribute to light harvesting and photocurrent generation. The calculated J_{SC} values obtained from the integral EQE curves are in good correlation with those from *J-V* measurement (within 5% mismatch). It is clear that the PTPTI-T70:*m*-ITIC blend has the highest photoresponse efficiency, with a maximum EQE value approaching 76% in the spectral range of 650–750 nm. These findings corroborate with the occurrence of the efficient hole-transfer process from the *m*-ITIC acceptor to PTPTI-Tx donor despite the small ΔHOMO between PTPTI-Tx polymers and *m*-ITIC.

Table 3. Photovoltaic parameters of the PTPTI-Tx:*m*-ITIC (1:1.25, w/w) solar cells under the illumination of AM1.5G, 100mW cm^{-2}.

Devices	V_{OC} [a] (V)	J_{SC} [a] (mA cm^{-2})	FF [a] (%)	PCE [a] (%)	Calculated J_{SC} [b] (mA cm^{-2})	μ_h $10^{-4}cm^2v^{-1}s^{-1}$	μ_e $10^{-4}cm^2v^{-1}s^{-1}$
PTPTI-T100:*m*-ITIC	0.957 0.954±0.004	13.90 13.84±0.13	68.34 67.67±1.06	9.10 8.97±0.09	13.21	5.79	2.66
PTPTI-T70:*m*-ITIC	0.929 0.928±0.006	17.12 16.90±0.21	69.26 68.23±1.08	11.02 10.86±0.12	16.34	7.15	5.02
PTPTI-T50:*m*-ITIC	0.911 0.914±0.007	14.97 14.72±0.23	65.66 65.06±1.10	8.95 8.79±0.13	14.23	4.39	1.71
PTPTI-T30:*m*-ITIC	0.908 0.903±0.005	14.40 14.38±0.30	62.14 63.00±1.14	8.13 7.99±0.15	13.76	4.02	1.06

[a] The average values are obtained from 15 devices with standard deviation. [b] The short-circuit current densities are integrated from the EQE spectra.

2.2.3. Thin Film Mophology Analysis

To understand the correlation between the structure and performance difference of NF-PSCs, grazing incidence wide-angle X-ray scattering (GIWAXS) measurements were first performed on the neat films. Upon blending the PTPTI-Tx polymers with *m*-ITIC, the (100) lamellar diffraction appeared along both the out-of-plane and in-plane axes, implying the coexistence of the edge-on and face-on crystallites in the blend films (**Figure 26**).

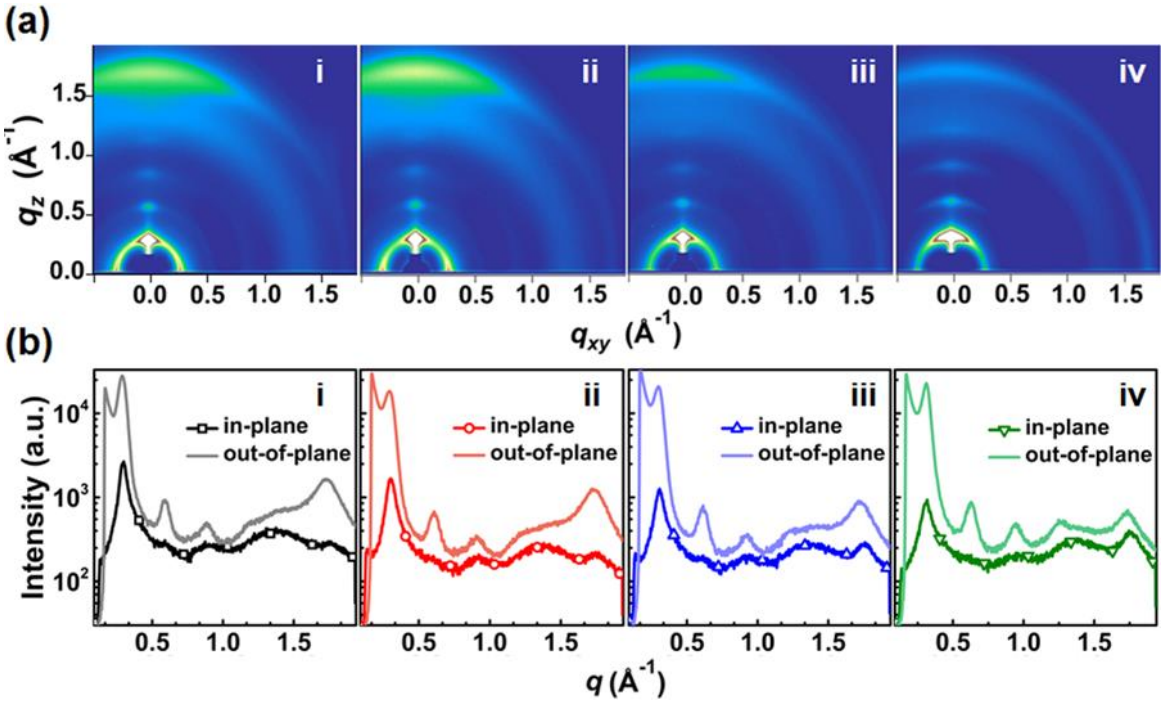

Figure 26. (a) GIWAXS images of the PTPTI-Tx:*m*-ITIC blend films: (i) PTPTI-T100:*m*-ITIC, (ii) PTPTI-T70:*m*-ITIC, (iii) PTPTI-T50:*m*-ITIC, (iv) PTPTI-T30:*m*-ITIC. (b) Corresponding in-plane and out-of-plane line cuts of the GIWAXS images of PTPTI-Tx:*m*-ITIC blend films.

The relative change in the orientation distribution of crystallites in the blend films was quantified by pole figure extraction from the (100) diffraction (**Figure 27**).[54, 106-107] The integrated intensities within the azimuthal angle (χ) are defined as fractions of face-on and edge-on crystallites, respectively. A spatially averaged value of the A_{xy} to A_z ratio (A_{xy}/A_z) was used to assess the ratio of face-on to edge-on crystallites. The A_{xy}/A_z values of PTPTI-T100, PTPTI-T70, PTPTI-T50, and PTPTI-T30 blend films were found to be 0.41, 0.54, 0.30, and 0.17, respectively, indicating a relatively larger population of the face-on crystallites in the best-performing PTPTI-T70:*m*-ITIC system. It can be observed that the variation in the A_{xy}/A_z values has the same trend as that in the J_{SC} and PCE values obtained from PTPTI-Tx-based NF-PSCs. The obtained findings agree with an actual consensus on the well-developed conjecture, that the face-on orientation geometry is more favorable for photovoltaic applications owing to the existence of vertical charge-transportation channels.[54, 108].

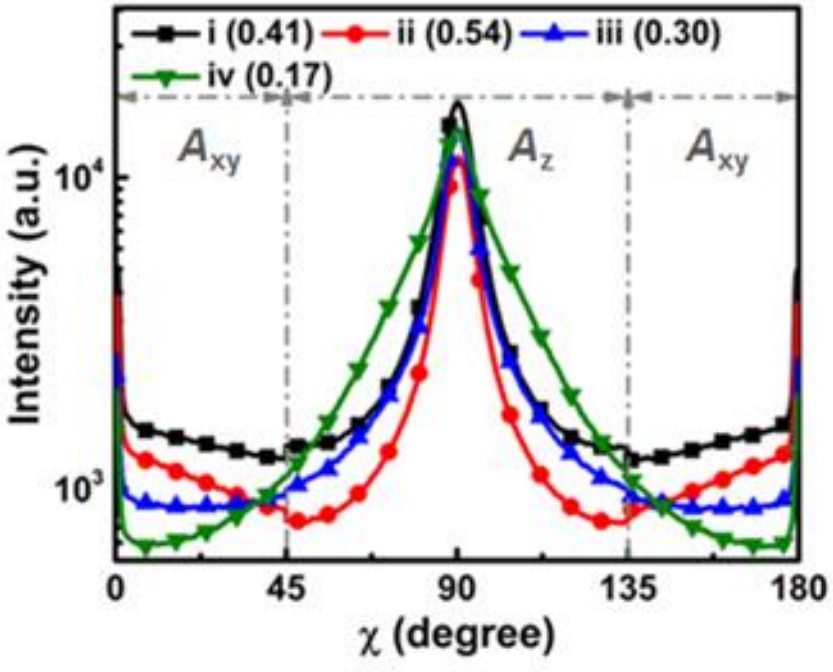

Figure 27. Pole figure plots from the (100) lamellar diffraction in the PTPTI-Tx:*m*-ITIC blend films: (i) PTPTI-T100:*m*-ITIC, (ii) PTPTI-T70:*m*-ITIC, (iii) PTPTI-T50:*m*-ITIC, (iv) PTPTI-T30:*m*-ITIC, the fraction values in parentheses are the ratios of integrated 0–45° and 135–180° (A_{xy}) to 45–135° (A_z) area.

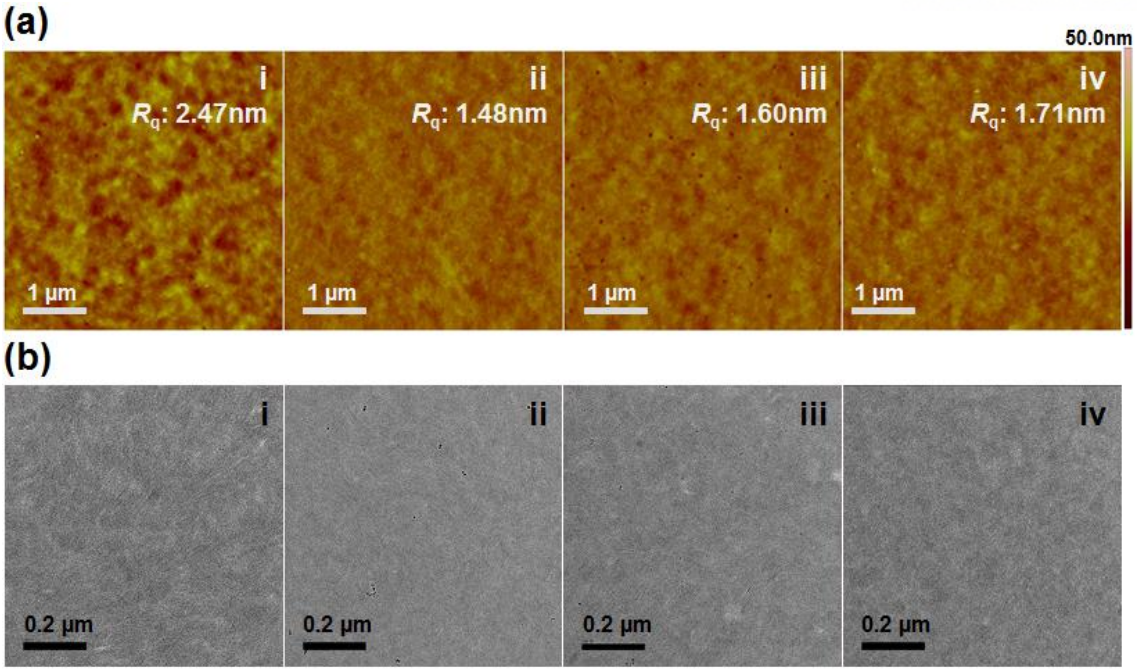

Figure 28. (a) AFM height images and (b) TEM images of the PTPTI-Tx:*m*-ITIC blend films: (i) PTPTI-T100:*m*-ITIC, (ii) PTPTI-T70:*m*-ITIC, (iii) PTPTI-T50:*m*-ITIC, (iv) PTPTI-T30:*m*-ITIC.

The top surface and bulk morphology of the blend films were further investigated via atomic force spectroscopy (AFM) and transmission electron microscopy (TEM), respectively. A relatively smooth surface (**Figure 28a**) with a low root-mean-square (R_q) value of 1.48 nm was observed in PTPTI-T70:*m*-ITIC, which implies that the miscibility between the donor and acceptor components improved within the blend. Furthermore, the donor–acceptor domains are just partially visible in the TEM images of all the blends (**Figure 28b**), and the distribution is more uniform in the PTPTI-T70:*m*-ITIC blend. It should be noted that the small-scale phase separation and well-distributed microstructure in PTPTI-T70:*m*-ITIC can promote effective exciton dissociation,[107] which is certainly important for the observed superior device performance.

2.2.4. Charge Generation, Separation and Transport Properties

The charge recombination process in the devices was evaluated by analyzing the *J–V* characteristics depending on the light intensity (*P*) (**Figures 29a and 29b**); J_{SC} and *P* are quantitatively scaled by a power-law functional relationship, $J_{SC} \propto P^{\alpha}$, where exponent α is close to unity when the bimolecular recombination is negligible.[109] The determined values of α were 0.988, 0.990, 0.958, and 0.957 for PTPTI-T100:*m*-ITIC, PTPTI-T70:*m*-ITIC, PTPTI-T50:*m*-ITIC, and PTPTI-T30:*m*-ITIC, respectively, indicating the relatively reduced bimolecular recombination in both PTPTI-T100:*m*-ITIC and PTPTI-T70:*m*-ITIC devices and accounting for their high *FF* values.

Additionally, the geminate or Shockley–Read–Hall recombination loss can be determined from the dependence of V_{OC} on *P*. The slope of V_{OC} versus the natural logarithm of the light intensity plot gives kT/q, where *k* is the Boltzmann's constant, *T* is the temperature in K, and *q* is the elementary charge.[60] The magnitude of the slope represents the degree of geminate recombination during the charge transport. The slopes for PTPTI-T100:*m*-ITIC, PTPTI-T70:*m*-ITIC, PTPTI-T50:*m*-ITIC, and PTPTI-T30:*m*-ITIC (**Figure 29b**) were determined to be $1.623kT/q$, $1.186kT/q$, $1.374kT/q$, and $1.490kT/q$, respectively, indicating that the geminate recombination loss was the least in the PTPTI-T70:*m*-ITIC device. This can be useful for explaining the higher J_{SC} value of the PTPTI-T70:*m*-ITIC device due to the previously described beneficial microstructural intermixing. The values of J_{SC} and PCE show an increasing trend depending on the T content in the polymer backbone (**Figure 29c**).

Further studies on the basic operational mechanism were performed to obtain the plots of photocurrent density (J_{ph}) versus effective voltage (V_{eff}) in the investigated devices (**Figure 29d**).[110] Note that J_{ph} reaches the saturation value (J_{sat}) at high V_{eff} (over 1.0 V) for all cells; at which all the photogenerated excitons are dissociated into free charge carriers and collected at electrodes. The higher J_{sat} value of the PTPTI-T70:*m*-ITIC indicates the overall enhancement in exciton generation.[111] Under the short-circuit condition, the values of exciton dissociation probabilities, $P(E,T)$, defined as J_{ph}/J_{sat}, are 88.39%, 95.74%, 92.04%, 90.63% for TPTI-T100:*m*-ITIC, PTPTI-T70:*m*-ITIC, PTPTI-T50:*m*-ITIC, and PTPTI-T30:*m*-ITIC, respectively. These results imply that in the case of the PTPTI-T70:*m*-ITIC device, the reduced geminate recombination loss facilitates exciton dissociation at the donor/acceptor interface and is the main reason for the significantly increased J_{SC} value.[107, 112]

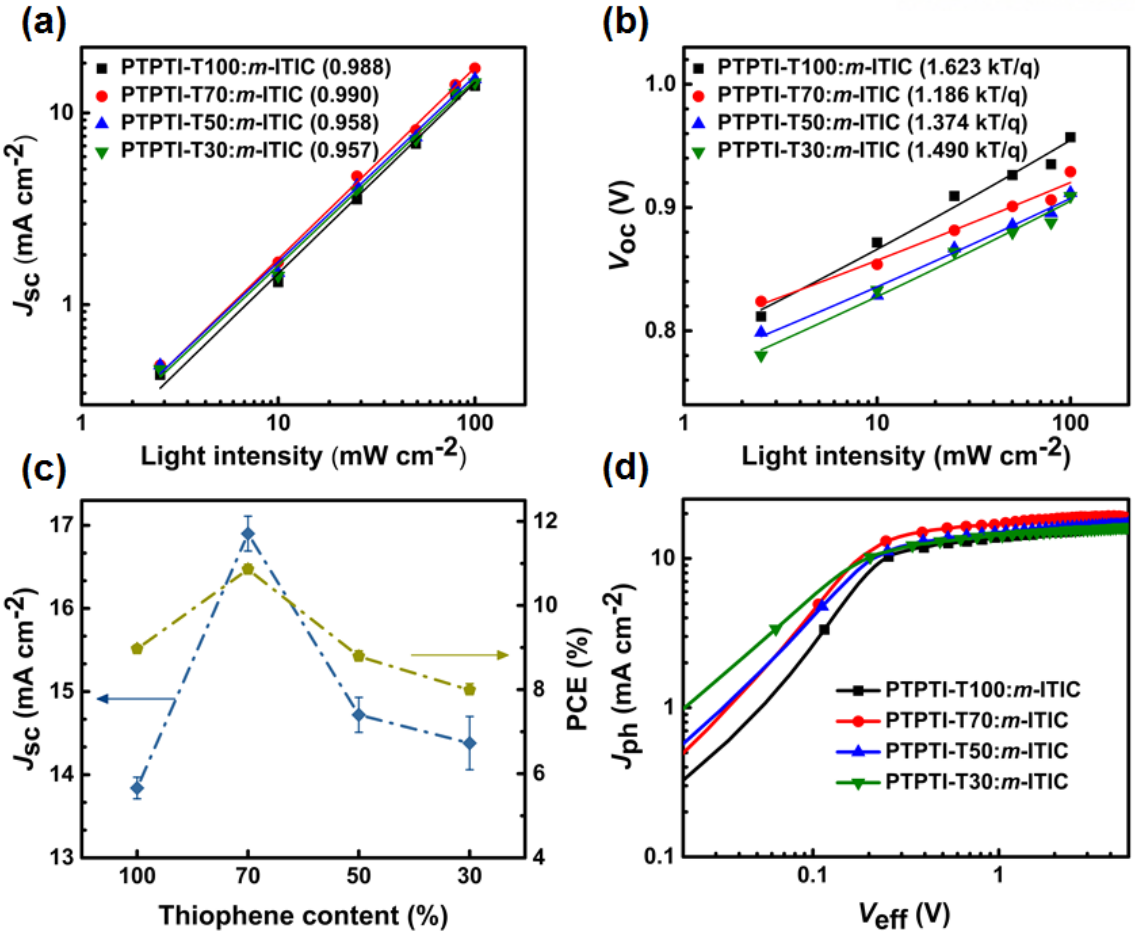

Figure 29. (a) Light intensity dependence of J_{SC} and (b) V_{OC} for the optimized PTPTI-Tx:*m*-ITIC devices. (c) J_{SC} and PCE values of the optimized PTPTI-Tx:*m*-ITIC solar cells versus the thiophene content in the donor polymer. (d) J_{ph} versus V_{eff} characterizes in the optimized devices.

2.3. Experimental Section

TPTI-Tx random terpolymers were synthesized with same method of chapter 1.

2.4. Conclusion

In **Chapter 2**, a successful approach was demonstrated in the single-junction NF-PSCs with a high PCE of 11.02% by utilizing the PTPTI-Tx random polymers containing two simple T and 2T units as donors and *m*-ITIC as an acceptor. Careful tailoring of the ratio of T and 2T units in the PTPTI-Tx backbone induced a remarkable change in the molecular orientation without causing any significant influence on the optical band gaps and energy levels. Precise control of the molecular orientation resulted in different morphological properties of the blend films in conjunction with *m*-ITIC. Furthermore, a small-scale phase separation with a high fraction of the face-on oriented crystallites was observed in the best-performing PTPTI-T70:*m*-ITIC device, thereby enabling efficient exciton dissociation and charge transport. This played a critical role in achieving a remarkably enhanced J_{SC} of 17.12 $mAcm^{-2}$ through this system.

Chapter 3. A Study on Tuning Molecular Weight and Alkyl Substituents of TIIG-Np-based polymers for OFETs

3.1. Introduction

π-Conjugated polymer-based organic field-effect transistors (OFETs) have received significant attention from both the academic and industrial communities, owing to their solution processability, tunability in structural modification, potential for large area device fabrication of low-cost, flexible and large-area electronic applications.[113-118] Benefiting from new molecular designs and device fabrication improvements, OFETs have made considerable progress in the past decade, resulting in excellent carrier mobility approaching or surpassing that of amorphous silicon (1 cm^2 V^{-1} s^{-1}).[119-122] In the design of semiconducting polymers, significant effort is focused on molecular packing and organization via the polymer backbones engineering, promoting the crystalline structures that in turn can facilitate the good charge carrier transport.[123-129] Therefore, the correlation between the backbone structures and OFET performances has been well established.[116-117, 130-135]

On the other hand, some recent studies have begun to observe that the molecular weight and the alkyl substituent of a given polymer platform have a profound influence on molecular ordering and microstructure, and additionally on optoelectronic and charge transport characteristics, thus making it one of the key parameters governing the device performance.[107, 127, 136-138] For example, it was found that not only increasing the molecular weight but also decreasing the size and the branching point away from backbones are linked to improved charge transport arising from better intergrain connectivity.[114, 139] However, to the best of our knowledge, the effects of molecular weight and alkyl substituent variations on polymer properties and device performances have been studied independently.[58, 127, 138, 140-141]

Here, I synthesized a series of poly(thienoisoindigo-*alt*-naphthalene) (PTIIG-Np)-based polymers with alkyl substituents of 2-hexyldecyl (HD), 2-octyldodecyl (OD), and 2-decyltetradecyl (DT), where the control of each polymer M_ns is accomplished by modulating stoichiometric balance between the two monomers and the polymerization time. I aimed to investigate how the molecular weight and alkyl substituent variations influence photophysical and electrochemical properties, film morphology, and charge carrier transport in PTIIG-Np-based OFETs.

3.2. Results and discussion

3.2.1. Synthesis and Characterization

Three branched alkyl amines (2-hexyldecyl-1-, 2-octyldodecyl-1-, and 2-decyltetradecyl-1- amines) were first prepared from Gabriel synthesis,[142-143] followed by Ullmann coupling with 3-bromothiophene to afford the corresponding alkyl-thiophen-3-amine compounds. The TIIG-based key monomers were synthesized according to the previous reported procedures in three laboratory steps (intramolecular Friedel-Crafts cyclization with oxalyl chloride, dimerization with Lawesson's reagent, and bromination with *N*-bromosuccinimide (NBS)).[52, 144-147] A series of TIIG-based polymers were synthesized via typical Pd-catalyzed Suzuki coupling ($Pd_2(dba)_3$/P(*o*-tol)$_3$)/K_3PO_4 system) using 2,6-bis(4,4,5,5-tetramethyl-1,3,2-dioxaborolan-2-yl)naphthalene co-monomer (**Scheme 1**). The general polymerization reaction was conducted in toluene at 90°C under inert atmosphere and the molecular weight controls can be achieved by varying the stoichiometric balance (r = A0/B0) between the two monomers and reaction time, where A0 and B0 are mole quantities of dibromide and diboronic ester monomers, respectively.

The samples with high molecular weights (H-PTIIGHD-Np, H- PTIIGOD-Np, and H- PTIIGDT-Np) were prepared using the exact stoichiometric balance (r = 1.00) and with sufficient reaction times to go to complete polymerization (over 5 days), while the stoichiometric imbalance (r = 0.77) with a 3-h reaction time gave the corresponding samples with low molecular weights (L-PTIIGHD-Np, L-PTIIGOD-Np, and L-PTIIGDT-Np), respectively.

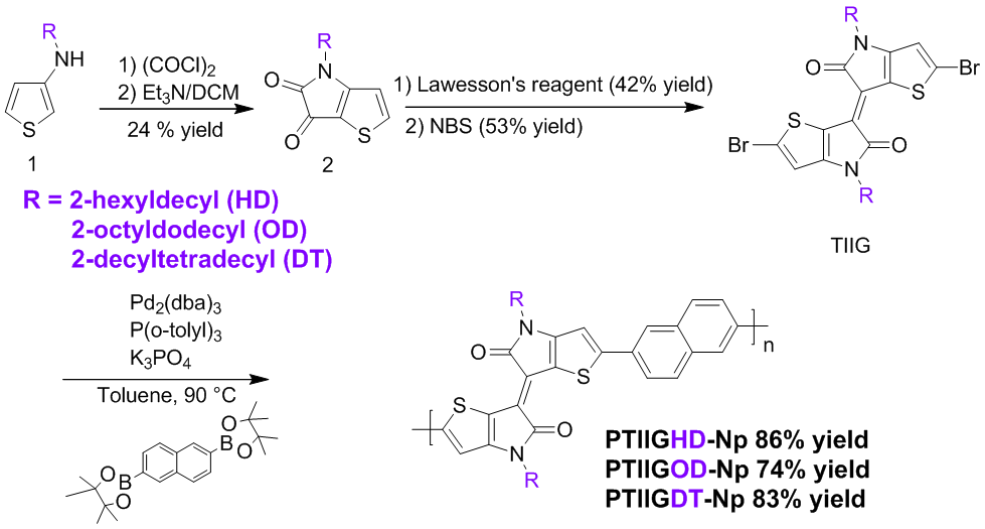

Scheme 1. Synthesis of PTIIG-Np polymers.

All the polymers were obtained as dark green solids. Their number-average molecular weight (M_n) and polydispersity index (PDI) values and the relevant data are summarized in **Table 4**.

Table 4. Optoelectrical and electrochemical properties of PTIIG-Np polymers.

copolymer	M_n [a] (kDa)	PDI	λ_{max}^{sol} (nm)	λ_{max}^{film} (nm)	ΔE_g^{opt} [b] (eV)	E_{HOMO} (eV)	E_{LUMO} (eV)	ΔE_g^{elec} [c] (eV)
L-PTIIGHD-Np	24.6	2.05	798	813	1.34	- 5.05	- 3.60	1.45
H-PTIIGHD-Np	61.3	2.11	813	819	1.34	- 5.01	- 3.60	1.41
L-PTIIGOD-Np	34.3	2.81	796	797	1.32	- 5.05	- 3.62	1.43
H-PTIIGOD-Np	63.8	3.19	799	810	1.34	- 5.06	- 3.61	1.45
L-PTIIGDT-Np	50.6	2.57	799	810	1.33	- 5.03	- 3.60	1.46
H-PTIIGDT-Np	108.7	3.79	808	819	1.32	- 5.05	- 3.61	1.44

[a]Estimated from the gel permeation chromatography (GPC) against polystyrene standard in tetrahydrofuran (THF) at 40°C; [b]Optical energy bandgap estimated from the absorption onset of the thin films. $\Delta Eg^{opt} = 1240/ \lambda_{onset}^{film}$; [c]$\Delta Eg^{elec}$ = LUMO-HOMO

3.2.2. Optical and Electrochemical Properties

The UV-Vis absorption spectra of the polymers are measured both in chloroform solution and as thin films. All the polymers displayed dual characteristic bands in the absorption spectra, wherein the absorption peak at ~425 nm can be ascribed to the π-π* transitions of the polymers backbone, while the absorption peak at ~810 nm can be attributed to the intramolecular charge transfer (ICT) effects from the donor to acceptor units.[58] The optical bandgaps (E_g^{opt}) of all the polymers, calculated from the film absorption onsets, are nearly identical within 1.32 – 1.34 eV.

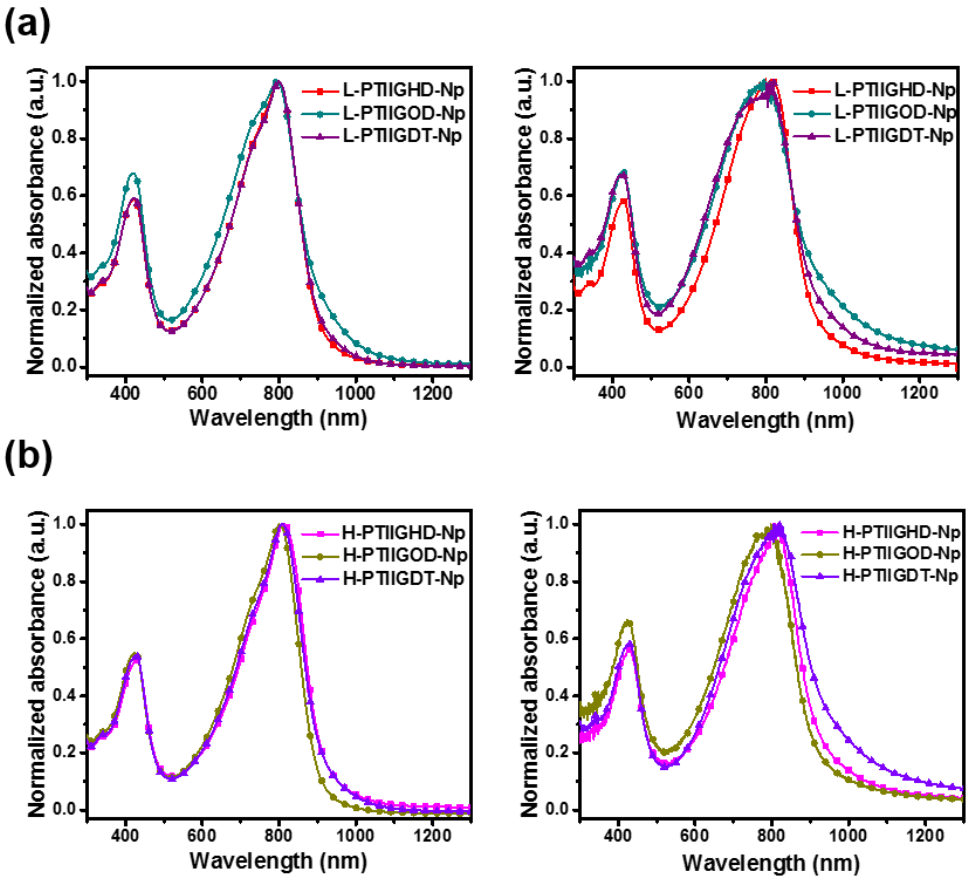

Figure 30. Normalized UV vis-absorption spectra of PTIIG-Np polymers with low (L-) molecular weight in $CHCl_3$ solution (left) and film (right) (a) and with high (H-) molecular weight in $CHCl_3$ solution (left) and film (right) (b).

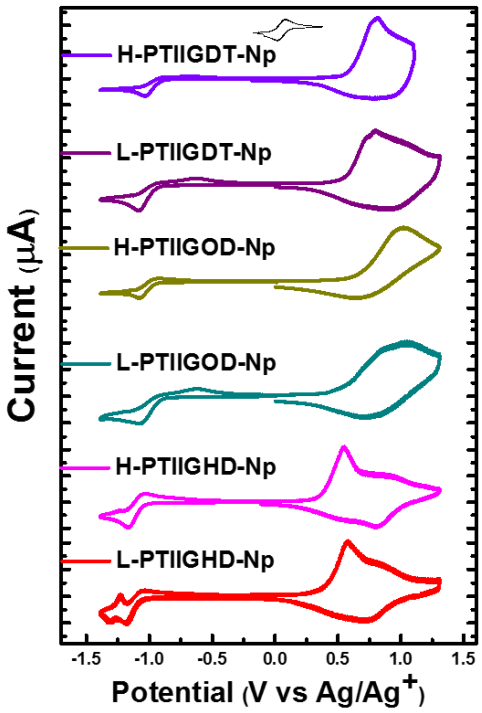

Figure 31. Cyclic voltamograms of PTIIG-Np polymers with different alkyl substituent (-HD, -OD, -DT) and low (L-) and high (H-) molecular weight.

The frontier molecular orbital energies (E_{HOMO} and E_{LUMO}) were determined using cyclic voltammetry (CV) in nitrogen atmosphere (**Figure 31**). The E_{HOMO} and E_{LUMO} values of all the polymers lie from -5.06 to -5.02 eV and from -3.62 to -3.60 eV, respectively, reflecting manipulation of the alkyl substituents and M_n of PTIIG-Np polymers has negligible effect on their energy levels.

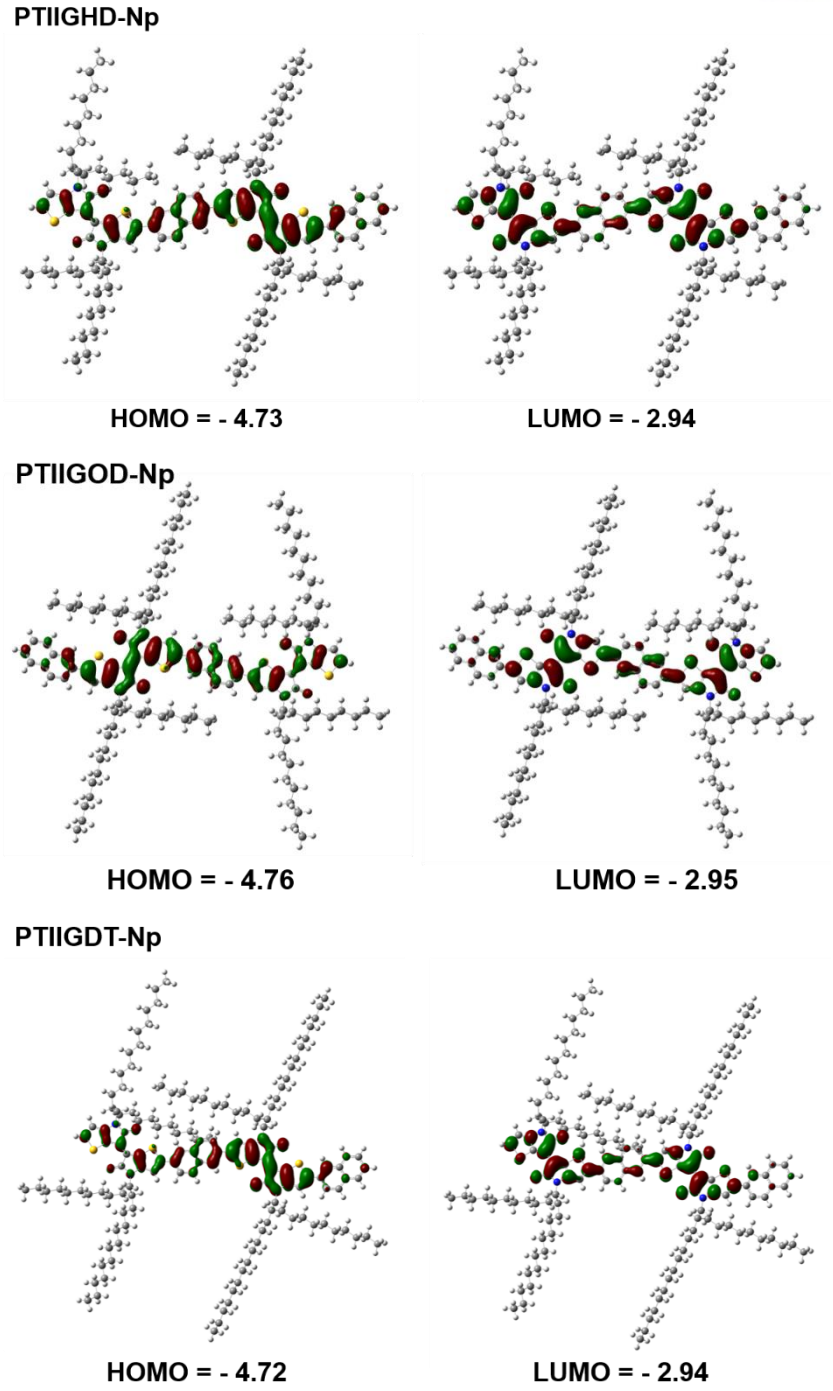

Figure 32. Optimized frontier molecular geometries, simulated HOMO (bottom) and LUMO (top) orbitals for the PTIIG-Np based dimers with different alkyl substituents (-HD, -OD, -DT), PTIIGHD-Np, PTIIGOD-Np, and PTIIGDT-Np, respectively.

In addition, to elucidate the HOMO and LUMO levels after optimizing the geometry of compound name using the same method, the computational calculation of the molecular geometries over the PTIIG-Np-based polymers with different alkyl substituents (-HD, -OD, -DT) were performed using the

Gaussian 09 package with the nonlocal hybrid Becke three-parameter Lee-Yang-Parr (B3LYP) function and the 6-31G* basis set (see **Figure 32**) For all cases, the HOMOs are mostly distributed along the polymer backbone, whereas the LUMOs are localized on the TIIG moiety. Besides, three models had an almost planar backbone structure with similar HOMO/LUMO values

3.2.3. Thin Film Mophology Analysis

To elucidate the effects of the alkyl substituents and M_ns on the film morphological structures (molecular packing/crystallinity) of the polymers, atomic force microscopy (AFM) and grazing incident X-ray diffraction (GIXD) were employed, where the polymer films were prepared under identical conditions by spin-coating from 1,2,4-trichlorobenzene and thermally annealed at 300 °C.[52] As shown in **Figure 33**, the AFM images of all the annealed films show fine interconnecting grains. The low-M_n batches (e.g., both PTIIGHD-Np and PTIIGDT-Np) exhibited a more defined fibril-like polymer microstructure than the corresponding high-M_n batch with a nodule-like feature, which is likely the result of the strong intermolecular π-π interactions, similar to other high performance OFET.[20, 148] In sharp contrast, such a fibrillar network is formed for H-PTIIGOD-Np rather than L-PTIIGOD-Np. Therefore, the observed behaviors of the polymer surface morphologies are well-correlated with that observed in the charge transport properties; that is, increasing M_ns triggered a rise in OFET mobility for PTIIGOD-Np, while adversely affecting that of PTIIGHD-Np and PTIIGDT-Np.

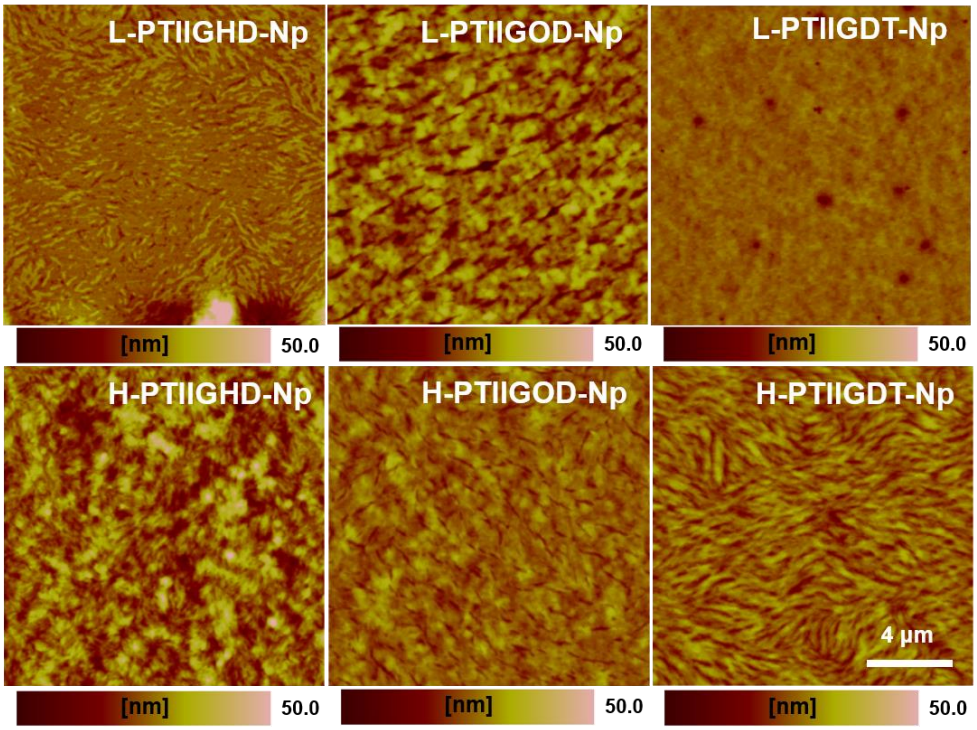

Figure 33. AFM height images of the PTIIG-Np polymers depending on the length of alkyl substituents (-HD, -OD, -DT) and low (L-) and high (H-) molecular weight, where inner scale bar is 4 μm.

As illustrated in **Figure 34**, all the polymer films appear to have dual textures of edge-on and face-on crystallites, as judged by the presence of the long-range ordered (h00) and strong π-π (010) stacking peaks in both out-of-plane (q_z axis) and in-plane (q_{xy} axis) orientations. Interestingly, the lamellar d-spacings (d_{100}) increase gradually with longer alkyl substitutes, namely PTIIGHD-Np (~21 Å) < PTIIGOD-Np (~24 Å) < PTIIGDT-Np (~27 Å), though they are almost insensitive to the variation of the M_ns (see **Figure 35a**). This indicates that the shorter HD chains are closely interdigitated with the other side chains in the adjacent layers. Note also that compared with the other samples, the PTIIGHD-Np film showed more-intense and more-distinct diffraction peaks, suggesting its better microstructural ordering.

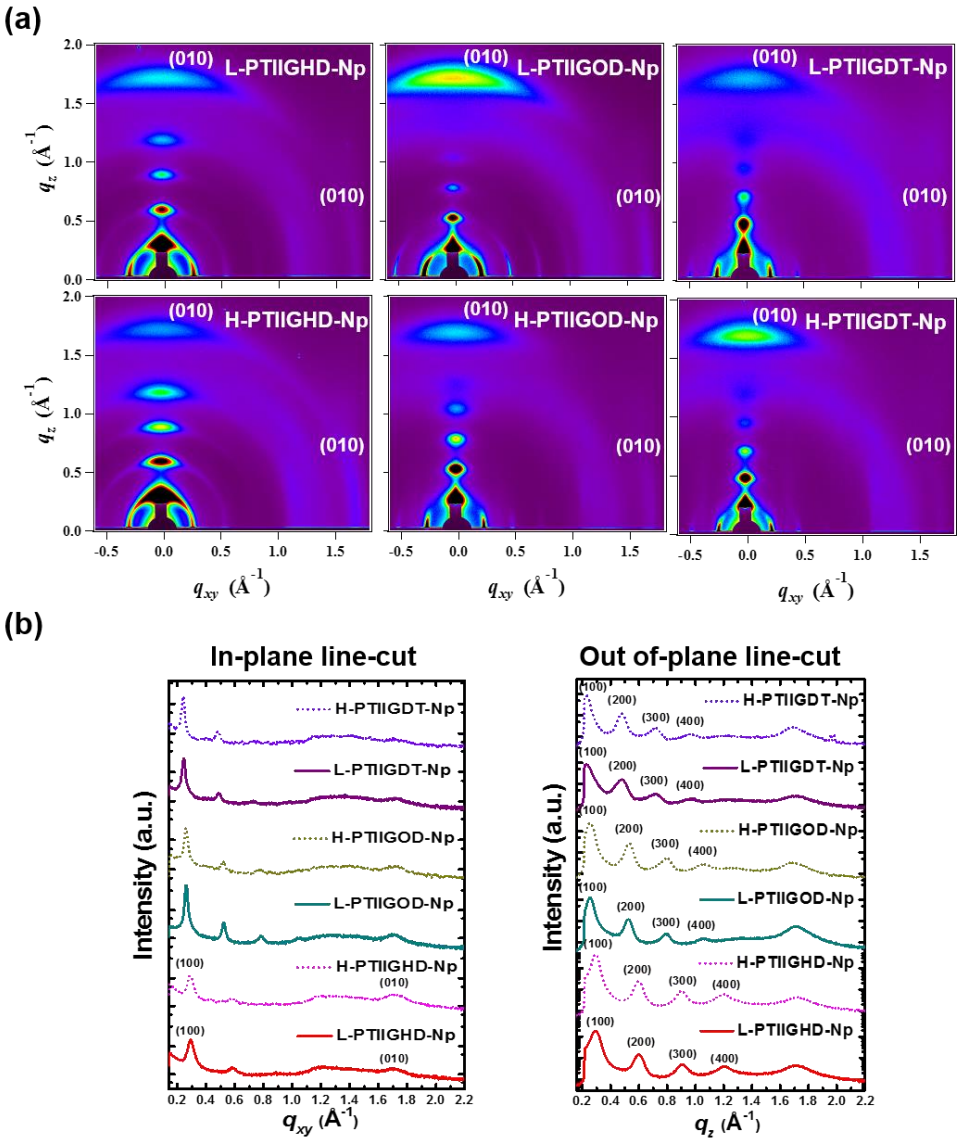

Figure 34. Grazing incidence X-ray diffraction (GIXD) patterns of pristine PTIIG-Np polymer thin films obtained with a 2D-image plates, where critical angle is 0.112° (a). In-plane (left) and out-of-plane line-cut profiles (right) of the pristine PTIIG-Np polymer thin films, each of which is characterized as low (L-) and high (H-) molecular weight (b).

I calculated the (010) crystal coherence length (CCL_{010}) along q_z using Debye Scherrer's equation,[106] where Gaussian fitting is used to obtain full widths at half-maximum (FWHM) values (**Figure 35a**). No systematic trends are found in the CCL_{010} values as a function of the alkyl substituents. Nevertheless, it is apparent that in both cases of PTIIGOD-Np and PTIIGDT-Np, the CCL_{010} values of the high-M_n samples are larger than those of the low-M_n samples, whereas for PTIIGHD-Np, the relatively increased CCL_{010} value is observed in the low-M_n case. This result suggests that the π-stacking crystallites size is more likely to be governed by M_n variations than by the changed alkyl substituents of the polymers.

The pole figures of the (100) reflection were also used to quantitatively compare the relative degree of bimodal orientation of the polymer films.[54, 56, 149] **Figure 35b** compares the intensities of azimuthal angle (χ) of 45–135° (A_z) and χ of 0–45° and 135–180° (A_{xy}), attributed to the edge-on crystallites and face-on crystallites, respectively. Thereby, the ratios of A_{xy} to A_z (A_{xy}/A_z) signify the relative face-on and edge-on crystallite populations. Although distinguishing trends with varying alkyl substituents were not observed, low-M_n batches have clearly higher ratio values than the corresponding high-M_ns cases; that is, the population of the face-on crystallites decreases with M_ns values.

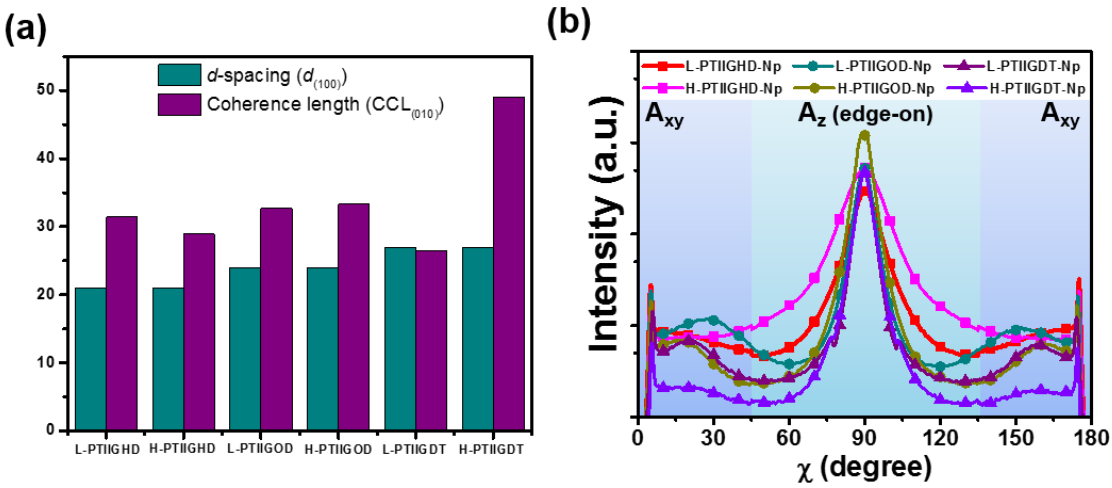

Figure 35. Values of *d*-spacing and coherence length of PTIIG-Np polymers depending on different alkyl substituents (-HD, -OD, -DT) and low (L-) and high (H-) molecular weight (a). Pole figures extracted from (100) diffraction of PTIIG-Np polymer thin films on the SiO_2/Si substrates, indicating that A_{xy} and A_z are region of face-on and edge-on crystallites, respectively (α_i = 0.12°, critical angle), where from the integrated intensity of the azimuthal angle (χ) of 45–135° (A_z) and χ of 0–45° and 135–180° (A_{xy}), attributed to the edge-on crystallites and face-on crystallites, respectively (b).

3.2.4. Field-effect Performance

Top gate and bottom-contact (TG-BC)-based OFET characteristics of the polymers as a channel semiconductor were investigated using a poly(methyl methacrylate) (PMMA) gate dielectric.[52] The enhanced mobility of the PTIIG-Np polymers upon thermal annealing was reported in our previous work, and therefore all the OFET devices were subsequently annealed at the optimized temperature of 300 °C.

Table 5. Summary of PTIIG-Np polymer OFET performances with different alkyl substituents and low (L-) or high (H-) molecular weights

copolymers	M_n (kDa)	μ_{hole} ($cm^2\ V^{-1}\ s^{-1}$) [a),b)]	V_T (V)	I_{on}/I_{off}	$\mu_{electron}$ ($cm^2\ V^{-1}\ s^{-1}$) [a),c)]	V_T (V)
L-PTIIGHD-Np	24.6	1.31 (1.87)	-55.3 ~ --64.2	160 ~ 411	1.61×10^{-2} (3.44×10^{-2})	68.9 ~ 73.7
H-PTIIGHD-Np	61.3	1.17 (1.64)	-59.2 ~ -65.0	588 ~ 1357	1.611×10^{-2} (1.89×10^{-2})	70.3 ~ 72.5
L-PTIIGOD-Np	34.3	6.35×10^{-2} (1.11×10^{-1})	-55.2 ~ -61.2	217 ~ 413	2.58×10^{-3} (4.02×10^{-3})	69.4 ~ 72.7
H-PTIIGOD-Np	63.8	3.46×10^{-1} (6.06×10^{-1})	-55.0 ~ -63.5	347 ~ 520	1.356×10^{-2} (1.49×10^{-2})	74.7 ~ 77.2
L-PTIIGDT-Np	50.6	1.54×10^{-1} (3.56×10^{-1})	-45.6 ~ -60.5	36 ~ 84	2.66×10^{-2} (4.78×10^{-2})	61.4 ~ 66.1
H-PTIIGDT-Np	108.7	7.48×10^{-2} (1.08×10^{-1})	-48.0 ~ -56.1	49 ~ 92	1.14×10^{-2} (1.63×10^{-2})	61.5 ~ 65.6

[a)] Average values of hole or electron mobilities are indicated with over ten devices, and maximum values are in parenthesis.[b)] Measured at V_{DS} = -100 V. [c)] Measured at V_{DS} = +100 V.

All OFET parameters (e.g., hole (μ_{hole}) and electron ($\mu_{electron}$) mobilities, threshold voltage (V_T), and on/off current ratio (I_{on}/I_{off}) of the annealed polymer films are summarized in **Table 5**. All the polymer films showed hole dominant p-channel characteristics with good drain-current modulation. Clearly, PTIIGHD-Np polymers exhibit higher μ_{hole} values over 1.0 $cm^2\ V^{-1}\ s^{-1}$ than those of other polymers. By increasing the M_ns of both PTIIGHD-Np and PTIIGDT-Np, the μ_{hole} values slightly decrease, while H-PTIIGOD-Np exhibits relatively higher mobility than L-PTIIGOD-Np. Ultimately, the highest μ_{hole} value is 1.87 $cm^2\ V^{-1}\ s^{-1}$, seen in the L-PTIIGHD OFET, which is about one order of magnitude higher than those of other samples.

3.3. Experimental Section

Synthesis of 4-(2-decyltetradecyl)-4H-thieno[3,2-b]pyrrole-5,6-dione (2): Isolated yield = 24 %. ^{1}H NMR (400 MHz, $CDCl_3$): δ (ppm) 7.98 (d, 1H, J = 0.015), 6.75 (d, 1H, J = 0.002), 3.55 (d, 2H, J = 0.019), 1.77 (m, 1H), 1.30−1.25 (m, 40H), 0.90−0.86 (m, 6H). ^{13}C NMR (100 MHz, $CDCl_3$): δ (ppm) 173.31, 165.85, 162.07, 144.05, 113.45, 111.38, 46.80, 37.32, 32.25, 32.23, 31.73, 30.24, 30.00, 29.97, 29.94, 29.88, 29.69, 29.66, 29.64, 26.70, 23.02, 14.44, 14.43. MALDI-TOF MS (m/z) calcd: 489.36. Found: 480.92 (MH^+).

Synthesis of (E)-4,4'-bis(2-decyltetradecyl)-[6,6'-bithieno[3,2-b]pyrrolylidene]-5,5'(4H,4'H)-dione: Compound 2 (1 equiv.) and Lawesson's reagent (0.5 equiv.) in *o*-xylene was put in the two-neck round flask and stirred at 60 °C for 2 h (color changed into violet blue). After cooling down to the room temperature, the solvent was concentrated by evaporation. The crude was purified by column chromatography on silica gel with hexane:dichloromethane to obtain the product. Isolated yield = 42 %. ^{1}H NMR (400 MHz, $CDCl_3$): δ (ppm) 7.51 (d, 2H, J = 0.012), 6.77 (d, 2H, J = 0.013), 3.68 (d, 4H, J = 0.019), 1.89 (m, 2H), 1.31−1.22 (m, 80H), 0.88−0.85 (m, 12H). ^{13}C NMR (100 MHz, $CDCl_3$): δ (ppm) 171.65, 151.88, 134.53, 121.40, 114.58, 111.67, 46.49, 37.49, 32.28, 32.26, 31.81, 30.30, 30.02, 30.00, 29.97, 29.91, 29.71, 29.68, 26.76, 23.04, 14.47. Elemental Analysis: Anal. Calcd for $C_{60}H_{102}N_2O_2S_2$: C, 76.05; H, 10.85; N, 2.96; S, 6.77 Found: C, 75.56; H, 10.87; N, 2.98; S, 6.69. MALDI-TOF MS (m/z) calcd: 946.74. Found: 946.70 (MH^+).

Synthesis of (E)-2,2'-Dibromo-4,4'-bis(2-decyltetradecyl)-[6,6'-bithieno[3,2-b]pyrrolylidene]-5,5'(4H,4'H)-dione: To a solution of TIIG in THF in a two-neck round flask with an ice bath, add *N*-bromosuccinimide (NBS) dropwise over 30 min. After TLC check, the reaction was quenched by addition of water. The crude was taken up in 200 ml of dichloromethane, washed three times with water and once with brine. After drying by $MgSO_4$, the crude was purified by column chromatography on silica gel with hexane:dichloromethane. Isolated yield = 53 %. ^{1}H NMR (400 MHz, $CDCl_3$): δ (ppm) 6.82 (s, 2H), 3.62 (d, 4H, J = 0.019), 1.83 (m, 2H), 1.28−1.24 (m, 80H), 0.89−0.86 (m, 12H). ^{13}C NMR (100 MHz, $CDCl_3$): δ (ppm) 170.66, 150.49, 123.41, 119.96, 115.28, 115.02, 46.51, 37.53, 32.28, 32.27, 31.74, 30.30, 30.04, 30.02, 30.01, 29.99, 29.91, 29.72, 29.69, 26.71, 23.04, 14.47. Elemental Analysis: Anal. Calcd for $C_{60}H_{100}Br_2N_2O_2S_2$: C, 65.19; H, 9.12; N, 2.53; S, 5.80 Found: C, 65.47; H, 9.33; N, 2.54; S, 5.78. MALDI-TOF MS (m/z) calcd: 1104.56. Found: 1122.06 (MH^+).

Typical synthesis procedure of PTIIG-Np by Suzuki polymerization: In a Schlenk flask, dibromide TIIG and diboronic ester naphthalene were dissolved in anhydrous toluene (5 mL), a solution of K_3PO_4, P(*o*-toyl)$_3$, and deionized water (3 mL) with Aliquat 336 was added. The mixture was vigorously stirred at room temperature under argon. After 30 min, $Pd_2(dba)_3$ was added to the reaction mixture. The crude product was poured into a mixture of methanol and ammonia (4:1 v/v, 250 mL). The resulting solid was filtered off and subjected to sequential Soxhlet extraction with methanol (1 d), acetone (1 d), and hexane

(1 d) to remove impurities of the materials. The residue was extracted with chloroform to produce a dark-green product after precipitating again from methanol and drying in *vacuo*.

For low-M_n polymer cases: The dibromide TIIG (79.4 mmol, 1.0 equiv.), diboronic ester naphathalene (103.29 mmol, 1.3 equiv.), $Pd_2(dba)_3$ (1.45 mg, 2 mol%), P(*o*-toyl)$_3$ (84. 3 mg, 8 mol %), and K_3PO_4 (84.3 mg, 5 equiv.) were placed in Schlenk flask, and kept at 90 °C for 3 hour-reaction time.

L-PTIIGHD-Np: Isolated yield = 72%. GPC analysis (THF as eluent); M_n = 24.6 kDa, M_w = 50.4 kDa and PDI = 2.05. ^{1}H NMR (400 MHz, $CDCl_3$): δ (ppm) 8.33-6.96 (br, 8H), 3.76-3.69 (br, 4H) 2.02-2.00 (br, 2H), 1.25-1.23 (br, 48H), 0.84 (br,12H).

L-PTIIGOD-Np: GPC analysis (THF as eluent); M_n = 34.3 kDa, M_w = 96.5 kDa and PDI = 2.81. ^{1}H NMR (400 MHz, $CDCl_3$): δ(ppm) 8.33-6.96 (br, 8H), 3.76-3.69 (br, 4H) 2.02-2.00 (br, 2H), 1.25-1.23 (br, 64H), 0.84 (br,12H).

L-PTIIGDT-Np-L: Isolated yield = 73 %. GPC analysis (THF as eluent); M_n = 50.6 kDa, M_w = 130.4 kDa and PDI = 2.57. ^{1}H NMR (400 MHz, $CDCl_3$): δ(ppm) 8.33-6.96 (br, 8H), 3.76-3.69 (br, 4H) 2.02-2.00 (br, 2H), 1.25-1.23 (br, 80H), 0.84 (br,12H). Elemental Analysis: Anal. Calcd: C, 78.45; H, 9.97; N, 2.61; O, 2.99; S, 5.98.

For high-M_n polymer cases: The dibromide TIIG (79.4 mmol, 1.0 equiv.), diboronic ester naphathalene (79.4 mmol, 1.0 equiv.), $Pd_2(dba)_3$ (1.45 mg, 2 mol%), P(*o*-toyl)$_3$ (84. 3 mg, 8 mol %), and K_3PO_4 (84.3 mg, 5 equiv.) were placed in Schlenk flask, and kept at 90 °C for 24 hour-reaction time.

H-IIGHD-Np: Isolated yield = 86 %. GPC analysis (THF as eluent); M_n = 61.3 kDa, M_w = 129.5 kDa and PDI = 2.11.

H-PTIIGOD-Np: Isolated yield = 68%. GPS analysis (THF as eluent); M_n = 63.8 kDa, M_w = 204.0 kDa and PDI = 3.19.

H-PTIIGDT-Np: Isolated yield = 83 %. GPC analysis (THF as eluent); M_n = 108.7 kDa, M_w = 412.0 kDa and PDI = 3.79.

3.4. Conclusion

In **Chapter 3**, we synthesized a series of PTIIG-Np-based polymers and simultaneously investigated the influence of their M_n and alkyl substituent variations on the photophysics, film morphology, and OFET performances. The optical properties, such as band shape and absorption shiftiness are clearly affected by varying M_ns and alkyl substituent chains of the polymers, whereas the frontier energy levels (E_{HOMO} and E_{LUMO}) remain almost unchanged. The lamellar *d*-spacings (d_{100}) of the polymers increased from PTIIGHD-Np to PTIIGOD-Np, and to PTIIGDT-Np with similar π-stacking distances (~3.7 Å), as the length of alkyl substituents increase. In addition, the CCL values of both PTIIGOD-Np to PTIIGDT-Np exhibited a clear increasing trend in high-M_n samples, except for PTIIGHD-Np where a relatively larger CCL value was observed in its low-M_n case. Consequently, L-PTIIGHD-Np formed a more compacted lamellar structure with large π-stacking crystallites, which led to the highest μ_{hole} of 1.87 $cm^2 V^{-1} s^{-1}$, outperforming the other polymer-based OFETs.

Chapter 4. A Study on PVDF based Graft Copolymers for Triboelectric Nanogenerators

4.1. Introduction

Dielectric materials, commonly referred to as electrical insulators, have received much attention owing to their strong electron bonding, good support of electric fields, and low energy loss.[150-154] Dielectrics have also been widely used in many applications such as transistors,[155-156] photovoltaic devices,[157-158] and electrical insulation.[159] Recently, triboelectric nanogenerator (TENG), which converts mechanical energy into electricity, has been suggested as a new energy harvesting technology. Since 2012, it has been proven as a cost effective, simple, and efficient technique for the realization of various self-powered systems, such as sensors,[160-161] charging systems,[162-163] etc. However, greater output performance is essential for the implementation of TENG in practical applications. Although various strategies to enhance the output performance have been reported, an effective dielectric for creating the device with high performance should be developed because the output power is critically and basically dependent on the density of the charges transferred.[164-165] So far, various dielectric materials such as polydimethylsiloxane (PDMS),[166] poly(methyl methacrylate) (PMMA),[167] polyimide (PI),[168] polyvinylidene fluoride (PVDF),[169]and polytetrafluoroethylene (PTFE)[170] have been used without any modifications and the electrical signals were not enough.[171-172] PVDF, a dielectric polymer with a good piezoelectric/pyroelectric response and low acoustic impedance, has been considered as one of the most widely studied dielectric materials in mechanical energy harvesting technologies. In particular, it can be formed in a variety of nanostructures such as nanowire, nanofibers, nanotubes, etc., and can be flexible, therefore, the use of PVDF has been successfully demonstrated in a number of devices, such as capacitors and sensors, as well as TENG.[173-175]

Here, I designed and synthesize PVDF graft copolymers to incorporate poly(tert-butyl acrylate) (PtBA) through an atom transfer radical polymerization (ATRP) technique, as an efficient dielectric to enhance the output performance of the TENGs. The TENG fabricated with the graft copolymer generated the output voltage and current density of 64.4 V and 18.9 μA/cm^2, twice the enhancement in both, compared to pristine PVDF based TENG.

4.2. Results and discussion

4.2.1. Synthesis and characterization

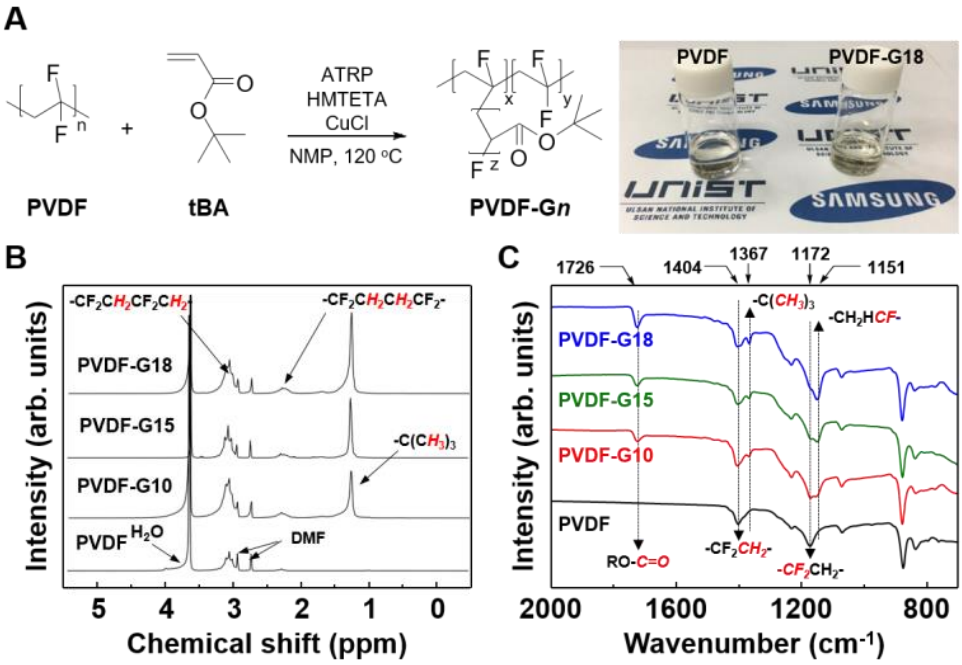

Figure 36. Synthesis of PVDF-Gn graft copolymers. (a) Synthesis of PVDF-Gn graft copolymers and photograph of the PVDF and PVDF-G18 NMP solutions, respectively (b) ^{1}H NMR, (c) FT-IR of PVDF and PVDF-Gn.

The PtBA-grafted PVDF copolymers were prepared by using ATRP (**Figure 36a**), in accordan ce with previously established methods in the literature.[176] The grafting ratios were controlled as a function of various reaction times (12 – 72 h) under the same conditions, yielding three samples with a different number of average molecular weights (Mn = 180.0 – 218.5 kDa). In a carful inspection of ^{1}H NMR spectra of the samples (**Figure 36b**), the composition of the graft copolymers was calculated on a mole basis from the integral ratio of the two noticeable resonances at 2.3 – 2.5 and 2.9 – 3.2 ppm attributed to head-to-head and head-to-tail config urations of PVDF and the signals at 1.4 – 1.65 ppm associated with the tert-butyl group in PtBA, by using the following equations;[177]

$$x = \frac{(\text{Integral}_{1.4-1.65})/9}{(\text{Integral}_{2.3-2.5} + \text{Integral}_{2.9-3.2})/2} \quad (1)$$

$$\text{PtBA mole percent (mol\%)} = \frac{x}{1+x} \times 100 \quad (2)$$

The mole percent of PtBA in the graft copolymer was determined as 10, 15 and 18%, respec tively. The graft copolymers were designated PVDF-Gn in this study, where Gn refers to the

mole percent of PtBA grafting. In addition, as shown in **Figure 36c**, the FT-IR spectra of th e PVDF-Gn showed the appearance of the absorption bands at 1725 cm^{-1} assigned to the stre tching vibrations of the ester carbonyl groups, in contrast with pristine PVDF. Also, as the gr afting ratios of PtBA were increased, the gradually enhanced intensity of the carbonyl bands r elative to the methylene stretching bands of PVDF at about 1404 cm^{-1} was observed, which f urther substantiates the PtBA content determined above.

4.2.2. TENG performance

As for a dielectric, the solutions were casted on the very flat Si/SiO_2 substrate with the blocking layer. After annealing process, the film was peeled off from the substrate and glued on Al film by using the Kapton film, followed by the attachment of Al electrode to fabricate the TENG, as shown in **Figure 37a and b**. The detailed experimental procedures are also described in experimental section. **Figure 37b** also shows that the resultant film appears white and quite flexible after peeled off. The TENG has 2 cm × 2 cm of active area with the spacer between the bottom electrode and the PVDF-Gn film made of four springs in each corner. The output voltages and current densities of the TENGs were measured and plotted in **Figure 37d**. Cycled compressive force of around 50 N at an applied frequency of 10 Hz was applied. The TENG with pristine PVDF film shows small AC-type electrical output performance of less than approximately 32.9 V and 7.7 μA/cm^2. For the PVDF-G10, the output voltage and current density were increased to 45 V and 8.3 μA/cm^2, respectively. Furthermore, the highest enhancement (with an output voltage of 64.4 V and current density of 18.9 μA/cm^2) was observed in PVDF-G18 under the same mechanical force.

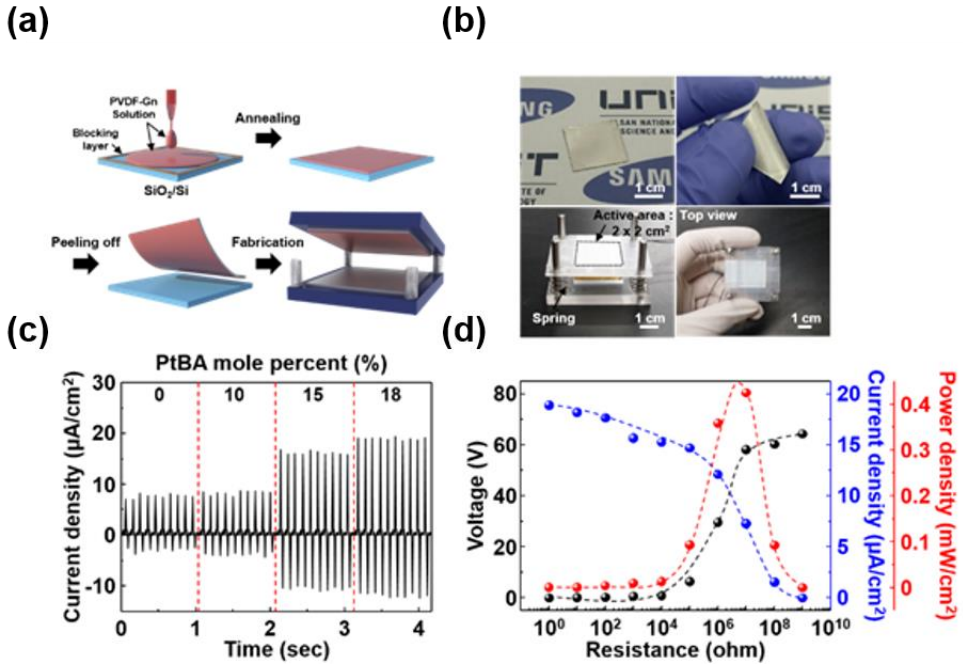

Figure 37. Fabrication of PVDF-Gn based TENGs and its output performance. (**a**) Schematic diagrams of the fabrication process for the PVDF-Gn based TENGs. (**b**) Photographs of a flexible PVDF-Gn film after peeled off and a PVDF-Gn based TENG. (**c**) The output current densities generated by the PVDF-based TENGs as a function of the PtBA mole percent ranging from 0 to 18%. (**d**) The output voltages, current densities, and the output power densities of the PVDF-G18 based TENG with the resistance of external loads from 1 to 10^9 Ω.

We measured the frequency dependent dielectric properties of the PVDF-based films over the frequency range of 10^2 Hz to 10^6 Hz at room temperature, plotted in **Figure 38**. To measure the dielectric constants, PVDF-based films were prepared on an Au/Si substrate, and Au as a top electrode was then deposited by using an E-beam evaporator. For pristine PVDF film, the dielectric constant was measured to be approximately 8.6 in the frequency range of 10^2 – 10^5 Hz; almost the same as in previous reports.[178-179] There is a significant drop in dielectric constant in the higher frequency range (10^5 – 10^6 Hz). This is because the dipole relaxation of the polymers cannot catch up with the external oscillating field. As the grafting ratios in the backbone increased, the dielectric constant gradually increased. Consequentially, the PVDF-G18 shows a superior dielectric constant value of up to 16.5 (**Figure 38**). There is no significant change in the loss tangent (~ 0.03) of all samples, except those in the higher frequency range. This means that the dielectric constant values are quite reliable. In principle, the dielectric constant has a strong correlation with polarizability and free volume of the elements present in the materials, as formulated in the Clausius-Mossotti equation.[180] The π-bonding and polar characteristics of the ester groups (–COO–) in the PtBA are able to not only hold relatively great polarizability, but also increase the net dipole moment in the backbone, which are considered to be major factors contributing to the improvement of dielectric constant values in the graft copolymers.[180]

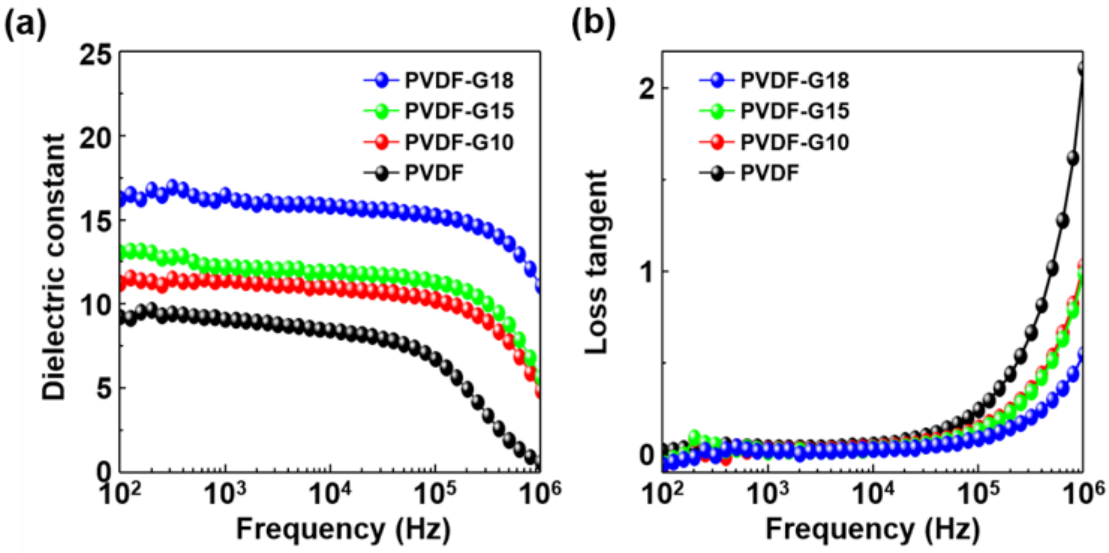

Figure 38. Dielectric constant and loss tangent for PVDF-Gn films. Frequency dependence of (a) dielectric constant values and (b) loss tangent for PVDF-based films with various PtBA m ole percent ranging from 0 to 18%.

4.2.3. Thin Film Mophology Analysis

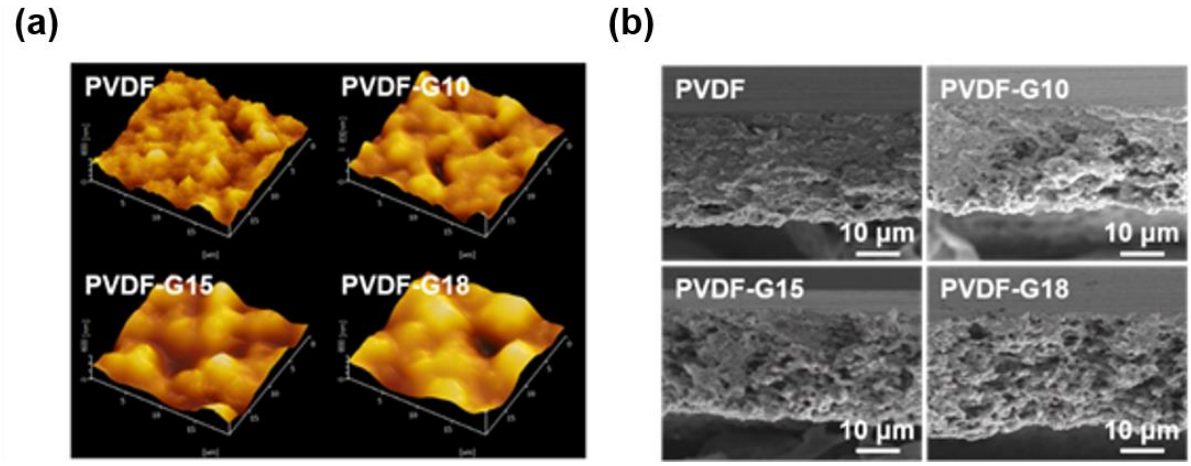

Figure 39. AFM and SEM images of the PVDF-Gn films. (a) 3-dimensional AFM images and (b) Cross-sectional SEM images for PVDF-based films with various PtBA mole percent ranging from 0 to 18%.

I evaluated the surface morphology of the PVDF-Gn films measured by using atomic force microscopy (AFM), as shown in **Figure 39a**. The root-mean-square (RMS) roughness value was measured to be approximately 98.11 nm at the PVDF-G18 and there is no significant change as the mole percent decreases from 18 to 0 %. These results may imply that the effect of the roughness on the output power is negligible. The cross-sectional scanning electron microscope (SEM) images of the PVDF-Gn films with the grafting ratio were shown in **Figure 39b**. Here, the thickness of all the films was fixed to approximately 30 μm. Importantly, all the films were quite porous, which is most likely due to the slow solvent removal process at low temperature (~ 60 ºC) to remove solvents. Such porous structures have been proven to be so effective in enhancing the output power because the output performance was significantly dependent on compressibility.[165]

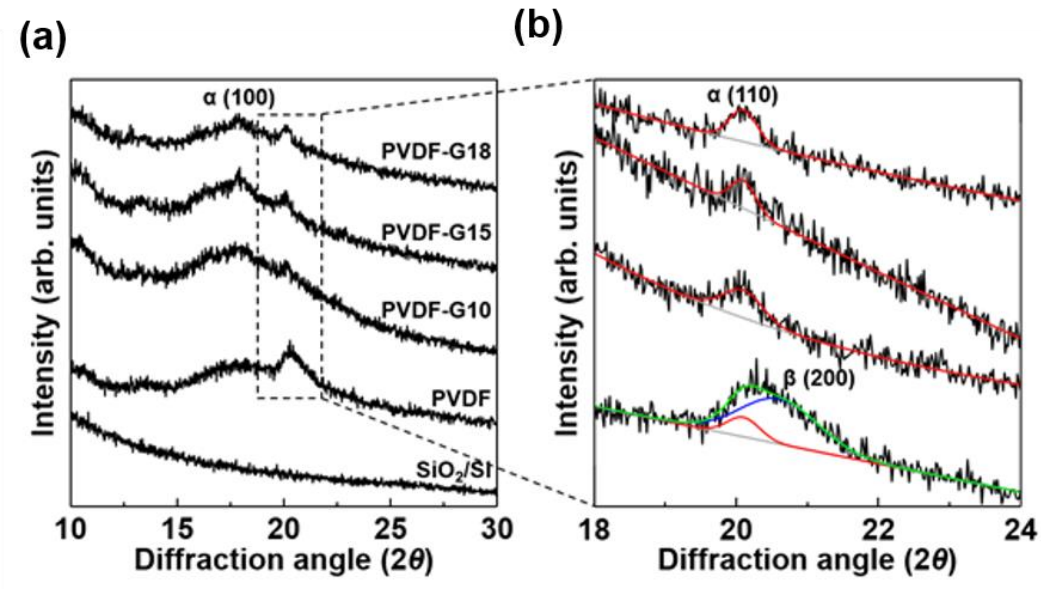

Figure 40. XRD pattern of PVDF-Gn films. (a) The high-resolution XRD patterns of pristine PVDF and PVDF-Gn films as a function of PtBA mole percent. (b) The expanded view of t he 2nd peak in Fig. 7A. The peak can be deconvoluted into two peaks, α (110) (red) and β (200) phase (blue).

The decrease of the work function in PVDF-G18 may be explained in terms of microstructu ral change. The crystalline properties of PVDF-based films were characterized by X-ray diffra ction (XRD), compared with PVDF film and plotted in **Figure 40a**. For the PVDF film, two representative peaks at 17.9 ° and 20.6 ° were observed. We thought that the two peaks woul d correspond to the (100) plane of α phase and the (200) plane of β phase, respectively. Ho wever, it was found that the β (200) peak, which was quite asymmetric, could be deconvolut ed into two peaks, α (110) and β (200),[181] as shown in **Figure 40b**. With the grafting, the p eak intensity of α (110) significantly increased, while the β (200) peak almost disappeared. In general, β phase is known to be formed due to the rotation of the CF_2 chains when anneale d.[182] The chain mobility is strongly related to the structure of the molecules, molecular weigh t, chain length, etc.[183] This implies that the increase in the molecular weight and the steric b ulkiness can suppress the rotation of the chains in PVDF-Gn films, thereby, β phase is not li kely to be formed.

4.3. Experimental Section

Materials and Instruments: PVDF (KF1100, M_n = 168.8 kDa, PDI = 2.94) was purchased from Kureha. *tert*-Butyl acrylate (tBA) was purchased from Sigma-Aldrich and was passed through an aluminum oxide column to remove the inhibitor before use. Copper (I) chloride (CuCl, 99.999%) and 1,1,4,7,10,10-hexamethyltriethylenetetramine (HMTETA) were purchased from Alfa Aesar Chemical Company. 1-Methyl-2-pyrrolidone (NMP) was purchased from JUNSEI. All solvents were reagent grade, and all reagents were used as received. The molecular weights of PVDF and the graft copolymers were measured by gel permeation chromatography (GPC) conducted at 23 °C in DMF at a flow rate of 1 mL/min, using a Agilent 1260 Infinity GPC system equipped with a PL gel 5 μm mixed B column (Polymer Laboratories) and differential refractive index detectors. Monodisperse PS standard (Polymer Laboratories) was used for calibration. ^{1}H NMR was performed in deuterated DMF, using a 400-MR DD2 (Agilent, USA) 400 MHz spectrometer. The Fourier transform infrared (FT-IR) spectra were recorded on a 670-IR (Agilent, USA) spectrophotometer.

Synthesis of PVDF-Gn graft copolymers: PVDF (3.0 g) was dissolved in NMP (30 ml) at 60 °C. Once the PVDF had completely dissolved in NMP, *tert*-butyl acrylate (18.02 g, 93.5 mmol), CuCl (0.03 g, 0.202 mmol), and HMTETA (0.127 g, 0.367 mmol) were added to the PVDF solution at room temperature under an argon atmosphere. Then, the reaction mixture was heated at 120 °C for a certain reaction time (either 12, 24 or 72 h). After cooling to room temperature, the copolymer solution was poured into water–methanol (1:4 v/v) and filtered off. The precipitated copolymer was stirred overnight in a large volume of hexane. Then, the copolymer was recovered by filtration, re-dissolved in NMP, and precipitated into the water: methanol (1:4 v/v). Finally, the graft copolymers were dried under a vacuum. ^{1}H NMR (400 MHz, C_3D_7NO): δ (ppm) 2.9–3.2 (br, 2H, -CF_2-CH_2-CF_2-CH_2-), 2.3–2.5 (br, 2H, -CF_2-CH_2-CH_2-CF_2-), 1.4–1.65 (br, 9H, -C(CH_3)$_3$). PVDF-G10: M_n = 180.0 kDa, PDI = 1.58, PVDF-G15: M_n = 201.8 kDa, PDI = 1.56, PVDF-G18: M_n = 218.5 kDa, PDI = 1.47.

4.4. Conclusion

In **Chapter 4**, we report an approach to enhance the output power of TENG with the successful synthesis of PtBA-grafted PVDF copolymers for dielectric constant control. The PtBA-grafted PVDF copolymers were prepared by using ATRP and the mole concentrations of the PtBA were controlled as 10, 15, and 18 %. In high-resolution XRD spectra, it was found that the β phases significantly decreased, thus, the copolymers were mainly composed of α phases. The TENG fabricated with the graft copolymers, generated an output voltage and current density of 64.4 V and 18.9 μA/cm^2, twice the enhancement in both, compared to pristine PVDF based TENG. The enhancement was attributed to the increase of the dielectric constant values from 8.6 to 16.5 due to the increase of the dipole moments obtained from KPFM results. Further increase in the output power was also observed by poling the film to align the dipole direction to increase the work function difference with the Al.

Reference

(1) Kang, T. E.; Kim, K.-H.; Kim, B. J., Design of terpolymers as electron donors for highly efficient polymer solar cells. *J. Mater. Chem. A.* **2014,** *2* (37), 15252-15267.

(2) Hinchet, R.; Seung, W.; Kim, S.-W., Recent Progress on Flexible Triboelectric Nanogenerators for SelfPowered Electronics. *ChemSusChem* **2015,** *8* (14), 2327-2344.

(3) Baran, D.; Ashraf, R. S.; Hanifi, D. A.; Abdelsamie, M.; Gasparini, N.; Rohr, J. A.; Holliday, S.; Wadsworth, A.; Lockett, S.; Neophytou, M.; Emmott, C. J. M.; Nelson, J.; Brabec, C. J.; Amassian, A.; Salleo, A.; Kirchartz, T.; Durrant, J. R.; McCulloch, I., Reducing the efficiency-stability-cost gap of organic photovoltaics with highly efficient and stable small molecule acceptor ternary solar cells. *Nat. Mater.* **2017,** *16* (3), 363-369.

(4) Bin, H.; Gao, L.; Zhang, Z.-G.; Yang, Y.; Zhang, Y.; Zhang, C.; Chen, S.; Xue, L.; Yang, C.; Xiao, M.; Li, Y., 11.4% Efficiency non-fullerene polymer solar cells with trialkylsilyl substituted 2D-conjugated polymer as donor. *Nat. Commun.* **2016,** *7*, 13651.

(5) Chen, J.-D.; Cui, C.; Li, Y.-Q.; Zhou, L.; Ou, Q.-D.; Li, C.; Li, Y.; Tang, J.-X., Single-Junction Polymer Solar Cells Exceeding 10% Power Conversion Efficiency. *Adv. Mater.* **2015,** *27* (6), 1035-1041.

(6) Lu, L.; Zheng, T.; Wu, Q.; Schneider, A. M.; Zhao, D.; Yu, L., Recent Advances in Bulk Heterojunction Polymer Solar Cells. *Chemical Reviews* **2015,** *115* (23), 12666-12731.

(7) Kan, B.; Zhang, Q.; Li, M.; Wan, X.; Ni, W.; Long, G.; Wang, Y.; Yang, X.; Feng, H.; Chen, Y., Solution-Processed Organic Solar Cells Based on Dialkylthiol-Substituted Benzodithiophene Unit with Efficiency near 10%. *J. Am. Chem. Soc.* **2014,** *136* (44), 15529-15532.

(8) Li, Z.; Jiang, K.; Yang, G.; Lai, J. Y. L.; Ma, T.; Zhao, J.; Ma, W.; Yan, H., Donor polymer design enables efficient non-fullerene organic solar cells. *Nat. Commun.* **2016,** *7*, 13094.

(9) Liu, Y.; Zhao, J.; Li, Z.; Mu, C.; Ma, W.; Hu, H.; Jiang, K.; Lin, H.; Ade, H.; Yan, H., Aggregation and morphology control enables multiple cases of high-efficiency polymer solar cells. *Nat. Commun.* **2014,** *5*, 5293.

(10) Ye, L.; Zhao, W.; Li, S.; Mukherjee, S.; Carpenter, J. H.; Awartani, O.; Jiao, X.; Hou, J.; Ade, H., High-Efficiency Nonfullerene Organic Solar Cells: Critical Factors that Affect Complex Multi-Length Scale Morphology and Device Performance. *Adv. Energy Mater.* **2017,** *7* (7), 1602000-n/a.

(11) Yu, G.; Gao, J.; Hummelen, J. C.; Wudl, F.; Heeger, A. J., Polymer Photovoltaic Cells: Enhanced Efficiencies via a Network of Internal Donor-Acceptor Heterojunctions. *Science* **1995,** *270* (5243), 1789-1791.

(12) Zhao, J.; Li, Y.; Lin, H.; Liu, Y.; Jiang, K.; Mu, C.; Ma, T.; Lin Lai, J. Y.; Hu, H.; Yu, D.; Yan, H., High-efficiency non-fullerene organic solar cells enabled by a difluorobenzothiadiazole-based

donor polymer combined with a properly matched small molecule acceptor. *Energy Environ Sci.* **2015,** *8* (2), 520-525.

(13) Zhao, J.; Li, Y.; Yang, G.; Jiang, K.; Lin, H.; Ade, H.; Ma, W.; Yan, H., Efficient organic solar cells processed from hydrocarbon solvents. *Nat. Energy.* **2016,** *1*, 15027.

(14) Bin, H.; Zhang, Z.-G.; Gao, L.; Chen, S.; Zhong, L.; Xue, L.; Yang, C.; Li, Y., Non-Fullerene Polymer Solar Cells Based on Alkylthio and Fluorine Substituted 2D-Conjugated Polymers Reach 9.5% Efficiency. *J. Am. Chem. Soc.* **2016,** *138* (13), 4657-4664.

(15) Gao, L.; Zhang, Z.-G.; Bin, H.; Xue, L.; Yang, Y.; Wang, C.; Liu, F.; Russell, T. P.; Li, Y., High-Efficiency Nonfullerene Polymer Solar Cells with Medium Bandgap Polymer Donor and Narrow Bandgap Organic Semiconductor Acceptor. *Adv. Mater.* **2016,** *28* (37), 8288-8295.

(16) Liao, S.-H.; Jhuo, H.-J.; Cheng, Y.-S.; Chen, S.-A., Fullerene Derivative-Doped Zinc Oxide Nanofilm as the Cathode of Inverted Polymer Solar Cells with Low-Bandgap Polymer (PTB7-Th) for High Performance. *Adv. Mater.* **2013,** *25* (34), 4766-4771.

(17) Zhao, W.; Qian, D.; Zhang, S.; Li, S.; Inganäs, O.; Gao, F.; Hou, J., Fullerene-Free Polymer Solar Cells with over 11% Efficiency and Excellent Thermal Stability. *Adv. Mater.* **2016,** *28* (23), 4734-4739.

(18) Duan, C.; Gao, K.; van Franeker, J. J.; Liu, F.; Wienk, M. M.; Janssen, R. A. J., Toward Practical Useful Polymers for Highly Efficient Solar Cells via a Random Copolymer Approach. *J. Am. Chem. Soc.* **2016,** *138* (34), 10782-10785.

(19) Jung, J. W.; Liu, F.; Russell, T. P.; Jo, W. H., Semi-crystalline random conjugated copolymers with panchromatic absorption for highly efficient polymer solar cells. *Energy Environ Sci.* **2013,** *6* (11), 3301-3307.

(20) Kang, T. E.; Cho, H.-H.; Kim, H. j.; Lee, W.; Kang, H.; Kim, B. J., Importance of Optimal Composition in Random Terpolymer-Based Polymer Solar Cells. *Macromolecules* **2013,** *46* (17), 6806-6813.

(21) Kang, T. E.; Choi, J.; Cho, H.-H.; Yoon, S. C.; Kim, B. J., Donor–Acceptor Random versus Alternating Copolymers for Efficient Polymer Solar Cells: Importance of Optimal Composition in Random Copolymers. *Macromolecules* **2016,** *49* (6), 2096-2105.

(22) Kim, G.; Song, S.; Lee, J.; Kim, T.; Lee, T. H.; Walker, B.; Kim, J. Y.; Yang, C., Control of Charge Dynamics via Use of Nonionic Phosphonate Chains and Their Effectiveness for Inverted Structure Solar Cells. *Adv. Energy Mater.* **2015,** *5* (18), 1500844-n/a.

(23) Ko, E. Y.; Park, G. E.; Lee, D. H.; Um, H. A.; Shin, J.; Cho, M. J.; Choi, D. H., Enhanced Performance of Polymer Solar Cells Comprising Diketopyrrolopyrrole-Based Regular Terpolymer Bearing Two Different π-Extended Donor Units. *ACS Appl. Mater. Interfaces* **2015,** *7* (51), 28303-28310.

(24) Zhang, M.; Wu, F.; Cao, Z.; Shen, T.; Chen, H.; Li, X.; Tan, S., Improved photovoltaic properties of terpolymers containing diketopyrrolopyrrole and an isoindigo side chain. *Polym. Chem.* **2014,** *5* (13), 4054-4060.

(25) Lee, J. W.; Ahn, H.; Jo, W. H., Conjugated Random Copolymers Consisting of Pyridine- and Thiophene-Capped Diketopyrrolopyrrole as Co-Electron Accepting Units To Enhance both JSC and VOC of Polymer Solar Cells. *Macromolecules* **2015,** *48* (21), 7836-7842.

(26) Marzano, G.; Kotowski, D.; Babudri, F.; Musio, R.; Pellegrino, A.; Luzzati, S.; Po, R.; Farinola, G. M., Tin-Free Synthesis of a Ternary Random Copolymer for BHJ Solar Cells: Direct (Hetero)arylation versus Stille Polymerization. *Macromolecules* **2015,** *48* (19), 7039-7048.

(27) Sharma, S.; Kolhe, N. B.; Gupta, V.; Bharti, V.; Sharma, A.; Datt, R.; Chand, S.; Asha, S. K., Improved All-Polymer Solar Cell Performance of n-Type Naphthalene Diimide–Bithiophene P(NDI2OD-T2) Copolymer by Incorporation of Perylene Diimide as Coacceptor. *Macromolecules* **2016,** *49* (21), 8113-8125.

(28) Jiang, T.; Yang, J.; Tao, Y.; Fan, C.; Xue, L.; Zhang, Z.; Li, H.; Li, Y.; Huang, W., Random terpolymer with a cost-effective monomer and comparable efficiency to PTB7-Th for bulk-heterojunction polymer solar cells. *Polym. Chem.* **2016,** *7* (4), 926-932.

(29) Kim, K.-H.; Park, S.; Yu, H.; Kang, H.; Song, I.; Oh, J. H.; Kim, B. J., Determining Optimal Crystallinity of Diketopyrrolopyrrole-Based Terpolymers for Highly Efficient Polymer Solar Cells and Transistors. *Chem. Mater.* **2014,** *26* (24), 6963-6970.

(30) Ye, L.; Jiao, X.; Zhang, S.; Yao, H.; Qin, Y.; Ade, H.; Hou, J., Control of Mesoscale Morphology and Photovoltaic Performance in Diketopyrrolopyrrole-Based Small Band Gap Terpolymers. *Adv. Energy Mater.* **2017,** *7* (3), 1601138-n/a.

(31) Li, X.; Sun, P.; Wang, Y.; Shan, H.; Xu, J.; Song, X.; Xu, Z.-x.; Chen, Z.-K., A random copolymer approach to develop nonfullerene acceptors for all-polymer solar cells. *J. Mater. Chem. C.* **2016,** *4* (11), 2106-2110.

(32) Li, Z.; Xu, X.; Zhang, W.; Meng, X.; Ma, W.; Yartsev, A.; Inganäs, O.; Andersson, M. R.; Janssen, R. A. J.; Wang, E., High Performance All-Polymer Solar Cells by Synergistic Effects of Fine-Tuned Crystallinity and Solvent Annealing. *J. Am. Chem. Soc.***2016,** *138* (34), 10935-10944.

(33) Cao, J.; Liao, Q.; Du, X.; Chen, J.; Xiao, Z.; Zuo, Q.; Ding, L., A pentacyclic aromatic lactam building block for efficient polymer solar cells. *Energy Environ Sci.* **2013,** *6* (11), 3224-3228.

(34) Zuo, C.; Cao, J.; Ding, L., A Fused-Ring Acceptor Unit in D–A Copolymers Benefits Photovoltaic Performance. *Macromol. Rapid Commun.* **2014,** *35* (15), 1362-1366.

(35) Li, J.; Ong, K.-H.; Lim, S.-L.; Ng, G.-M.; Tan, H.-S.; Chen, Z.-K., A random copolymer based on dithienothiophene and diketopyrrolopyrrole units for high performance organic solar cells. *Chem. Commun.* **2011,** *47* (33), 9480-9482.

(36) Liao, Q.; Cao, J.; Xiao, Z.; Liao, J.; Ding, L., Donor-acceptor conjugated polymers based on a pentacyclic aromatic lactam acceptor unit for polymer solar cells. *Phys. Chem. Chem. Phys.* **2013,** *15* (46), 19990-19993.

(37) Scharber, M. C.; Mühlbacher, D.; Koppe, M.; Denk, P.; Waldauf, C.; Heeger, A. J.; Brabec, C. J., Design Rules for Donors in Bulk-Heterojunction Solar Cells—Towards 10 % Energy-Conversion Efficiency. *Adv. Mater.* **2006,** *18* (6), 789-794.

(38) Thompson, B. C.; Fréchet, J. M. J., Polymer–Fullerene Composite Solar Cells. *Angew. Chem. Int. Ed.* **2008,** *47* (1), 58-77.

(39) Li, H.; Cao, J.; Zhou, Q.; Ding, L.; Wang, J., High-performance inverted PThTPTI:PC71BM solar cells. *Nano Energy* **2015,** *15*, 125-134.

(40) Ye, L.; Zhang, S.; Ma, W.; Fan, B.; Guo, X.; Huang, Y.; Ade, H.; Hou, J., From Binary to Ternary Solvent: Morphology Fine-tuning of D/A Blends in PDPP3T-based Polymer Solar Cells. *Adv. Mater.* **2012,** *24* (47), 6335-6341.

(41) Meng, D.; Fu, H.; Xiao, C.; Meng, X.; Winands, T.; Ma, W.; Wei, W.; Fan, B.; Huo, L.; Doltsinis, N. L.; Li, Y.; Sun, Y.; Wang, Z., Three-Bladed Rylene Propellers with Three-Dimensional Network Assembly for Organic Electronics. *J. Am. Chem. Soc.* **2016,** *138* (32), 10184-10190.

(42) Lee, J.; Sin, D. H.; Moon, B.; Shin, J.; Kim, H. G.; Kim, M.; Cho, K., Highly crystalline low-bandgap polymer nanowires towards high-performance thick-film organic solar cells exceeding 10% power conversion efficiency. *Energy Environ Sci.* **2017,** *10* (1), 247-257.

(43) Lin, Y.; Zhao, F.; Wu, Y.; Chen, K.; Xia, Y.; Li, G.; Prasad, S. K. K.; Zhu, J.; Huo, L.; Bin, H.; Zhang, Z.-G.; Guo, X.; Zhang, M.; Sun, Y.; Gao, F.; Wei, Z.; Ma, W.; Wang, C.; Hodgkiss, J.; Bo, Z.; Inganäs, O.; Li, Y.; Zhan, X., Mapping Polymer Donors toward High-Efficiency Fullerene Free Organic Solar Cells. *Adv. Mater.* **2017,** *29* (3), 1604155-n/a.

(44) Liu, C.; Wang, K.; Gong, X.; Heeger, A. J., Low bandgap semiconducting polymers for polymeric photovoltaics. *Chem. Soc. Rev.* **2016,** *45* (17), 4825-4846.

(45) Heeger, A. J., 25th Anniversary Article: Bulk Heterojunction Solar Cells: Understanding the Mechanism of Operation. *Adv. Mater.* **2014,** *26* (1), 10-28.

(46) Gupta, D.; Bag, M.; Narayan, K. S., Area dependent efficiency of organic solar cells. *Appl. Phys. Lett.* **2008,** *93* (16), 163301.

(47) Li, G.; Shrotriya, V.; Huang, J.; Yao, Y.; Moriarty, T.; Emery, K.; Yang, Y., High-efficiency solution processable polymer photovoltaic cells by self-organization of polymer blends. *Nat. Mater.* **2005,** *4* (11), 864-868.

(48) Renaud, G.; Lazzari, R.; Leroy, F., Probing surface and interface morphology with Grazing Incidence Small Angle X-Ray Scattering. *Surface Science Reports* **2009,** *64* (8), 255-380.

(49) Wernecke, J.; Okuda, H.; Ogawa, H.; Siewert, F.; Krumrey, M., Depth-Dependent Structural Changes in PS-b-P2VP Thin Films Induced by Annealing. *Macromolecules* **2014,** *47* (16), 5719-5727.

(50) Yoneda, Y., Anomalous Surface Reflection of X Rays. *Physical Review* **1963,** *131* (5), 2010-2013.

(51) Huang, Y.; Kramer, E. J.; Heeger, A. J.; Bazan, G. C., Bulk Heterojunction Solar Cells: Morphology and Performance Relationships. *Chem. Rev.* **2014,** *114* (14), 7006-7043.

(52) Kim, G.; Kang, S.-J.; Dutta, G. K.; Han, Y.-K.; Shin, T. J.; Noh, Y.-Y.; Yang, C., A Thienoisoindigo-Naphthalene Polymer with Ultrahigh Mobility of 14.4 cm2/V·s That Substantially Exceeds Benchmark Values for Amorphous Silicon Semiconductors. *J. Am. Chem. Soc.* **2014,** *136* (26), 9477-9483.

(53) Müller-Buschbaum, P., The Active Layer Morphology of Organic Solar Cells Probed with Grazing Incidence Scattering Techniques. *Adv. Mater.* **2014,** *26* (46), 7692-7709.

(54) Vohra, V.; Kawashima, K.; Kakara, T.; Koganezawa, T.; Osaka, I.; Takimiya, K.; Murata, H., Efficient inverted polymer solar cells employing favourable molecular orientation. *Nat. Photon.* **2015,** *9* (6), 403-408.

(55) Sirringhaus, H.; Brown, P. J.; Friend, R. H.; Nielsen, M. M.; Bechgaard, K.; Langeveld-Voss, B. M. W.; Spiering, A. J. H.; Janssen, R. A. J.; Meijer, E. W.; Herwig, P.; de Leeuw, D. M., Two-dimensional charge transport in self-organized, high-mobility conjugated polymers. *Nature* **1999,** *401* (6754), 685-688.

(56) Kim, Y.; Long, D. X.; Lee, J.; Kim, G.; Shin, T. J.; Nam, K.-W.; Noh, Y.-Y.; Yang, C., A Balanced Face-On to Edge-On Texture Ratio in Naphthalene Diimide-Based Polymers with Hybrid Siloxane Chains Directs Highly Efficient Electron Transport. *Macromolecules* **2015,** *48* (15), 5179-5187.

(57) Pivrikas, A.; Sariciftci, N. S.; Juška, G.; Österbacka, R., A review of charge transport and recombination in polymer/fullerene organic solar cells. *Progress in Photovoltaics: Research and Applications* **2007,** *15* (8), 677-696.

(58) Lee, W.; Lee, C.; Yu, H.; Kim, D.-J.; Wang, C.; Woo, H. Y.; Oh, J. H.; Kim, B. J., Side Chain Optimization of Naphthalenediimide–Bithiophene-Based Polymers to Enhance the Electron Mobility and the Performance in All-Polymer Solar Cells. *Adv. Funct. Mater.* **2016,** *26* (10), 1543-1553.

(59) He, Z.; Zhong, C.; Huang, X.; Wong, W.-Y.; Wu, H.; Chen, L.; Su, S.; Cao, Y., Simultaneous Enhancemen of Open-Circuit Voltage, Short-Circuit Current Density, and Fill Factor in Polymer Solar Cells. *Adv. Mater.* **2011,** *23* (40), 4636-4643.

(60) Cowan, S. R.; Banerji, N.; Leong, W. L.; Heeger, A. J., Charge Formation, Recombination, and Sweep-Out Dynamics in Organic Solar Cells. *Adv. Funct. Mater.* **2012,** *22* (6), 1116-1128.

(61) Proctor, C. M.; Nguyen, T.-Q., Effect of leakage current and shunt resistance on the light intensity dependence of organic solar cells. *Appl. Phys. Lett.* **2015,** *106* (8), 083301.

(62) Dou, L.; Liu, Y.; Hong, Z.; Li, G.; Yang, Y., Low-Bandgap Near-IR Conjugated Polymers/Molecules for Organic Electronics. *Chem. Rev.* **2015,** *115* (23), 12633-12665.

(63) Endres, J.; Pelczer, I.; Rand, B. P.; Kahn, A., Determination of Energy Level Alignment within an Energy Cascade Organic Solar Cell. *Chem. Mater.* **2016,** *28* (3), 794-801.

(64) Gao, L.; Zhang, Z.-G.; Xue, L.; Min, J.; Zhang, J.; Wei, Z.; Li, Y., All-Polymer Solar Cells Based on Absorption-Complementary Polymer Donor and Acceptor with High Power Conversion Efficiency of 8.27%. *Adv. Mater.* **2016,** *28* (9), 1884-1890.

(65) Nielsen, C. B.; Holliday, S.; Chen, H.-Y.; Cryer, S. J.; McCulloch, I., Non-Fullerene Electron Acceptors for Use in Organic Solar Cells. *Acc. Chem. Res.* **2015,** *48* (11), 2803-2812.

(66) Stoltzfus, D. M.; Donaghey, J. E.; Armin, A.; Shaw, P. E.; Burn, P. L.; Meredith, P., Charge Generation Pathways in Organic Solar Cells: Assessing the Contribution from the Electron Acceptor. *Chem. Rev.* **2016,** *116* (21), 12920-12955.

(67) Zhan, C.; Yao, J., More than Conformational "Twisting" or "Coplanarity": Molecular Strategies for Designing High-Efficiency Nonfullerene Organic Solar Cells. *Chem. Mater.* **2016,** *28* (7), 1948-1964.

(68) Zhou, H.; Yang, L.; You, W., Rational Design of High Performance Conjugated Polymers for Organic Solar Cells. *Macromolecules* **2012,** *45* (2), 607-632.

(69) Bin, H.; Gao, L.; Zhang, Z.-G.; Yang, Y.; Zhang, Y.; Zhang, C.; Chen, S.; Xue, L.; Yang, C.; Xiao, M.; Li, Y., 11.4% Efficiency non-fullerene polymer solar cells with trialkylsilyl substituted 2D-conjugated polymer as donor. **2016,** *7*, 13651.

(70) Dai, S.; Zhao, F.; Zhang, Q.; Lau, T.-K.; Li, T.; Liu, K.; Ling, Q.; Wang, C.; Lu, X.; You, W.; Zhan, X., Fused Nonacyclic Electron Acceptors for Efficient Polymer Solar Cells. *J. Am. Chem. Soc.* **2017,** *139* (3), 1336-1343.

(71) Li, S.; Ye, L.; Zhao, W.; Zhang, S.; Mukherjee, S.; Ade, H.; Hou, J., Energy-Level Modulation of Small-Molecule Electron Acceptors to Achieve over 12% Efficiency in Polymer Solar Cells. *Adv. Mater.* **2016,** *28* (42), 9423-9429.

(72) Li, Z.; Jiang, K.; Yang, G.; Lai, J. Y. L.; Ma, T.; Zhao, J.; Ma, W.; Yan, H., Donor polymer design enables efficient non-fullerene organic solar cells. **2016,** *7*, 13094.

(73) Liu, F.; Zhou, Z.; Zhang, C.; Vergote, T.; Fan, H.; Liu, F.; Zhu, X., A Thieno[3,4-b]thiophene-Based Non-fullerene Electron Acceptor for High-Performance Bulk-Heterojunction Organic Solar Cells. *J. Am. Chem. Soc.* **2016,** *138* (48), 15523-15526.

(74) Park, G. E.; Choi, S.; Park, S. Y.; Lee, D. H.; Cho, M. J.; Choi, D. H., Eco-Friendly Solvent-Processed Fullerene-Free Polymer Solar Cells with over 9.7% Efficiency and Long-Term Performance Stability. *Adv. Energy Mater.*, 1700566-n/a.

(75) Qin, Y.; Uddin, M. A.; Chen, Y.; Jang, B.; Zhao, K.; Zheng, Z.; Yu, R.; Shin, T. J.; Woo, H. Y.; Hou, J., Highly Efficient Fullerene-Free Polymer Solar Cells Fabricated with Polythiophene Derivative. *Adv. Mater.* **2016,** *28* (42), 9416-9422.

(76) Yang, Y.; Zhang, Z.-G.; Bin, H.; Chen, S.; Gao, L.; Xue, L.; Yang, C.; Li, Y., Side-Chain Isomerization on an n-type Organic Semiconductor ITIC Acceptor Makes 11.77% High Efficiency Polymer Solar Cells. *J. Am. Chem. Soc.* **2016,** *138* (45), 15011-15018.

(77) Zheng, Z.; Awartani, O. M.; Gautam, B.; Liu, D.; Qin, Y.; Li, W.; Bataller, A.; Gundogdu, K.; Ade, H.; Hou, J., Efficient Charge Transfer and Fine-Tuned Energy Level Alignment in a THF-Processed Fullerene-Free Organic Solar Cell with 11.3% Efficiency. *Adv. Mater.* **2017,** *29* (5), 1604241-n/a.

(78) Kim, H.; Lee, H.; Seo, D.; Jeong, Y.; Cho, K.; Lee, J.; Lee, Y., Regioregular Low Bandgap Polymer with Controlled Thieno[3,4-b]thiophene Orientation for High-Efficiency Polymer Solar Cells. *Chem. Mater.* **2015,** *27* (8), 3102-3107.

(79) Qin, T.; Zajaczkowski, W.; Pisula, W.; Baumgarten, M.; Chen, M.; Gao, M.; Wilson, G.; Easton, C. D.; Müllen, K.; Watkins, S. E., Tailored Donor–Acceptor Polymers with an A–D1–A–D2 Structure: Controlling Intermolecular Interactions to Enable Enhanced Polymer Photovoltaic Devices. *J. Am. Chem. Soc.* **2014,** *136* (16), 6049-6055.

(80) Wang, M.; Wang, H.; Yokoyama, T.; Liu, X.; Huang, Y.; Zhang, Y.; Nguyen, T.-Q.; Aramaki, S.; Bazan, G. C., High Open Circuit Voltage in Regioregular Narrow Band Gap Polymer Solar Cells. *J. Am. Chem. Soc.* **2014,** *136* (36), 12576-12579.

(81) Ye, L.; Zhang, S.; Huo, L.; Zhang, M.; Hou, J., Molecular Design toward Highly Efficient Photovoltaic Polymers Based on Two-Dimensional Conjugated Benzodithiophene. *Acc. Chem. Res.* **2014,** *47* (5), 1595-1603.

(82) Ying, L.; Hsu, B. B. Y.; Zhan, H.; Welch, G. C.; Zalar, P.; Perez, L. A.; Kramer, E. J.; Nguyen, T.-Q.; Heeger, A. J.; Wong, W.-Y.; Bazan, G. C., Regioregular Pyridal[2,1,3]thiadiazole π-Conjugated Copolymers. *J. Am. Chem. Soc.* **2011,** *133* (46), 18538-18541.

(83) Zhong, H.; Li, C.-Z.; Carpenter, J.; Ade, H.; Jen, A. K. Y., Influence of Regio- and Chemoselectivity on the Properties of Fluoro-Substituted Thienothiophene and Benzodithiophene Copolymers. *J. Am. Chem. Soc.* **2015,** *137* (24), 7616-7619.

(84) Dang, M. T.; Hirsch, L.; Wantz, G.; Wuest, J. D., Controlling the Morphology and Performance of Bulk Heterojunctions in Solar Cells. Lessons Learned from the Benchmark Poly(3-

hexylthiophene):[6,6]-Phenyl-C61-butyric Acid Methyl Ester System. *Chem. Rev.* **2013,** *113* (5), 3734-3765.

(85) Wu, J.-S.; Cheng, S.-W.; Cheng, Y.-J.; Hsu, C.-S., Donor-acceptor conjugated polymers based on multifused ladder-type arenes for organic solar cells. *Chem. Soc. Rev.* **2015,** *44* (5), 1113-1154.

(86) Zhang, S.; Ye, L.; Hou, J., Breaking the 10% Efficiency Barrier in Organic Photovoltaics: Morphology and Device Optimization of Well-Known PBDTTT Polymers. *Adv. Energy Mater.* **2016,** *6* (11), 1502529-n/a.

(87) Lin, Y.; Wang, J.; Zhang, Z.-G.; Bai, H.; Li, Y.; Zhu, D.; Zhan, X., An Electron Acceptor Challenging Fullerenes for Efficient Polymer Solar Cells. *Adv. Mater.* **2015,** *27* (7), 1170-1174.

(88) Betley, T. A.; Peters, J. C., Dinitrogen Chemistry from Trigonally Coordinated Iron and Cobalt Platforms. *J. Am. Chem. Soc.* **2003,** *125* (36), 10782-10783.

(89) Chang, W.-H.; Gao, J.; Dou, L.; Chen, C.-C.; Liu, Y.; Yang, Y., Side-Chain Tunability via Triple Component Random Copolymerization for Better Photovoltaic Polymers. *Adv. Energy Mater.* **2014,** *4* (4), 1300864-n/a.

(90) Chen, Y.-T.; Huang, T.-W.; Wang, C.-L.; Hsu, C.-S., Influences of the backbone randomness on the properties, morphology and performances of the fluorinated benzoselenadiazole-benzothiadiazole based random copolymers. *Polym. Chem.* **2015,** *6* (19), 3728-3736.

(91) Deng, P.; Wu, B.; Lei, Y.; Cao, H.; Ong, B. S., Regioregular and Random Difluorobenzothiadiazole Electron Donor–Acceptor Polymer Semiconductors for Thin-Film Transistors and Polymer Solar Cells. *Macromolecules* **2016,** *49* (7), 2541-2548.

(92) Hwang, Y.-J.; Earmme, T.; Courtright, B. A. E.; Eberle, F. N.; Jenekhe, S. A., n-Type Semiconducting Naphthalene Diimide-Perylene Diimide Copolymers: Controlling Crystallinity, Blend Morphology, and Compatibility Toward High-Performance All-Polymer Solar Cells. *J. Am. Chem. Soc.* **2015,** *137* (13), 4424-4434.

(93) Yang, Y.; Chen, W.; Dou, L.; Chang, W.-H.; Duan, H.-S.; Bob, B.; Li, G.; Yang, Y., High-performance multiple-donor bulk heterojunction solar cells. *Nat. Photon.* **2015,** *9* (3), 190-198.

(94) Yao, J.; Yu, C.; Liu, Z.; Luo, H.; Yang, Y.; Zhang, G.; Zhang, D., Significant Improvement of Semiconducting Performance of the Diketopyrrolopyrrole–Quaterthiophene Conjugated Polymer through Side-Chain Engineering via Hydrogen-Bonding. *J. Am. Chem. Soc.* **2016,** *138* (1), 173-185.

(95) Yuan, J.; McDowell, C.; Mai, C.-K.; Bazan, G. C.; Ma, W., Ternary D1–D2–A–D2 Structured Conjugated Polymer: Efficient “Green” Solvent-Processed Polymer/Neat-C70 Solar Cells. *Chem. Mater.* **2016,** *28* (20), 7479-7486.

(96) Zhang, Q.; Kelly, M. A.; Hunt, A.; Ade, H.; You, W., Comparative Photovoltaic Study of Physical Blending of Two Donor–Acceptor Polymers with the Chemical Blending of the Respective Moieties. *Macromolecules* **2016,** *49* (7), 2533-2540.

(97) Jo, J. W.; Jung, J. W.; Ahn, H.; Ko, M. J.; Jen, A. K. Y.; Son, H. J., Effect of Molecular Orientation of Donor Polymers on Charge Generation and Photovoltaic Properties in Bulk Heterojunction All-Polymer Solar Cells. *Adv. Energy Mater.* **2017,** *7* (1), 1601365-n/a.

(98) Faist, M. A.; Kirchartz, T.; Gong, W.; Ashraf, R. S.; McCulloch, I.; de Mello, J. C.; Ekins-Daukes, N. J.; Bradley, D. D. C.; Nelson, J., Competition between the Charge Transfer State and the Singlet States of Donor or Acceptor Limiting the Efficiency in Polymer:Fullerene Solar Cells. *J. Am. Chem. Soc.* **2012,** *134* (1), 685-692.

(99) Kawashima, K.; Tamai, Y.; Ohkita, H.; Osaka, I.; Takimiya, K., High-efficiency polymer solar cells with small photon energy loss. **2015,** *6*, 10085.

(100) Ran, N. A.; Love, J. A.; Takacs, C. J.; Sadhanala, A.; Beavers, J. K.; Collins, S. D.; Huang, Y.; Wang, M.; Friend, R. H.; Bazan, G. C.; Nguyen, T.-Q., Harvesting the Full Potential of Photons with Organic Solar Cells. *Adv. Mater.* **2016,** *28* (7), 1482-1488.

(101) Veldman, D.; Meskers, S. C. J.; Janssen, R. A. J., The Energy of Charge-Transfer States in Electron Donor–Acceptor Blends: Insight into the Energy Losses in Organic Solar Cells. *Adv. Funct. Mater.* **2009,** *19* (12), 1939-1948.

(102) Zhang, Z.-G.; Qi, B.; Jin, Z.; Chi, D.; Qi, Z.; Li, Y.; Wang, J., Perylene diimides: a thickness-insensitive cathode interlayer for high performance polymer solar cells. *Energy Environ Sci.* **2014,** *7* (6), 1966-1973.

(103) Burke, T. M.; Sweetnam, S.; Vandewal, K.; McGehee, M. D., Beyond Langevin Recombination: How Equilibrium Between Free Carriers and Charge Transfer States Determines the Open-Circuit Voltage of Organic Solar Cells. *Adv. Energy Mater.* **2015,** *5* (11), 1500123-n/a.

(104) Janssen, R. A. J.; Nelson, J., Factors Limiting Device Efficiency in Organic Photovoltaics. *Adv. Mater.* **2013,** *25* (13), 1847-1858.

(105) Scharber, M. C., On the Efficiency Limit of Conjugated Polymer:Fullerene-Based Bulk Heterojunction Solar Cells. *Adv. Mater.* **2016,** *28* (10), 1994-2001.

(106) Rivnay, J.; Mannsfeld, S. C. B.; Miller, C. E.; Salleo, A.; Toney, M. F., Quantitative Determination of Organic Semiconductor Microstructure from the Molecular to Device Scale. *Chem. Rev.* **2012,** *112* (10), 5488-5519.

(107) Zhou, N.; Dudnik, A. S.; Li, T. I. N. G.; Manley, E. F.; Aldrich, T. J.; Guo, P.; Liao, H.-C.; Chen, Z.; Chen, L. X.; Chang, R. P. H.; Facchetti, A.; Olvera de la Cruz, M.; Marks, T. J., All-Polymer Solar Cell Performance Optimized via Systematic Molecular Weight Tuning of Both Donor and Acceptor Polymers. *J. Am. Chem. Soc.* **2016,** *138* (4), 1240-1251.

(108) Tumbleston, J. R.; Collins, B. A.; Yang, L.; Stuart, A. C.; Gann, E.; Ma, W.; You, W.; Ade, H., The influence of molecular orientation on organic bulk heterojunction solar cells. *Nat. Photon.* **2014,** *8* (5), 385-391.

(109) Schilinsky, P.; Waldauf, C.; Brabec, C. J., Recombination and loss analysis in polythiophene based bulk heterojunction photodetectors. *Appl. Phys. Lett.* **2002,** *81* (20), 3885-3887.

(110) Lenes, M.; Morana, M.; Brabec, C. J.; Blom, P. W. M., Recombination-Limited Photocurrents in Low Bandgap Polymer/Fullerene Solar Cells. *Adv. Funct. Mater.* **2009,** *19* (7), 1106-1111.

(111) Lu, L.; Chen, W.; Xu, T.; Yu, L., High-performance ternary blend polymer solar cells involving both energy transfer and hole relay processes. **2015,** *6*, 7327.

(112) Chen, S.; An, Y.; Dutta, G. K.; Kim, Y.; Zhang, Z.-G.; Li, Y.; Yang, C., A Synergetic Effect of Molecular Weight and Fluorine in All-Polymer Solar Cells with Enhanced Performance. *Adv. Funct. Mater.* **2017,** *27* (2), 1603564-n/a.

(113) Fan, J.; Yuen, J. D.; Cui, W.; Seifter, J.; Mohebbi, A. R.; Wang, M.; Zhou, H.; Heeger, A.; Wudl, F., High-Hole-Mobility Field-Effect Transistors Based on Co-Benzobisthiadiazole-Quaterthiophene. *Adv. Mater.* **2012,** *24* (46), 6164-6168.

(114) Han, A. R.; Dutta, G. K.; Lee, J.; Lee, H. R.; Lee, S. M.; Ahn, H.; Shin, T. J.; Oh, J. H.; Yang, C., ε-Branched Flexible Side Chain Substituted Diketopyrrolopyrrole-Containing Polymers Designed for High Hole and Electron Mobilities. *Adv. Funct. Mater.* **2015,** *25* (2), 247-254.

(115) Kang, I.; Yun, H.-J.; Chung, D. S.; Kwon, S.-K.; Kim, Y.-H., Record High Hole Mobility in Polymer Semiconductors via Side-Chain Engineering. *J. Am. Chem. Soc.* **2013,** *135* (40), 14896-14899.

(116) Lei, T.; Cao, Y.; Fan, Y.; Liu, C.-J.; Yuan, S.-C.; Pei, J., High-Performance Air-Stable Organic Field-Effect Transistors: Isoindigo-Based Conjugated Polymers. *J. Am. Chem. Soc.* **2011,** *133* (16), 6099-6101.

(117) Wang, C.; Dong, H.; Hu, W.; Liu, Y.; Zhu, D., Semiconducting π-Conjugated Systems in Field-Effect Transistors: A Material Odyssey of Organic Electronics. *Chem. Rev.* **2012,** *112* (4), 2208-2267.

(118) Yan, H.; Chen, Z.; Zheng, Y.; Newman, C.; Quinn, J. R.; Dotz, F.; Kastler, M.; Facchetti, A., A high-mobility electron-transporting polymer for printed transistors. *Nature* **2009,** *457* (7230), 679-686.

(119) Cho, J.; Park, S. J.; Lee, S. M.; Ha, J. U.; Ahn, E. S.; Chang, S. T.; Kwon, S.-K.; Chung, D. S.; Kim, Y.-H., Synergetic Evolution of Diketopyrrolopyrrole-Based Polymeric Semiconductor for High Reproducibility and Performance: Random Copolymerization of Similarly Shaped Building Blocks. *Macromol. Rapid Commun.* **2016,** *37* (24), 2057-2063.

(120) Lei, T.; Cao, Y.; Zhou, X.; Peng, Y.; Bian, J.; Pei, J., Systematic Investigation of Isoindigo-Based Polymeric Field-Effect Transistors: Design Strategy and Impact of Polymer Symmetry and Backbone Curvature. *Chem. Mater.* **2012,** *24* (10), 1762-1770.

(121) Li, J.; Zhao, Y.; Tan, H. S.; Guo, Y.; Di, C.-A.; Yu, G.; Liu, Y.; Lin, M.; Lim, S. H.; Zhou, Y.; Su, H.; Ong, B. S., A stable solution-processed polymer semiconductor with record high-mobility for printed transistors. *Sci. Rep.* **2012,** *2*, 754.

(122) Zhang, W.; Smith, J.; Watkins, S. E.; Gysel, R.; McGehee, M.; Salleo, A.; Kirkpatrick, J.; Ashraf, S.; Anthopoulos, T.; Heeney, M.; McCulloch, I., Indacenodithiophene Semiconducting Polymers for High-Performance, Air-Stable Transistors. *J. Am. Chem. Soc.* **2010,** *132* (33), 11437-11439.

(123) Brinkmann, M., Structure and morphology control in thin films of regioregular poly(3-hexylthiophene). *J. Polym. Sci. Part B.* **2011,** *49* (17), 1218-1233.

(124) Nketia-Yawson, B.; Kang, H.; Shin, E.-Y.; Xu, Y.; Yang, C.; Noh, Y.-Y., Effect of electron-donating unit on crystallinity and charge transport in organic field-effect transistors with thienoisoindigo-based small molecules. *Organic Electronics* **2015,** *26*, 151-157.

(125) Park, W.-T.; Kim, G.; Yang, C.; Liu, C.; Noh, Y.-Y., Effect of Donor Molecular Structure and Gate Dielectric on Charge-Transporting Characteristics for Isoindigo-Based Donor–Acceptor Conjugated Polymers. *Adv. Funct. Mater.* **2016,** *26* (26), 4695-4703.

(126) Schuettfort, T.; Thomsen, L.; McNeill, C. R., Observation of a Distinct Surface Molecular Orientation in Films of a High Mobility Conjugated Polymer. *J. Am. Chem. Soc.* **2013,** *135* (3), 1092-1101.

(127) Tsao, H. N.; Cho, D. M.; Park, I.; Hansen, M. R.; Mavrinskiy, A.; Yoon, D. Y.; Graf, R.; Pisula, W.; Spiess, H. W.; Müllen, K., Ultrahigh Mobility in Polymer Field-Effect Transistors by Design. *J. Am. Chem. Soc.* **2011,** *133* (8), 2605-2612.

(128) Tseng, H.-R.; Ying, L.; Hsu, B. B. Y.; Perez, L. A.; Takacs, C. J.; Bazan, G. C.; Heeger, A. J., High Mobility Field Effect Transistors Based on Macroscopically Oriented Regioregular Copolymers. *Nano Letters* **2012,** *12* (12), 6353-6357.

(129) Zhang, X.; Bronstein, H.; Kronemeijer, A. J.; Smith, J.; Kim, Y.; Kline, R. J.; Richter, L. J.; Anthopoulos, T. D.; Sirringhaus, H.; Song, K.; Heeney, M.; Zhang, W.; McCulloch, I.; DeLongchamp, D. M., Molecular origin of high field-effect mobility in an indacenodithiophene–benzothiadiazole copolymer. *Nat. Commun.* **2013,** *4*, 2238.

(130) Kanimozhi, C.; Yaacobi-Gross, N.; Chou, K. W.; Amassian, A.; Anthopoulos, T. D.; Patil, S., Diketopyrrolopyrrole–Diketopyrrolopyrrole-Based Conjugated Copolymer for High-Mobility Organic Field-Effect Transistors. *J. Am. Chem. Soc.* **2012,** *134* (40), 16532-16535.

(131) Kim, J.; Han, A. R.; Hong, J.; Kim, G.; Lee, J.; Shin, T. J.; Oh, J. H.; Yang, C., Ambipolar Semiconducting Polymers with π-Spacer Linked Bis-Benzothiadiazole Blocks as Strong Accepting Units. *Chem. Mater.* **2014,** *26* (17), 4933-4942.

(132) Kim, J.; Yun, M. H.; Kim, G.-H.; Lee, J.; Lee, S. M.; Ko, S.-J.; Kim, Y.; Dutta, G. K.; Moon, M.; Park, S. Y.; Kim, D. S.; Kim, J. Y.; Yang, C., Synthesis of PCDTBT-Based Fluorinated Polymers for High Open-Circuit Voltage in Organic Photovoltaics: Towards an Understanding of Relationships between Polymer Energy Levels Engineering and Ideal Morphology Control. *ACS Appl. Mater. Interfaces* **2014,** *6* (10), 7523-7534.

(133) Kim, M. J.; Choi, S.; Lee, M.; Heo, H.; Lee, Y.; Cho, J. H.; Kim, B., Photoresponsive Transistors Based on a Dual Acceptor-Containing Low-Bandgap Polymer. *ACS Appl. Mater. Interfaces.* **2017**.

(134) Lee, S. M.; Lee, H. R.; Han, A. R.; Lee, J.; Oh, J. H.; Yang, C., High-Performance Furan-Containing Conjugated Polymer for Environmentally Benign Solution Processing. *ACS Appl. Mater. Interfaces* **2017,** *9* (18), 15652-15661.

(135) Lei, T.; Wang, J.-Y.; Pei, J., Roles of Flexible Chains in Organic Semiconducting Materials. *Chem. Mater.* **2014,** *26* (1), 594-603.

(136) An, T. K.; Jang, S. H.; Kim, S.-O.; Jang, J.; Hwang, J.; Cha, H.; Noh, Y. R.; Yoon, S. B.; Yoon, Y. J.; Kim, L. H.; Chung, D. S.; Kwon, S.-K.; Kim, Y.-H.; Lee, S.-G.; Park, C. E., Synthesis and Transistor Properties of Asymmetric Oligothiophenes: Relationship between Molecular Structure and Device Performance. *Chemistry – A European Journal* **2013,** *19* (42), 14052-14060.

(137) Chen, M. S.; Lee, O. P.; Niskala, J. R.; Yiu, A. T.; Tassone, C. J.; Schmidt, K.; Beaujuge, P. M.; Onishi, S. S.; Toney, M. F.; Zettl, A.; Fréchet, J. M. J., Enhanced Solid-State Order and Field-Effect Hole Mobility through Control of Nanoscale Polymer Aggregation. *J. Am. Chem. Soc.* **2013,** *135* (51), 19229-19236.

(138) Lee, J. S.; Son, S. K.; Song, S.; Kim, H.; Lee, D. R.; Kim, K.; Ko, M. J.; Choi, D. H.; Kim, B.; Cho, J. H., Importance of Solubilizing Group and Backbone Planarity in Low Band Gap Polymers for High Performance Ambipolar field-effect Transistors. *Chem. Mater.* **2012,** *24* (7), 1316-1323.

(139) Back, J. Y.; An, T. K.; Cheon, Y. R.; Cha, H.; Jang, J.; Kim, Y.; Baek, Y.; Chung, D. S.; Kwon, S.-K.; Park, C. E.; Kim, Y.-H., Alkyl Chain Length Dependence of the Field-Effect Mobility in Novel Anthracene Derivatives. *ACS Appl. Mater. Interfaces* **2015,** *7* (1), 351-358.

(140) Kline, R. J.; McGehee, M. D.; Kadnikova, E. N.; Liu, J.; Fréchet, J. M. J.; Toney, M. F., Dependence of Regioregular Poly(3-hexylthiophene) Film Morphology and Field-Effect Mobility on Molecular Weight. *Macromolecules* **2005,** *38* (8), 3312-3319.

(141) Tunc, A. V.; Ecker, B.; Dogruyol, Z.; Jüchter, S.; Ugur, A. L.; Erdogmus, A.; San, S. E.; Parisi, J.; von Hauff, E., Influence of molecular weight on the short-channel effect in polymer-based field-effect transistors. *J. Polym. Sci. Part B Polym. Phys.* **2012,** *50* (2), 117-124.

(142) Guo, X.; Watson, M. D., Conjugated Polymers from Naphthalene Bisimide. *Organic Letters* **2008,** *10* (23), 5333-5336.

(143) Shin, J.; Park, G. E.; Lee, D. H.; Um, H. A.; Lee, T. W.; Cho, M. J.; Choi, D. H., Bis(thienothiophenyl) Diketopyrrolopyrrole-Based Conjugated Polymers with Various Branched Alkyl Side Chains and Their Applications in Thin-Film Transistors and Polymer Solar Cells. *ACS Appl. Mater. Interfaces* **2015,** *7* (5), 3280-3288.

(144) Ashraf, R. S.; Kronemeijer, A. J.; James, D. I.; Sirringhaus, H.; McCulloch, I., A new thiophene substituted isoindigo based copolymer for high performance ambipolar transistors. *Chem. Commun.* **2012,** *48* (33), 3939-3941.

(145) Dutta, G. K.; Han, A. R.; Lee, J.; Kim, Y.; Oh, J. H.; Yang, C., Visible-Near Infrared Absorbing Polymers Containing Thienoisoindigo and Electron-Rich Units for Organic Transistors with Tunable Polarity. *Adv. Funct. Mater.* **2013,** *23* (42), 5317-5325.

(146) Kim, G.; Kim, H.; Jang, M.; Jung, Y. K.; Oh, J. H.; Yang, C., Ultra-narrow-bandgap thienoisoindigo polymers: structure-property correlations in field-effect transistors. *J. Mater. Chem. C* **2016,** *4* (40), 9554-9560.

(147) Van Pruissen, G. W. P.; Gholamrezaie, F.; Wienk, M. M.; Janssen, R. A. J., Synthesis and properties of small band gap thienoisoindigo based conjugated polymers. *J. Mater. Chem.* **2012,** *22* (38), 20387-20393.

(148) Kim, G.; Han, A. R.; Lee, H. R.; Lee, J.; Oh, J. H.; Yang, C., Acceptor-acceptor type isoindigo-based copolymers for high-performance n-channel field-effect transistors. *Chem. Commun.* **2014,** *50* (17), 2180-2183.

(149) Duong, D. T.; Toney, M. F.; Saileo, A., Role of Confinement and Aggregation in Charge Transport in Semicrystalline Polythiophene Thin Films. *Phys. Rev. B86: 205205, 2012* **2014**, Medium: X.

(150) Cao, Y.; Irwin, P. C.; Younsi, K., The future of nanodielectrics in the electrical power industry. *IEEE Transactions on Dielectrics and Electrical Insulation* **2004,** *11* (5), 797-807.

(151) Chen, Q.; Shen, Y.; Zhang, S.; Zhang, Q. M., Polymer-Based Dielectrics with High Energy Storage Density. *Annual Review of Materials Research* **2015,** *45* (1), 433-458.

(152) Chu, B.; Zhou, X.; Ren, K.; Neese, B.; Lin, M.; Wang, Q.; Bauer, F.; Zhang, Q. M., A Dielectric Polymer with High Electric Energy Density and Fast Discharge Speed. *Science* **2006,** *313* (5785), 334-336.

(153) Ducharme, S., An Inside-Out Approach to Storing Electrostatic Energy. *ACS Nano* **2009,** *3* (9), 2447-2450.

(154) Wu, S.; Li, W.; Lin, M.; Burlingame, Q.; Chen, Q.; Payzant, A.; Xiao, K.; Zhang, Q. M., Aromatic Polythiourea Dielectrics with Ultrahigh Breakdown Field Strength, Low Dielectric Loss, and High Electric Energy Density. *Adv. Mater.* **2013,** *25* (12), 1734-1738.

(155) Roberts, M. E.; Queraltó, N.; Mannsfeld, S. C. B.; Reinecke, B. N.; Knoll, W.; Bao, Z., Cross-Linked Polymer Gate Dielectric Films for Low-Voltage Organic Transistors. *Chem. Mater.* **2009,** *21* (11), 2292-2299.

(156) Yoon, M.-H.; Yan, H.; Facchetti, A.; Marks, T. J., Low-Voltage Organic Field-Effect Transistors and Inverters Enabled by Ultrathin Cross-Linked Polymers as Gate Dielectrics. *J. Am. Chem. Soc.* **2005,** *127* (29), 10388-10395.

(157) Dang, M. T.; Hirsch, L.; Wantz, G., P3HT:PCBM, Best Seller in Polymer Photovoltaic Research. *Adv. Mater.* **2011,** *23* (31), 3597-3602.

(158) Huo, L.; Zhang, S.; Guo, X.; Xu, F.; Li, Y.; Hou, J., Replacing Alkoxy Groups with Alkylthienyl Groups: A Feasible Approach To Improve the Properties of Photovoltaic Polymers. *Angew. Chem. Int. Ed.* **2011,** *50* (41), 9697-9702.

(159) Dadbin, S.; Frounchi, M.; Saeid, M. H.; Gangi, F., Molecular structure and physical properties of E-beam crosslinked low-density polyethylene for wire and cable insulation applications. *J. Appl. Polym. Sci.* **2002,** *86* (8), 1959-1969.

(160) Kim, J.-H.; Chun, J.; Kim, J. W.; Choi, W. J.; Baik, J. M., Self-Powered, Room-Temperature Electronic Nose Based on Triboelectrification and Heterogeneous Catalytic Reaction. *Adv. Funct. Mater.* **2015,** *25* (45), 7049-7055.

(161) Li, Z.; Chen, J.; Yang, J.; Su, Y.; Fan, X.; Wu, Y.; Yu, C.; Wang, Z. L., [small beta]-cyclodextrin enhanced triboelectrification for self-powered phenol detection and electrochemical degradation. *Energy Environ Sci.* **2015,** *8* (3), 887-896.

(162) Wang, S.; Lin, L.; Wang, Z. L., Nanoscale Triboelectric-Effect-Enabled Energy Conversion for Sustainably Powering Portable Electronics. *Nano Letters* **2012,** *12* (12), 6339-6346.

(163) Yang, Y.; Zhang, H.; Liu, Y.; Lin, Z.-H.; Lee, S.; Lin, Z.; Wong, C. P.; Wang, Z. L., Silicon-Based Hybrid Energy Cell for Self-Powered Electrodegradation and Personal Electronics. *ACS Nano* **2013,** *7* (3), 2808-2813.

(164) Chen, J.; Guo, H.; He, X.; Liu, G.; Xi, Y.; Shi, H.; Hu, C., Enhancing Performance of Triboelectric Nanogenerator by Filling High Dielectric Nanoparticles into Sponge PDMS Film. *ACS Appl. Mater. Interfaces* **2016,** *8* (1), 736-744.

(165) Chun, J.; Kim, J. W.; Jung, W.-s.; Kang, C.-Y.; Kim, S.-W.; Wang, Z. L.; Baik, J. M., Mesoporous pores impregnated with Au nanoparticles as effective dielectrics for enhancing triboelectric nanogenerator performance in harsh environments. *Energy Environ Sci.* **2015,** *8* (10), 3006-3012.

(166) Zhu, G.; Lin, Z.-H.; Jing, Q.; Bai, P.; Pan, C.; Yang, Y.; Zhou, Y.; Wang, Z. L., Toward Large-Scale Energy Harvesting by a Nanoparticle-Enhanced Triboelectric Nanogenerator. *Nano Letters* **2013,** *13* (2), 847-853.

(167) Zhu, G.; Pan, C.; Guo, W.; Chen, C.-Y.; Zhou, Y.; Yu, R.; Wang, Z. L., Triboelectric-Generator-Driven Pulse Electrodeposition for Micropatterning. *Nano Letters* **2012,** *12* (9), 4960-4965.

(168) Zhao, Z.; Pu, X.; Du, C.; Li, L.; Jiang, C.; Hu, W.; Wang, Z. L., Freestanding Flag-Type Triboelectric Nanogenerator for Harvesting High-Altitude Wind Energy from Arbitrary Directions. *ACS Nano* **2016,** *10* (2), 1780-1787.

(169) Bai, P.; Zhu, G.; Zhou, Y. S.; Wang, S.; Ma, J.; Zhang, G.; Wang, Z. L., Dipole-moment-induced effect on contact electrification for triboelectric nanogenerators. *Nano Research* **2014,** *7* (7), 990-997.

(170) Bai, P.; Zhu, G.; Lin, Z.-H.; Jing, Q.; Chen, J.; Zhang, G.; Ma, J.; Wang, Z. L., Integrated Multilayered Triboelectric Nanogenerator for Harvesting Biomechanical Energy from Human Motions. *ACS Nano* **2013,** *7* (4), 3713-3719.

(171) Zhou, Y. S.; Wang, S.; Yang, Y.; Zhu, G.; Niu, S.; Lin, Z.-H.; Liu, Y.; Wang, Z. L., Manipulating Nanoscale Contact Electrification by an Applied Electric Field. *Nano Letters* **2014,** *14* (3), 1567-1572.

(172) Lee, K. Y.; Chun, J.; Lee, J.-H.; Kim, K. N.; Kang, N.-R.; Kim, J.-Y.; Kim, M. H.; Shin, K.-S.; Gupta, M. K.; Baik, J. M.; Kim, S.-W., Hydrophobic Sponge Structure-Based Triboelectric Nanogenerator. *Adv. Mater.* **2014,** *26* (29), 5037-5042.

(173) Li, M.; Wondergem, H. J.; Spijkman, M.-J.; Asadi, K.; Katsouras, I.; Blom, P. W. M.; de Leeuw, D. M., Revisiting the δ-phase of poly(vinylidene fluoride) for solution-processed ferroelectric thin films. *Nat. Mater.* **2013,** *12* (5), 433-438.

(174) Shirinov, A. V.; Schomburg, W. K., Pressure sensor from a PVDF film. *Sensors and Actuators A: Physical* **2008,** *142* (1), 48-55.

(175) Song, Y.; Shen, Y.; Liu, H.; Lin, Y.; Li, M.; Nan, C.-W., Enhanced dielectric and ferroelectric properties induced by dopamine-modified BaTiO3 nanofibers in flexible poly(vinylidene fluoride-trifluoroethylene) nanocomposites. *J. Mater. Chem.* **2012,** *22* (16), 8063-8068.

(176) Fernández, E.; Mijangos, C.; Guenet, J.-M.; Cuberes, M. T.; López, D., New hydrogels based on the interpenetration of physical gels of agarose and chemical gels of polyacrylamide. *Eur. Polym. J.* **2009,** *45* (3), 932-939.

(177) Guan, F.; Yang, L.; Wang, J.; Guan, B.; Han, K.; Wang, Q.; Zhu, L., Confined Ferroelectric Properties in Poly(Vinylidene Fluoride-co-Chlorotrifluoroethylene)-graft-Polystyrene Graft Copolymers for Electric Energy Storage Applications. *Adv. Funct. Mater.* **2011,** *21* (16), 3176-3188.

(178) Dang, Z. M.; Lin, Y. H.; Nan, C. W., Novel Ferroelectric Polymer Composites with High Dielectric Constants. *Adv. Mater.* **2003,** *15* (19), 1625-1629.

(179) Luo, B.; Wang, X.; Wang, Y.; Li, L., Fabrication, characterization, properties and theoretical analysis of ceramic/PVDF composite flexible films with high dielectric constant and low dielectric loss. *J. Mater. Chem. A.* **2014,** *2* (2), 510-519.

(180) Ahmad, Z., Polymer Dielectric Materials. In *Dielectric Material*, Silaghi, M. A., Ed. InTech: Rijeka, 2012; p Ch. 01.

(181) Hao, Y.; Tao, H.; Mingxia, L.; Mengye, M.; Qinghong, Z.; Hongzhi, W., Enhanced power output of an electrospun PVDF/MWCNTs-based nanogenerator by tuning its conductivity. *Nanotechnology* **2013,** *24* (40), 405401.

(182) Gregorio, J. R.; Cestari, M., Effect of crystallization temperature on the crystalline phase content and morphology of poly(vinylidene fluoride). *J. Polym. Sci. Part B Polym. Phys.* **1994,** *32* (5), 859-870.

(183) Xu, L.; Selin, V.; Zhuk, A.; Ankner, J. F.; Sukhishvili, S. A., Molecular Weight Dependence of Polymer Chain Mobility within Multilayer Films. *ACS Macro Lett* **2013,** *2* (10), 865-868.

감사의 글

먼저 2년 반동안 저에게 연구자로서의 교육과 인생의 많은 가르침을 주신 양창덕 지도교수님께 진심으로 깊은 감사드립니다. 교수님께서 저의 부족한 점도 다 받아주시고 포용으로 가르쳐 주셨기에 학위도 무사히 마치고 많이 배우고 성장할 수 있었습니다. 교수님께서 해주셨던 충고와 따뜻한 격려, 말씀해주셨던 저의 장점들, 고쳐나가야 할 부분들을 항상 잊지 않으며 발전해나가며 살겠습니다. 또한 교수님께 배웠던 연구와 값진 경험들을 가지고 연구자로서 자질을 키워나가며 노력하겠습니다. 아직도 많이 부족하지만 계속 배움을 게을리 하지 않으며 사회에 좋은 일로 기여할 수 있는 연구자가 되도록 노력하겠습니다. 또한 석사 학위 논문 및 디펜스 발표를 검토해주신 유니스트 박혜성 교수님과 홍성유 교수님께 깊은 감사드립니다. 그리고 고분자 개질을 통한 인공번개 전하펌프 발전기, 태양 전지 및 유기박막 트랜지스터의 공동연구를 수행하면서 많은 도움을 주신 유니스트 백정민 교수님, 포항공대 박찬언 교수님 그리고 동국대 노용영 교수님께 감사드립니다. 그 외 이재원 학생과 김유진, chen, 강석주 박사님께도 깊은 감사 드립니다. 이 분들과의 공동연구로 인해 저의 실험이 더 잘되고 좋은 결실을 맺을 수 있었습니다. 그리고 학위 과정 동안 실험도 많이 가르쳐주시고 좋은 조언들을 해주셨던 이정훈 박사님, 김경식 박사님, 이규철 박사님, 처음 ATOMS에 들어와서 실험 사수로서 많이 가르쳐 주셨던 효진언니, 졸업 이후에도 많은 조언과 지지로 항상 용기 주셨던 미진언니, 같이 공동 연구를 한 것 외에도 많이 가르쳐주고 친언니처럼 정들었던 chen, 티격태격 많이 싸우기도 했지만 늘 도와주고 가르쳐줬던 상면이, 그외 ATOMS 식구들에게도 감사드립니다. 모두 하는 일들 잘되고 나중에 좋은 모습으로 만났으면 좋겠습니다. 1년 넘게 각각 같이 살면서 정들고 많이 의지했던 민지언니와 은이.. 다른 실험실에서 학위하며 서로 많이 의지하고 힘이 되었던 언영이와 종하오빠, 철원이에게도 감사합니다. 모두들 무사히

학위 마치고 연구자로서 나중에도 좋은 연을 이어갔으면 좋겠습니다. 또한 초등학교부터 대학교까지 함께 다니면서 멀리서 힘들 때 늘 힘이 되주고 응원해주던 고향 친구들.. 민지, 은지, 서희, 미옥이, 멀리 여수에서 혹은 영국에 유학을 가서도 늘 지지해주고 용기주던 대학동기 환수에게도 감사드립니다. 친구들의 응원과 저에 대한 믿음이 저를 버티게 하고 힘이 되주었습니다.. 또한 2년반 동안 울산에 있으며 보살펴주시고 도와주셨던 막내이모께도 감사드립니다.

마지막으로 항상 저를 걱정해주시고 응원해주시는 사랑하는 어머니, 아버지께 진심으로 감사드립니다. 부모님의 희생과 노고가 있었기에 지금까지 제가 하고 싶었던 학문도 할 수 있었다고 생각합니다. 또한 언제나 제가 잘 되길 응원해주고 도와주고 기도해주는 사랑하는 형제들 진원오빠, 혜민언니, 혜현 언니에게도 감사드립니다. 앞으로 가족들의 사랑에 보답하는 연구자가 되겠습니다. 감사드립니다.

Permission from all cited journal in this dissertation

Chapter 1. *Nano Energy*, *Volume 39*, *September 2017*, *Pages 229-237*

Copyright Clearance Center RightsLink®

Home | Account Info | Help

ELSEVIER

Title: Over 10% efficiency in single-junction polymer solar cells developed from easily accessible random terpolymers

Author: Hye Jin Cho,Yu Jin Kim,Shanshan Chen,Jungho Lee,Tae Joo Shin,Chan Eon Park,Changduk Yang

Publication: Nano Energy

Publisher: Elsevier

Date: September 2017

Logged in as:
Hye Jin Cho
LOGOUT

Custom Permission Request

Review the details below and click 'Submit Request'.
Elsevier will review and respond within 15 business days.

Licensed Content Publisher	Elsevier
Licensed Content Publication	Nano Energy
Licensed Content Title	Over 10% efficiency in single-junction polymer solar cells developed from easily accessible random terpolymers
Licensed Content Author	Hye Jin Cho,Yu Jin Kim,Shanshan Chen,Jungho Lee,Tae Joo Shin,Chan Eon Park,Changduk Yang
Licensed Content Date	September 2017
Licensed Content Volume	39
Licensed Content Issue	n/a
Licensed Content Pages	9
Type of Use	reuse in a thesis/dissertation
Portion	cover image
Quantity	1
Format	both print and electronic
Are you the author of this Elsevier article?	Yes
Will you be translating?	No
Order reference number	183
Title of your thesis/dissertation	Molecular Design and Modification of Organic Materials for Opto-electronic and Tribo-electric Devices
Expected completion date	Jul 2017
Estimated size (number of pages)	100
Elsevier VAT number	GB 494 6272 12
Requestor Location	Miss. Hye Jin Cho 50, UNIST-gil Ulsan 44919 Republic of Korea Ulsan, 670380 Korea, Republic Of Attn: Miss. Hye Jin Cho
Total	Not Available

Edit Order Details
Edit Requestor Location This location may be used to determine your tax liability.

BACK | SUBMIT REQUEST

Chapter 4. *Lee et al., Sci. Adv. 2017;3: e1602902*

DOI: 10.1126/sciadv.1602902

Copyright Clearance Center

Note: Copyright.com supplies permissions but not the copyrighted content itself.

1 PAYMENT 2 REVIEW 3 CONFIRMATION

Step 3: Order Confirmation

Thank you for your order! A confirmation for your order will be sent to your account email address. If you have questions about your order, you can call us 24 hrs/day, M-F at +1.855.239.3415 Toll Free, or write to us at info@copyright.com. This is not an invoice.

Confirmation Number: 11655072
Order Date: 07/10/2017

If you paid by credit card, your order will be finalized and your card will be charged within 24 hours. If you choose to be invoiced, you can change or cancel your order until the invoice is generated.

Payment Information

Hye Jin Cho
chj7440@naver.com
+82 1038577440
Payment Method: Invoice

Billing address:

50, UNIST-gil
Ulsan 44919
Ulsan, 670380
KR

Order Details

Course: USE IN A THESIS/DISSERTATION

University/Institution: UNIST
Start of term: 07/11/2017
Course number:
Number of students: 1
Instructor:
Your reference:
Accounting reference:
Order entered by:

Special Orders

Science advances

Order detail ID: 70596797
ISSN: 2375-2548
Publication Type: Journal
Rightsholder: AMERICAN ASSOCIATION FOR THE ADVANCEMENT OF SCIENCE
Author/Editor: American Association for the Advancement of Science,

Permission Status: Special Order
Special Order Update: Checking availability
Permission type: Use in print course materials
Article/Chapter: full article
Page range(s): 98-99
Total number of pages: 100
Number of students: 1

TBD

Total order items: 1

This is not an invoice.

Order Total: TBD